NASA CR-165261
FR-13083

EXTENDED FREQUENCY TURBOFAN MODEL

By: J. R. Mason, J. W. Park, R. F. Jaekel

Pratt & Whitney Aircraft Group
Government Products Divison

Prepared for
National Aeronautics and Space Administration

NASA Lewis Research Center
Contract NAS3-21607

Final Report

1 Report Number	2 Govt Accession No	3 Recipient's Catalog Number
CR-165261		

4 Title *(and Subtitle)*	5 Report Date
EXTENDED FREQUENCY TURBOFAN MODEL	15 December 1980
	6 Performing Organization Code

7 Author(s)	8 Performing Organization Report No.
J. R. Mason, J. W. Park, R. F. Jaekel	FR-13983

9 Performing Organization Name and Address	10 Work Unit No
United Technologies Corporation Pratt & Whitney Aircraft Group Government Products Division P.O. Box 2691, West Palm Beach, FL 33402	11 Contract or Grant No NAS3-21607

12 Sponsoring Agency Name and Address	13 Type of Report and Period Covered
National Aeronautics and Space Administration Washington, D.C. 20546	Contractor Report
	14 Sponsoring Agency Code

15 Supplementary Notes

Project Manager, Peter G. Batterton
NASA Lewis Research Center
Cleveland, Ohio 44135

16 Abstract

Previously, a TF30 Engine Model was optimized using strictly one-dimensional modeling techniques with limited success in matching the response of the engine data. This program developed a fan model using two dimensional modeling techniques to add dynamic radial coupling between the core stream and the bypass stream of the fan. When incorporated into a complete TF30 engine simulation, the fan model greatly improved compression system frequency response to planar inlet pressure disturbances up to 100 Hz. The improved simulation also matched engine stability limits at 15 Hz, whereas the one dimensional fan model required twice the inlet pressure amplitude to stall the simulation. With verification of the two-dimensional fan model, this program formulated a high frequency F100(3) engine simulation using row-by-row compression system characteristics. In addition to the F100(3) remote splitter fan, the program modified the model fan characteristics to simulate a proximate splitter version of the F100(3) engine. The response of the F100 models was compared to high frequency (50-60 Hz) augmentor rumble data with good comparison of phase, but differences in gain. The source of the F100 model inaccuracy was traced to the fan duct model.

17 Key Words	18 Distribution Statement
Digital Dynamic Simulation Frequency Response Transient Response 2 Dimensional Modeling Bypass Ratio Stability Limits	Turbofan

19 Security Classif. (of this report)	20 Security Classif. (of this page)	21 No. of Pages	22 Price*
		99	

*For sale by the National Technical Information Service, Springfield, Virginia 22151

TABLE OF CONTENTS

LIST OF ILLUSTRATIONS

LIST OF ILLUSTRATIONS (CONTINUED)

LIST OF ILLUSTRATIONS (CONTINUED)

LIST OF ILLUSTRATIONS (CONTINUED)

SUMMARY

Pratt & Whitney Aircraft Group, Government Products Division (P&WA/GPD) conducted this program under National Aeronautics and Space Administration (NASA) Contract NAS3 21607 to investigate techniques for improving turbofan engine digital model high frequency response. A previous contract, NAS3-20292, optimized the dynamic configuration of a TF30 engine model using strictly one-dimensional modeling techniques with limited success in matching the response of the engine data. This program developed a fan model using two dimensional modeling techniques to add dynamic radial coupling between the core stream and the bypass stream of the fan. When incorporated into a complete TF30 engine simulation, the fan model greatly improved compression system frequency response to planar inlet pressure disturbances up to 100 Hz. The improved simulation also matched engine stability limits at 15 Hz, whereas the one-dimensional fan model required twice the inlet pressure amplitude to stall the simulation. With verification of the two-dimensional fan model, this program formulated a high-frequency F100(3) engine simulation using row-by-row compression system characteristics. In addition to the F100(3) remote splitter fan, the program modified the model fan characteristics to simulate a proximate splitter version of the F100(3) engine. The response of the F100 models was compared to high-frequency (50-60 Hz) augmentor rumble data with good comparison of phase, but differences in gain. The source of the F100 model inaccuracy was traced to the fan duct model.

INTRODUCTION

Gas turbine engine system design stresses the importance of developing the capability to model high-frequency phenomena and, thus, properly simulate the effects of augmentor and inlet disturbances on compression system response and stability. For example, augmentor transient disturbances, which have been tracked forward through the fan duct and around the inlet splitter, produce destabilizing effects on the compression system. Design studies indicate that transient operation of fan duct burners, variable geometry, and air invertor valves also result in duct flow disturbances that impact compression system stability. Evaluation of dynamic engine stability early in the design process requires a good dynamic engine model to ensure propulsion system operational suitability.

NASA Contract NAS3-20292 developed a high-frequency TF30 turbofan engine model with the objective of achieving reponse characteristics up to 100Hz. Modifications to the compression system improved the dynamic response characteristics of the engine simulation based on an investigation of the influence of size and number of finite elements using strictly one-dimensional modeling techniques. Based on the results of this program, high-frequency engine simulations using finite elements can be assembled to optimize the engine dynamic configuration with respect to dynamic characteristics and computer execution time. Resizing the compression system finite elements improved the dynamic characteristics of the engine simulation, but showed that additional refinements were required to obtain close agreement between simulation and actual engine dynamic characteristics.

Modeling of the fan bypass/core stream dynamic coupling and the transient splitter aerodynamics proved to be the main areas of needed improvement. Previous TF30 model results indicated a pressure disturbance must be twice the amplitude observed in tests to generate model instability. The simulation showed the fan to be the stability-limiting component where test data shows rotating stall to be initiated in the low-pressure compressor. The frequency response at the fan discharge of the model did not match recorded engine data above approximately 20Hz. The gain of fan discharge pressures in response to spatially uniform (planar) periodic pressure disturbances introduced at the engine inlet did not compare as well as desired with engine data.

The technical approach of the turbofan model frequency response improvement program conducted under contract NAS3-21607 sought to provide dynamic radial coupling in the fan by describing the gas path flowfield of the fan in a two-dimensional format of radial as well as axial directions. Three describing equations of continuity, energy, and momentum across a finite element were provided in the radial direction between the finite elements representing the fan core stream and the fan bypass stream.

This two-dimensional fan concept was constructed into a computer model and integrated into a complete turbofan engine model. Using TF30 engine component characteristics, the frequency response of the turbofan model was compared to measured engine data. When significant frequency response improvements resulted in the new TF30 model compared to the one-dimensional model, the F100(3) engine was then modeled. In addition to the baseline remote splitter F100 model, a proximate splitter F100 model was also constructed. The response of both F100 models was compared to measured engine test data.

TWO-DIMENSIONAL FAN MODEL

Model Concept

A majority of turbofan operation occurs with a radial warpage in discharge pressure across the span of the fan. The sensitivity of the turbofan cycle balance requires a fan model to account for this pressure warpage during all operating conditions. An average bypass fan section and an average core fan section, as shown in figure 1, accomplishes this in the cost effective, one-dimensional gas path modeling technique. A great deal of accuracy has been obtained in steady-state simulations by proper correlation of this warpage with some parameter, such as bypass ratio.

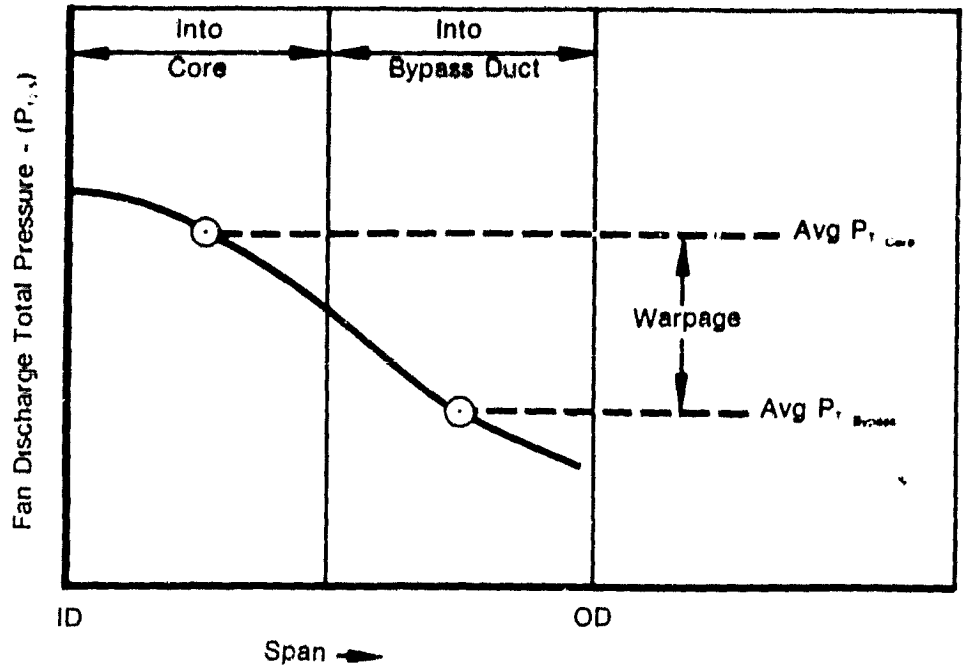

Figure 1. Turbofan One-Dimensional Modeling Technique Must Use Two Sections at Fan Discharge

However, steady-state correlations of warpage, which couple the bypass fan representation with the core fan representation, are not necessarily sufficient for a dynamic representation. Determination of transient response for stability and suitability investigations requires definition of accurate transient flow paths for components in the model. Proper definition of these paths, symbolized by the shift in bypass and core dividing streamlines as a function of time, further requires the incorporation of radial dynamic coupling in the fan component.

This refined modeling technique allows radial communication between control volumes that describe the inside diameter (ID) and outside diameter (OD) characteristics of the fan. In a previous NASA contract (NAS3 20292), the dividing streamline, based on the steadystate operating bypass ratio of the fan, set the characteristics of the control volumes for the bypass and core streams. However, no direct communication path existed between the control volumes in the radial direction during a transient. The new model accomplishes this communication by solving the basic unsteady flow equations for the radial direction in additional to axial direction calculations, as shown in figure 2.

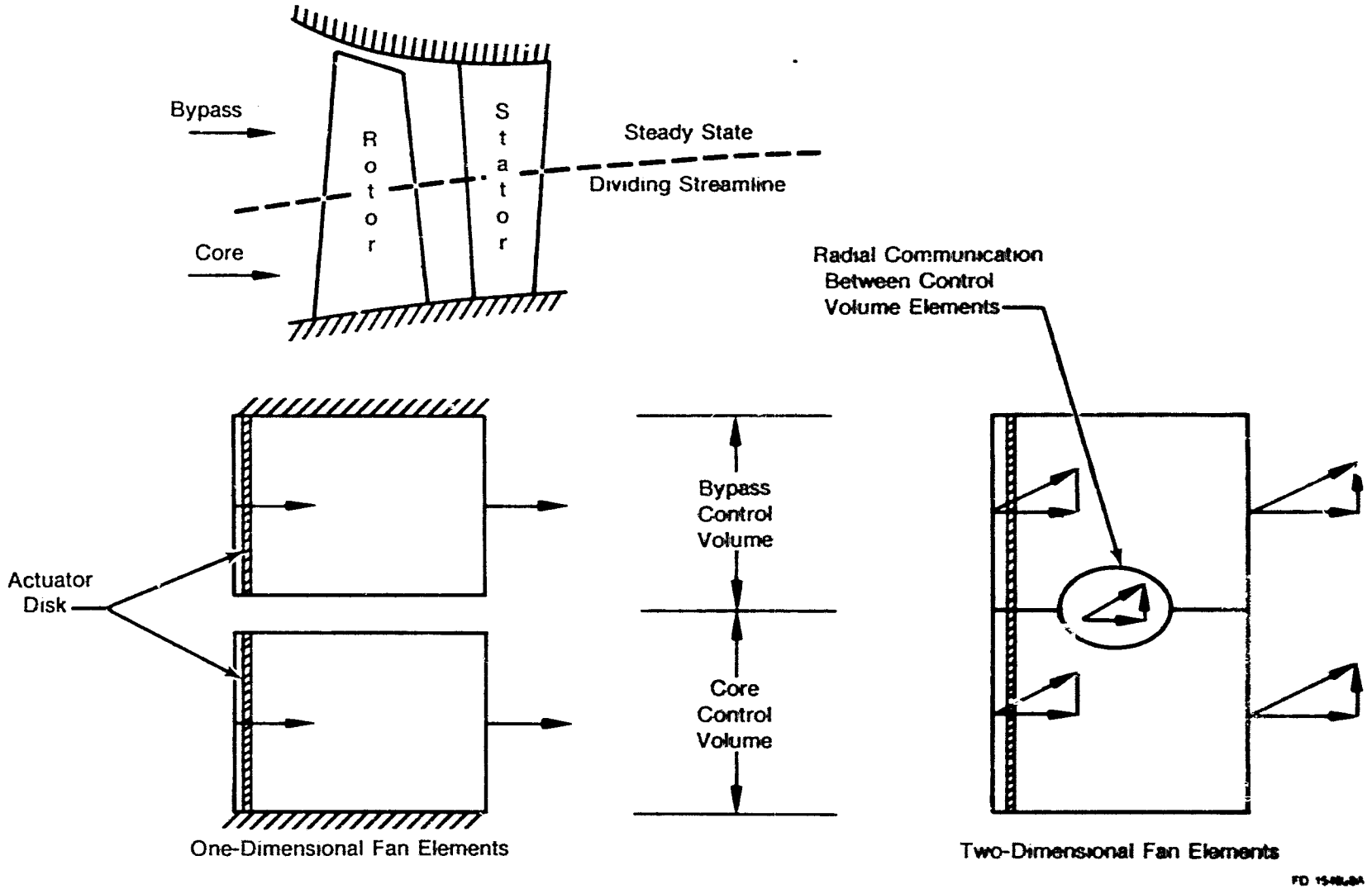

Figure 2. Dynamic Modeling of Fan Elements for Radial Coupling

Row Characteristics

The one-dimensional fan model utilized the row-by-row characteristics of NAS3-18535 as a base for the TF30 engine and NAS3-[illegible]310 as a base for the F100 engine. These empirical characteristics describe the fan performance in the core (ID) stream and in the bypass (OD) stream. A "dividing" streamline, as shown in figure 3, separates the core stream and bypass stream. Since the flow per unit area remains approximately constant, separate OD and ID pressure rise characteristics were described for each rotor and stator, independent of the streamline position. These characteristics, shown in Appendix B for the F100 fan, utilized the following definitions:

$$\Phi \quad \frac{W\sqrt{\theta_1}}{\delta A} \quad \left[\frac{(N/\sqrt{\theta_1})_{\text{corrs}}}{(N/\sqrt{\theta_1})} \right] \tag{1}$$

$$\Psi \quad \frac{\Delta P}{P} \left[\frac{(N/\sqrt{\theta_1})_{\text{corrs}}}{(N/\sqrt{\theta_1})} \right] \tag{2}$$

$$\lambda \quad \frac{\Delta T}{T} \left[\frac{(N/\sqrt{\theta_1})_{\text{corrs}}}{(N/\sqrt{\theta_1})} \right] \tag{3}$$

The total and static pressures required for the calculations of Φ and Ψ are related through Mach Number:

$$P \quad P \quad \left[1.0 + \frac{\gamma - 1.0}{2.0} M \right]^{\frac{\gamma}{\gamma - 1}} \tag{4}$$

where:

A	flow area
M	Mach number
N	rotor speed
P	pressure
T	temperature
Δ	pressure, temperature differential
δ	pressure/standard pressure
θ	temperature/standard temperature

Subscripts:

s	static
T	total

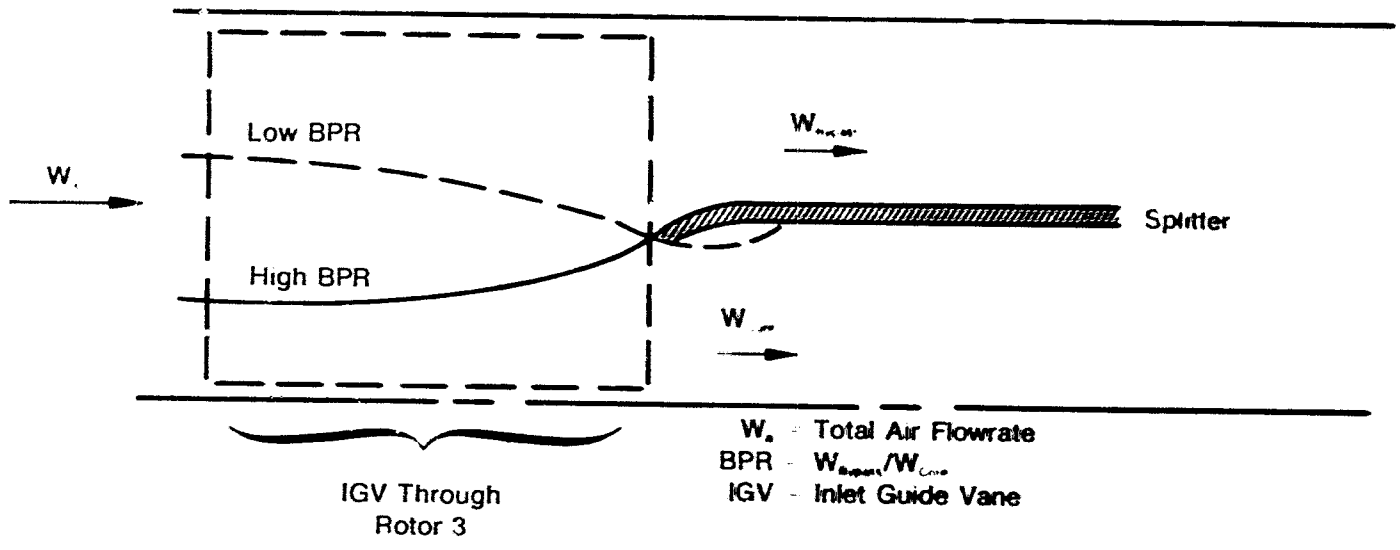

Figure 3. Fan Core Stream and Bypass Stream Separated by Dividing Streamline

Two-Dimensional Equations

The mathematical approach to the two-dimensional flowfield follows as a natural extension of the basic one-dimensional flow through a finite element, as described in Appendix A. Conceptually, the elements parallel each other with a primary flowpath in the axial direction and a secondary flowpath in the radial direction. This generates the grid that makes up the boundaries of the finite elements, as shown in figure 4. The velocity at the entrance and exit of the element contains both axial and radial components. A four-point averaging of two adjacent elements enables the computation of velocity at the radial boundary between the elements. The basic flow equations required to define the unsteady flow in an element are continuity, momentum, and energy. Each equation describes a basic property of the fluid flow: namely mass, momentum, and energy. It should be noted that the properties of mass and energy within the finite element are scalar quantities, while momentum is a vector quantity.

The following equations for time derivatives of the properties can be written for Element A in figure 4.

Continuity Equation

$$\left(\frac{dM}{dt}\right)_A = \left(\frac{dM}{dt}\right)_{in} - \left(\frac{dM}{dt}\right)_{out} - \left(\frac{dM}{dt}\right)_{in}$$

$$\left(\frac{dM}{dt}\right)_A = \rho_{in} A_{in} V_{in} - \rho_{out} A_{out} V_{out} - \rho_{in} A_{in} V_{in} \tag{5}$$

Where:

V	axial velocity component
V	radial velocity component

Momentum Equation

$$\left(\frac{dMOM}{dt}\right)_A = \left(\frac{dMOM}{dt}\right)_{in} - \left(\frac{dMOM}{dt}\right)_{out} + \left(\frac{dMOM}{dt}\right)_{in}$$

Axial $\left(\frac{dMOM}{dt}\right)_A = \rho_{in} A_{in} V_{in} - \rho_{out} A_{out} V_{out} - \rho_{in} A_{in} V_{in} V_{in} +$

$$P_{in} A_{in} - P_{out} A_{out} - P_{in} \pi (r_{in} - r_{out})$$

$$P_{out} ((\pi r_{in} + A_{in}) - (\pi r_{out} + A_{out})) + F' \tag{6}$$

Radial $\left(\frac{dMOM}{dt}\right)_A = \rho_{in} A_{in} V_{in} V_{out} - \rho_{out} A_{out} V_{out} V_{in}$

$$\rho_{in} A_{in} V_{in} V_{in} + P_{in} A_{in} - P_{out} A_{out} -$$

$$(P_{out} + P_{in})/2 (A_{out} - A_{in}) + R' \tag{7}$$

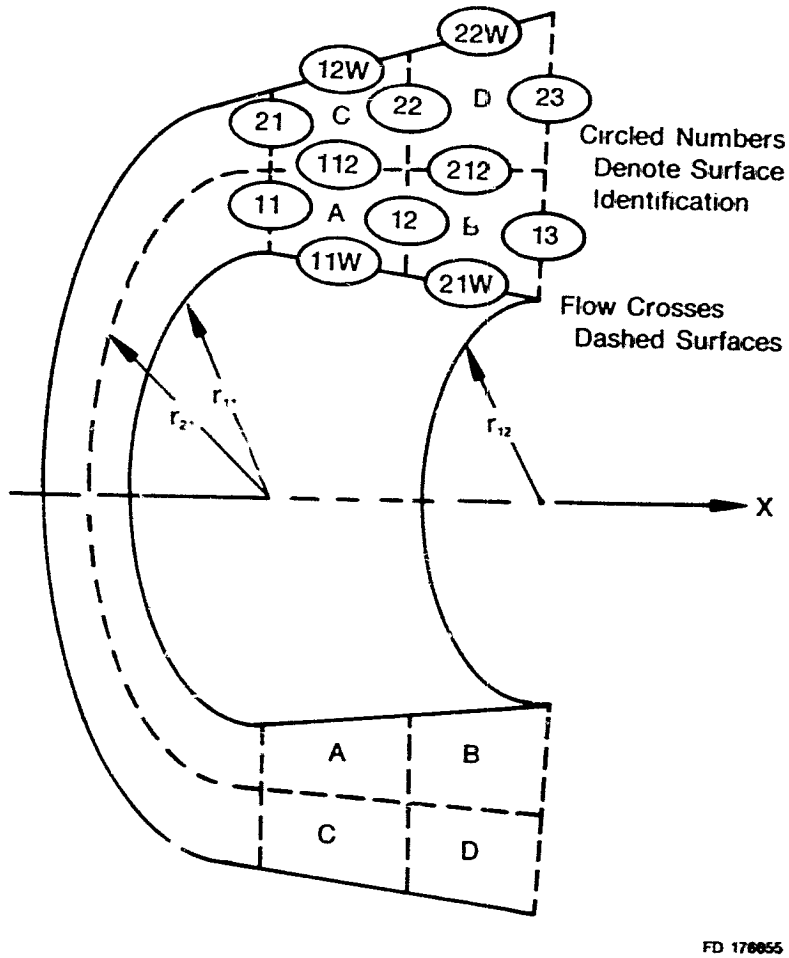

Figure 4. Finite Element Grid

Energy Equation

$$\left(\frac{dE}{dt}\right)_{\quad} \left(\frac{dE}{dt}\right)_{\quad} \left(\frac{dE}{dt}\right)_{\quad} \left(\frac{dE}{dt}\right)_{\quad}$$

$$\left(\frac{dE}{dt}\right) \left(h + \frac{1}{2g} V^{\quad}\right) \rho A V$$

$$\left(h + \frac{1}{2g} V^{\quad}\right) \rho A V$$

$$\left(h + \frac{1}{2g} V^{\quad}\right) \rho A V$$

$$\frac{dW}{dt} \frac{dQ}{dt} \tag{8}$$

Where:

$$h \int_{T}^{T} C_p \, dT \tag{9}$$

$$V \quad V \quad V \tag{10}$$

Nomenclature:

A	cross sectional area
C_p	specific heat at constant pressure (function of T)
C_v	specific heat at constant volume
E	energy in the element
F	force on the fluid due to turbomachinery
M	mass in the element
MOM	momentum in the element
P	static pressure
Q	heat addition across the element boundaries
R	term to account for turbomachinery radial warpage
r	radius
T	static temperature
V	velocity
W	mechanical work
ρ	density

Subscripts

A	element A of figure 4
r	radial direction
Tur	turbomachinery effects inside element
x	axial direction
1,2,...	nodal coordinates of figure 4

The continuity equation defines the time rate of change of mass in the element in terms of the flow in and out of the element. The momentum equation expresses the time rate of change of momentum in the element due to mass transfer and forces on the fluid in the axial direction, as well as the radial direction of flow. The energy equation represents the time rate of change of energy as the sum of the kinetic and potential energies of the fluid, the rate of mechanical work done on the fluid, and the rate of heat addition to the fluid. Expressed in an integral form, the equations define the quantities of mass, momentum, and energy within the finite element in the following manner:

Continuity Equation

$$M \quad \int \rho d(\text{Volume}) \quad \int \rho(x) A(x) \qquad (11)$$

The equation integrates by assuming a linear distribution of properties across the finite element as follows:

$$\rho(x) \quad \rho \quad + \quad \frac{(\rho \quad \rho)}{\Delta x} \, dx \qquad (12)$$

$$A(x) \quad A \quad + \quad \frac{(A \quad A)}{\Delta x} \, dx \qquad (13)$$

Thus, the continuity equation becomes

$$(M) \quad (2\rho \, A \quad + 2\rho \, A \quad + \rho \, A \quad + \rho \, A) \, \frac{\Delta x}{6} \qquad (14)$$

which satifies the continuity principle:

$$(M) \quad \int (\text{equation No. 5}) \, dt \quad \int (\rho A V \quad \rho A V \quad \rho A V) \, dt$$

$$(2\rho \, A \quad + 2\rho \, A \quad + \rho A \quad + \rho A) \, \frac{\Delta x}{6} \qquad (15)$$

Similar expressions have been derived for the momentum and energy equations. Equations 14 through 21 define the fluid conditions in Element A of figure 4.

$$\text{Axial (MOM)} \quad \int [\rho A V \quad P A \quad P A \quad \rho A V V \quad +$$

$$P A \quad P A \quad P \pi (r \quad r)$$

$$P (\pi r \quad A) \quad (\pi r \quad A)) + F] \, dt \qquad (16)$$

$$[(3A \quad A) \rho V \quad + (A \quad 3A) \rho V \quad +$$

$$(A \quad A)(\rho V \quad \rho V)] \, \frac{\Delta x}{12.} \qquad (17)$$

Radial (MOM),

$$\int [\rho_{in} A_{in} V_{x,in} V_{r,in} - \rho_{ex} A_{ex} V_{x,ex} V_{r,ex} + \rho_{in} A_{in} V_{in}^2 + P_{in} A_{in} - P_{ex} A_{ex} - (P_{in} + P_{ex})/2 \cdot (A_{in} - A_{ex}) + R'] \, dt \tag{18}$$

$$[(3A_{in} + A_{ex}) \rho_{in} V_{in}^2 + (A_{in} + 3A_{ex}) \rho_{ex} V_{ex}^2 + (A_{in} + A_{ex})(\rho_{in} V_{in}^2 + \rho_{ex} V_{ex}^2)] \frac{\Delta X}{12.} \tag{19}$$

(E),

$$\int \left[\left(h_{in} + \frac{1}{2g} V_{in}^2 \right) \rho_{in} A_{in} V_{x,in} - \left(h_{ex} + \frac{1}{2g} V_{ex}^2 \right) \rho_{ex} A_{ex} V_{x,ex} + \left(h_{in} + \frac{1}{2g} V_{in}^2 \right) \rho_{in} A_{in} V_{x,in} + \frac{d\omega}{dt} + \frac{dQ}{dt} \right] dt \tag{20}$$

$$\left[V_{in}^2 \left(A_{in} \left(\frac{\rho_{in}}{5} + \frac{\rho_{ex}}{20} \right) + A_{ex} \left(\frac{\rho_{in}}{20} + \frac{\rho_{ex}}{30} \right) \right) + V_{ex}^2 \left(A_{in} \left(\frac{\rho_{in}}{30} + \frac{\rho_{ex}}{20} \right) + A_{ex} \left(\frac{\rho_{in}}{20} + \frac{\rho_{ex}}{5} \right) \right) + V_{in} V_{ex} \left(A_{in} \left(\frac{\rho_{in}}{10} + \frac{\rho_{ex}}{15} \right) + A_{ex} \left(\frac{\rho_{in}}{15} + \frac{\rho_{ex}}{10} \right) \right) \right] \frac{\Delta X}{2} +$$

$$C_p [(3A_{in} + A_{ex}) \rho_{in} T_{in} + (A_{in} + 3A_{ex}) \rho_{ex} T_{ex} + (A_{in} + A_{ex})(\rho_{in} T_{in} + \rho_{ex} T_{ex})] \frac{\Delta X}{12} \tag{21}$$

Radial Term

Because the one-dimensional core stream and bypass stream characteristics represent average pressures in their respective streams, as shown in figure 1, a radial profile in pressure may exist at a steady-state operating point. An increment in radial momentum flux (R' in the above equations) balances the effect of this pressure profile. Effort was extended without success during the contract period to analytically predict this radial term as a function of blading design and operating conditions. Thus, the model results reported herein consist of calculating the required steady-state radial momentum term and retaining the vector angle between the radial and axial momentum fluxes as a constant during transients. For small transients away from a steady-state point, this method is probably adequate. However, a new technique should be developed for large excursions.

TF30 ENGINE MODEL

The TF30 is a twin-spool augmented turbofan engine that mixes bypass and core gas flows in the afterburner duct. The low-pressure spool is composed of a three-stage fan and a six-stage compressor driven by a three-stage turbine. The high-pressure spool consists of a seven-stage compressor driven by a one-stage, air-cooled turbine. The combustor is a can type surrounded by a secondary chamber that uses high-pressure compressor discharge air to cool the burner cans and dilute the fuel-air mixture. Surge bleeds are incorporated at the seventh and twelfth stage of the compression system

Engine Test Data

NASA Lewis Research Center (LeRC) tested a TF30-P-3 engine to investigate engine dynamics. These high frequency response results enabled an evaluation of the dynamic characteristics of the engine simulation in the contract. Testing occurred in an altitude chamber using the LeRC air jet system described in Reference 2, which induced dynamic pressure variations at the front end of the engine. The average inlet conditions for the test produced a Reynolds number index of 0.5 at an inlet pressure of 50.7 to 54.5 kPa abs (7.35 to 7.90 psia). Engine exhaust pressure was set at 16.5 kPa abs (2.4 psia) for all tests. As illustrated in figure 5, high-response total pressure instrumentation locations included the engine air inlet (Sta. 2.0), the fan first-stator passage (Sta. 2.1), the fan core stream discharge (Sta. 2.3), fan bypass stream discharge (Sta. 2.3F), low-pressure compressor discharge (Sta. 3.0), twelfth-stage stator passage (Sta. 3.12), and high-pressure compressor discharge (Sta. 4.0).

NASA devoted a portion of the test program to an investigation of the engine dynamic response to spatially uniform (planar) periodic pressure disturbances induced at the engine inlet. By using the frequency-sweep test technique described in Reference 2, gain and phase characteristics of response to the engine inlet pressure were established for pressures at the internal engine stations of 2.3, 2.3F, 3.0, and 4.0. Figures 6 through 9 show the Sta. 2.3 and Sta. 2.3F gain and phase characteristics of the engine operating at 8600 $N1/\sqrt{\theta}$ used for comparisons in this contract. Although the air jet stream was mechanically capable of frequencies up to 200 Hz, Reference 2 cautions against using the data above 80 Hz because of the measurable amplitudes in the engine-inlet and fan-compressor system pressures. Investigations also included engine stability limits during the NASA test program. During these tests, discrete frequency inlet pressures were induced and amplitude increased until either stall/surge was encountered or the amplitude limits of the air jet system were reached. Results of these tests in terms of P_{t2} amplitude at stall for 15 Hz frequency, as shown in figure 10, provided data for comparison to the stability limits of the simulation.

Baseline Element Configuration

This modeling technology improvement program investigated methods to improve turbofan engine system model response in the frequency range up to 100 Hz. A previous NASA contract (NAS3-20292) utilized the TF30 mixed flow turbofan engine in strictly one-dimensional simulation technology studies. Through reduced-order analysis of the compression system simulation element breakup, NAS3-20292 showed that the dynamic characteristics of a stage-by-stage simulation at 100 Hz could be obtained with a more simplified dynamic configuration, while realizing substantial savings in computer execution time. The analysis showed that the dynamic elements should be uniformly sized to achieve the best frequency response. The optimum dynamic element configuration for the TF30 engine under this program was 27 elements. This became the baseline for the present contract to investigate simulation improvement by utilizing two-dimensional effects in the fan.

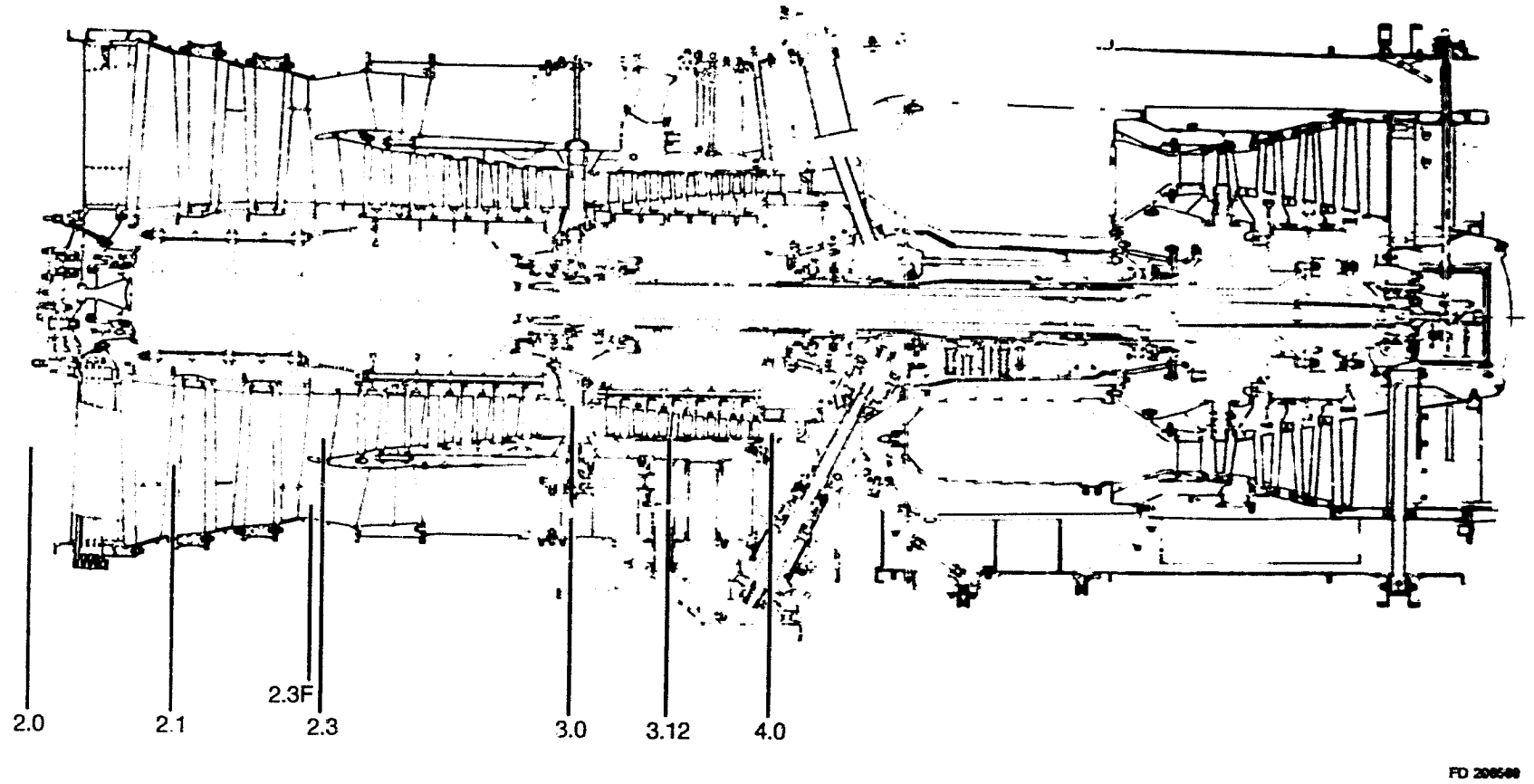

Figure 5. TF30 Engine Cross Section with High-Response Total Pressure Instrumentation Locations

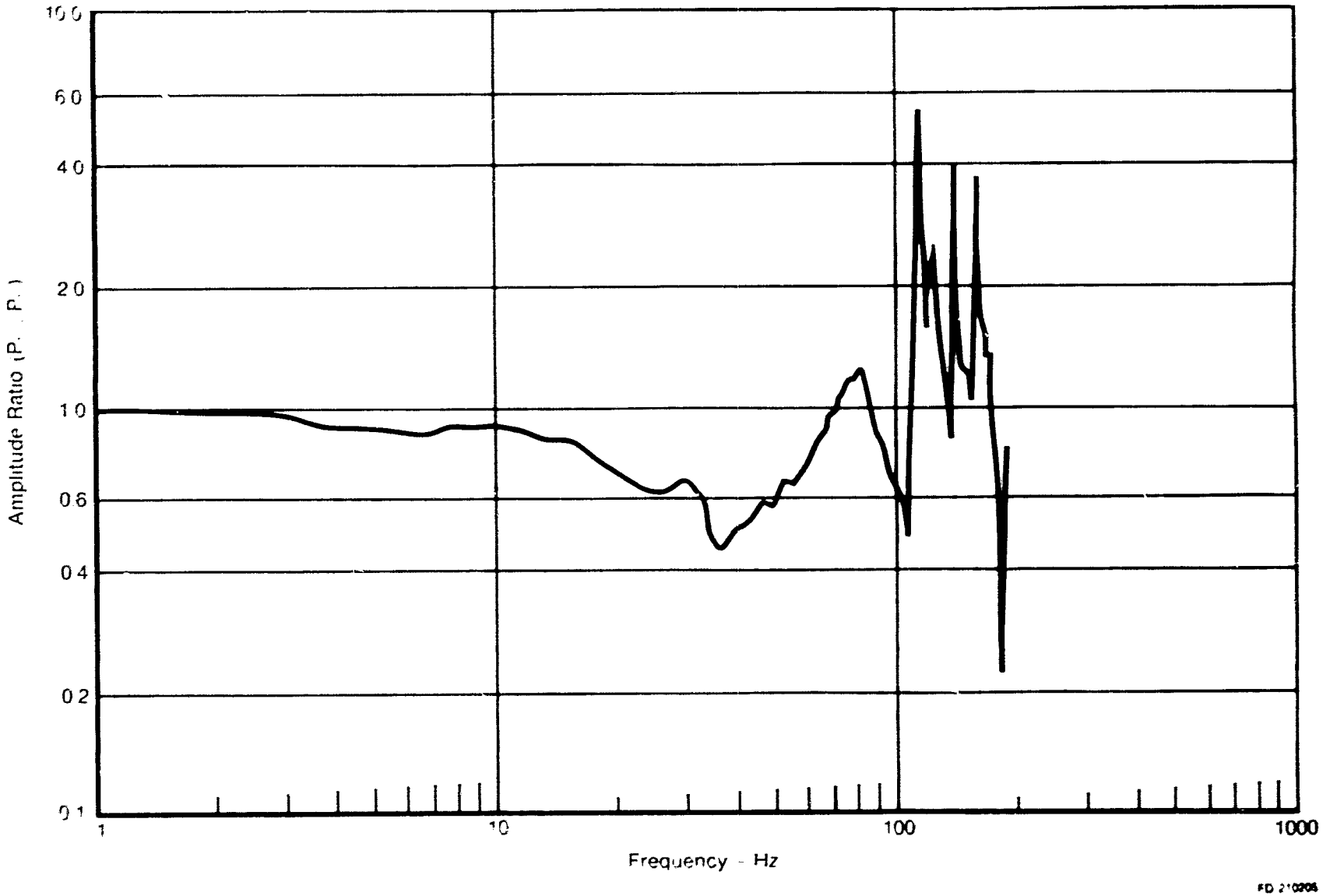

Figure 6. Fan Core Stream Amplitude Ratio - TF30 NASA Data

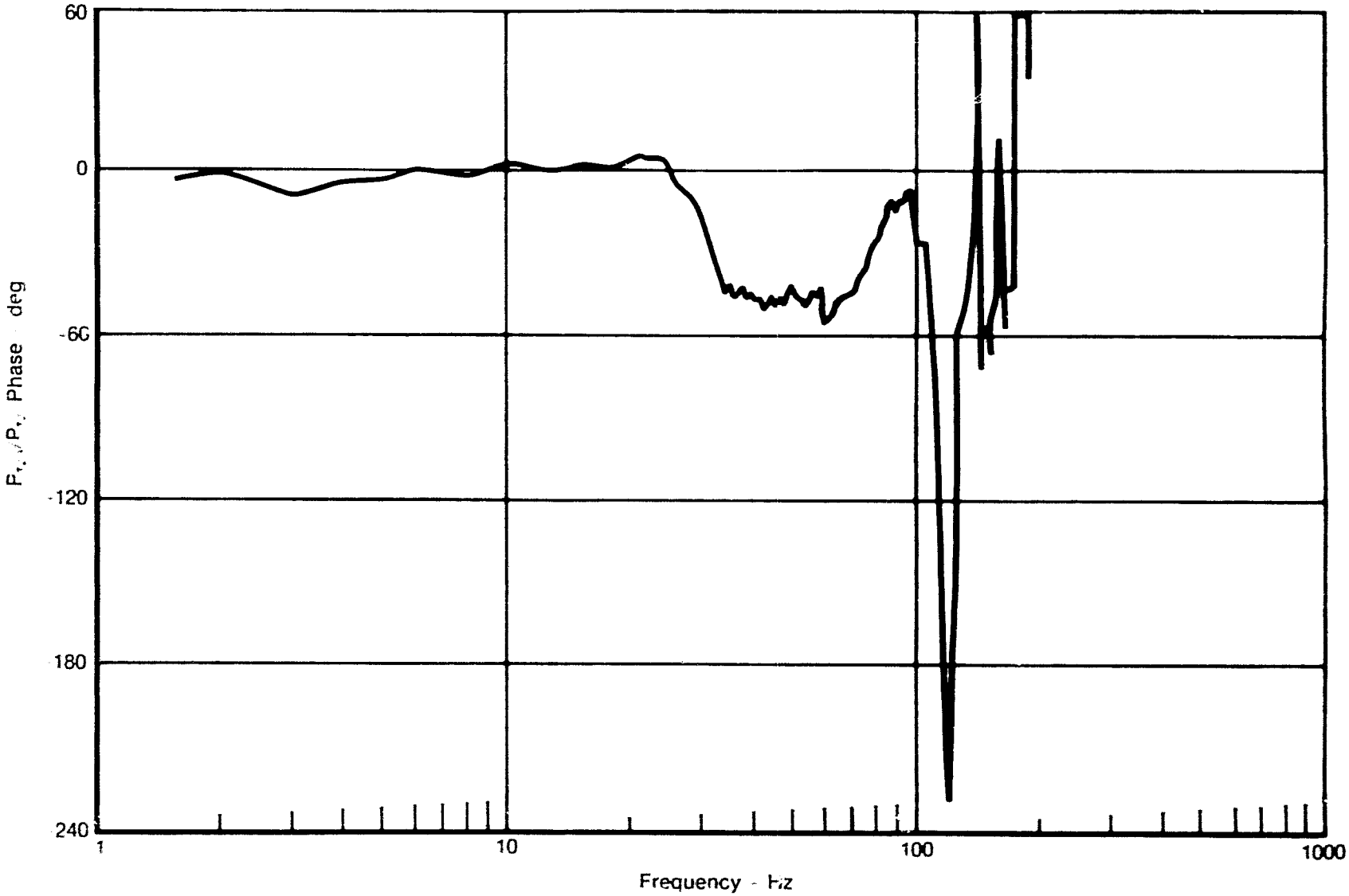

Figure 7. Fan Core Stream Phase - TF30 NASA Data

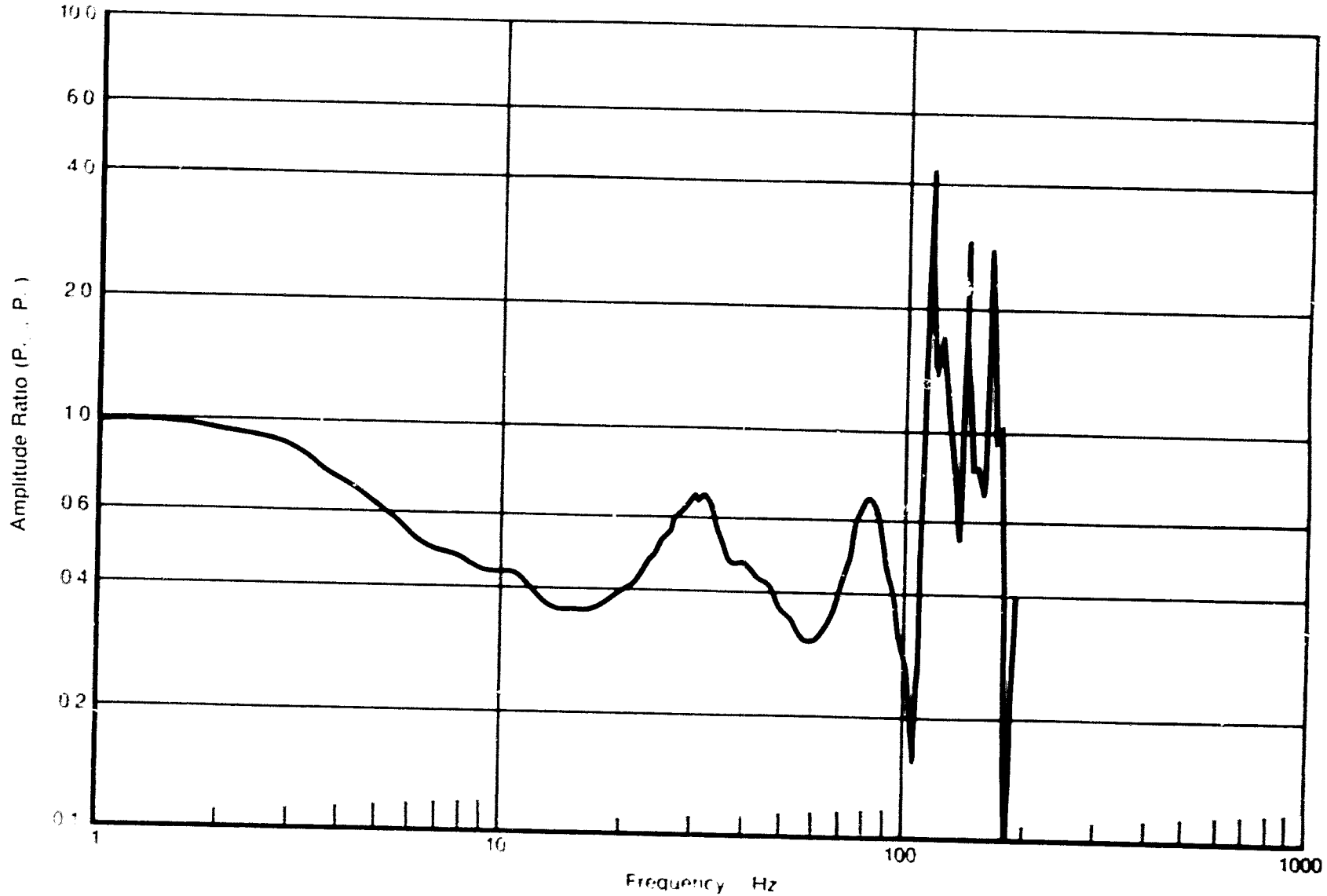

Figure 8. Fan Bypass Stream Amplitude Ratio - TF30 P&WA Data

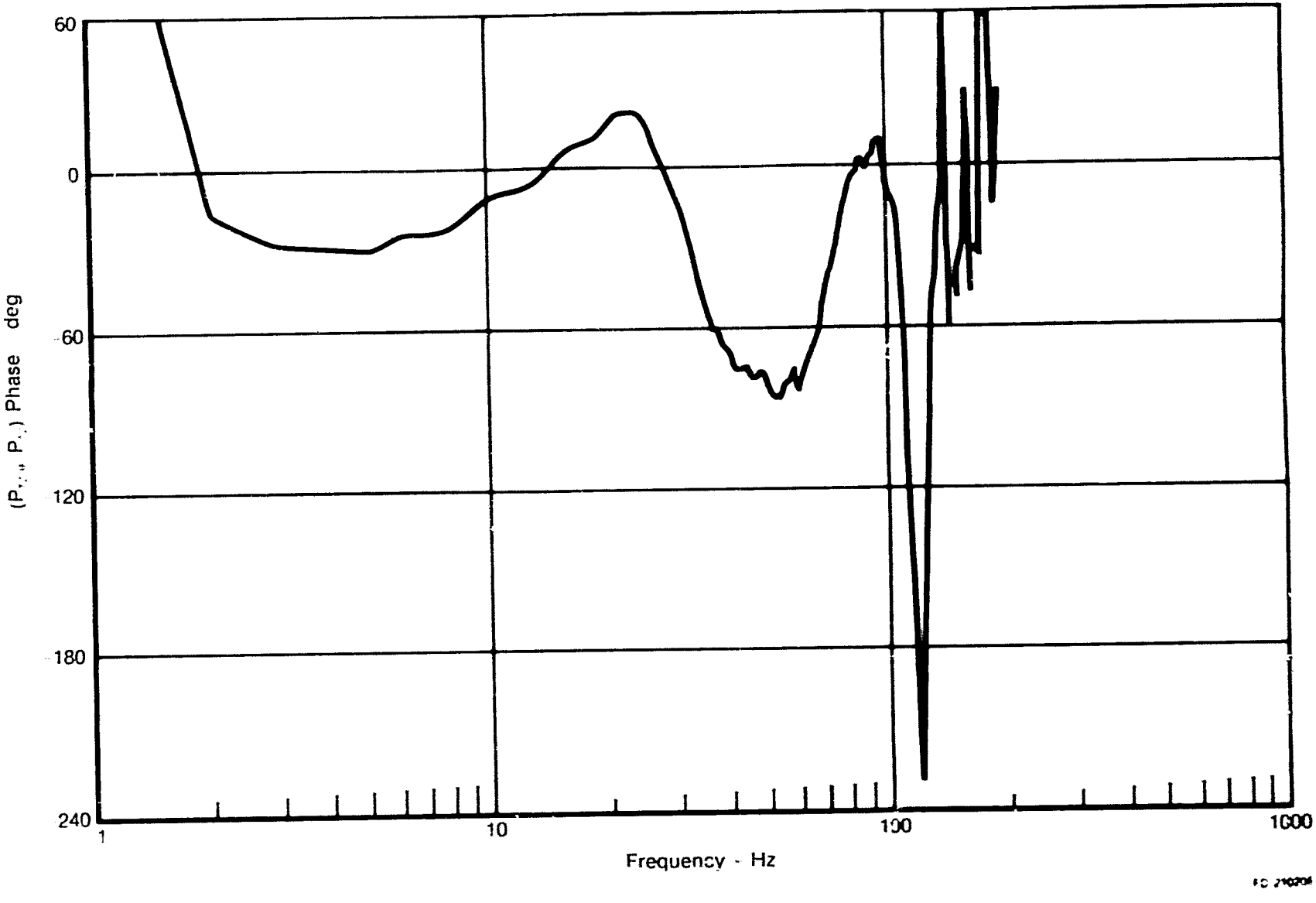

Figure 9. Fan Bypass Stream Phase - TF30 NASA Data

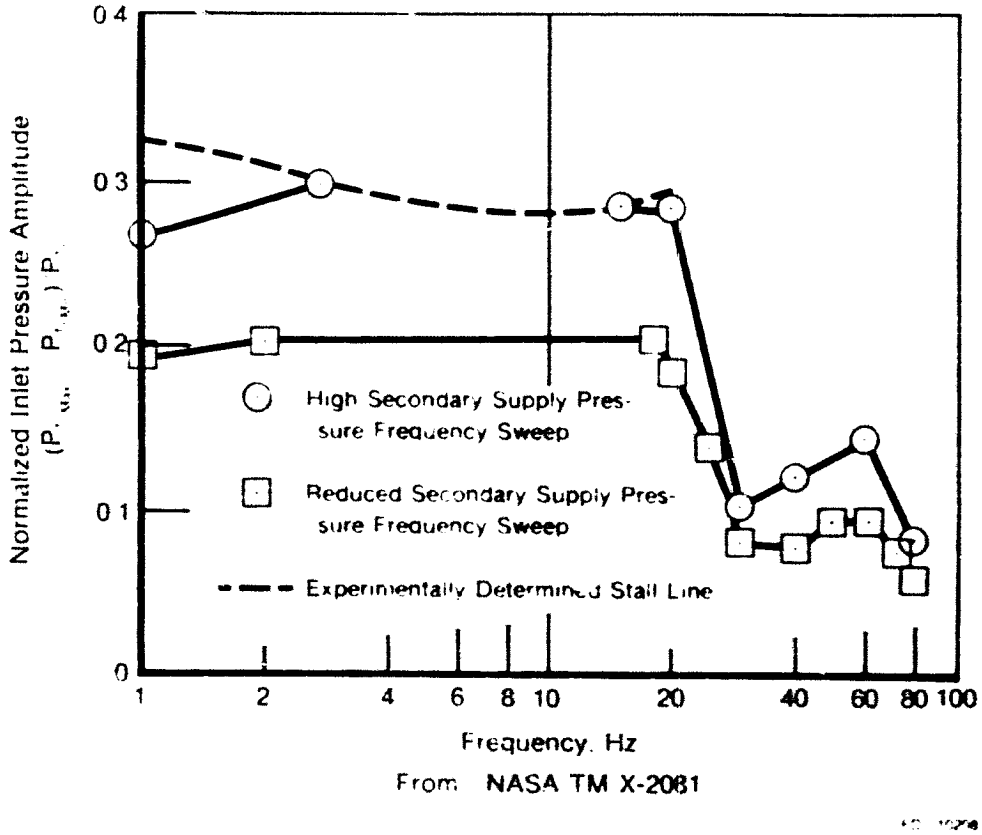

Figure 10. TF30 Engine NASA Test Data Stall Limit and Operating Characteristics During Cyclic P_{T2} Variations

The baseline 27 dynamic elements of the TF30 engine, shown in figure 11, consist of 10 elements in the compression system and 17 elements for the remaining components of the engine. One modification was performed to the configuration of NAS3-20292 involving the interface location of the fan elements. The boundary location of the fan discharge elements was relocated from aft of Stator 3 to forward of Stator 3 for both the fan bypass and core streams. This allows the dynamic element boundaries to coincide with the test data probe (Sta. 2.3 and Sta. 2.3F) locations. This dynamic element configuration with four fan elements (two in the core stream and two in the bypass stream) made up the baseline TF30 configuration. The model was operated with only one-dimensional effects to enable comparison with the two-dimensional fan model. As will be discussed later, the four-element fan was also configured with six and eight elements to investigate fan element configuration influence on model response.

Frequency Response Comparison

Frequency response of the fan discharge pressure appears on bodie plots (gain and phase) in figures 12 and 13 for the fan core stream and fan bypass stream, respectively. The engine plots originate from test frequency data and the model plots come from the linearized transfer function method described in Appendix A. The baseline two-dimensional fan model response shows improvement over the one-dimensinal fan model. The fan core stream of the two-dimensional model, as shown in figure 12, achieves resonant responses, whereas the one-dimensional model produced only a gradual roll-off in gain and phase. At the low frequencies (less than 25 Hz), the two-dimensional model is more attenuated than engine data, but achieving resonant frequencies is much more important for this extended frequency model. These resonant frequencies of the model at 33 and 70 Hz compare with engine data of 30 and 82 Hz. Even though the one-dimensional fan showed resonant frequencies in the bypass stream, shown in figure 13, the overall trend of the two-dimensional model more closely duplicates engine data and the large attenuation at 7 Hz has disappeared.

Discrete Frequency Comparison

The model was exercised with discrete sinusoidal frequencies of 15, 30, 60, 82, and 100 Hz on P_{t_2}. These frequencies were selected because of resonant peaks and valleys in engine data. This study generated data for comparison of model response with large amplitudes (identical to engine data) to the linearized transfer function method wherein the partials were generated with only 0.1% steps, as shown in Appendix A. In addition to determining the non-linear effects due to the large amplitudes, the results could be compared to discrete frequency engine data.

Surprisingly, the model results of the discrete frequency analysis closely approximated the linearized transfer function analysis, as shown in figures 14 and 15, with only differences in phase denoted for high frequencies. Only three cycles were run at each frequency, but by examining the transient pressure traces shown in figures 16 through 20 the startup inaccuracies appear to be gone. Tables 1 and 2 present the detailed results of the discrete frequency analysis.

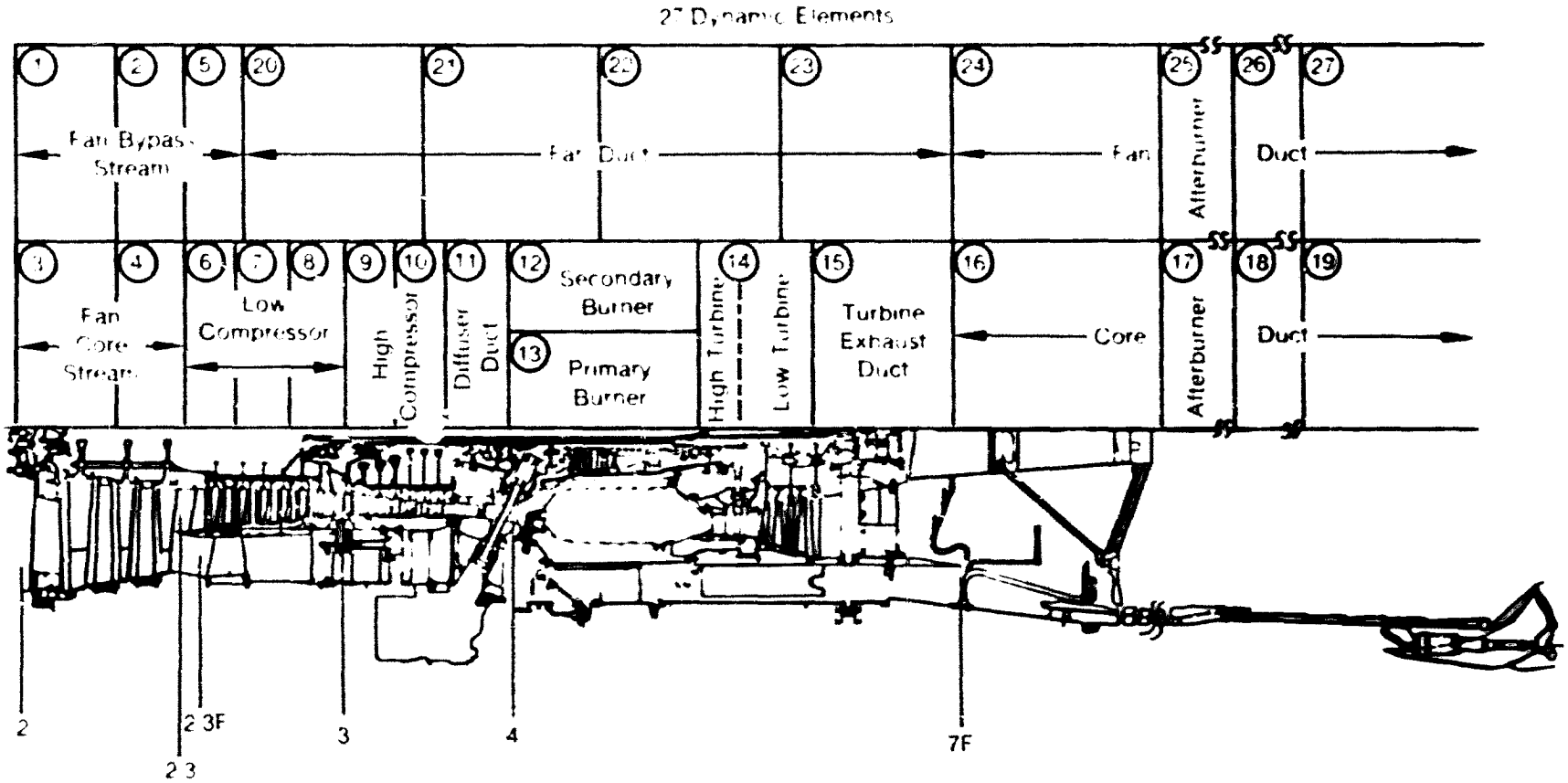

FD 20857D

Figure 11. Configuration of Baseline TF30 Engine Simulation

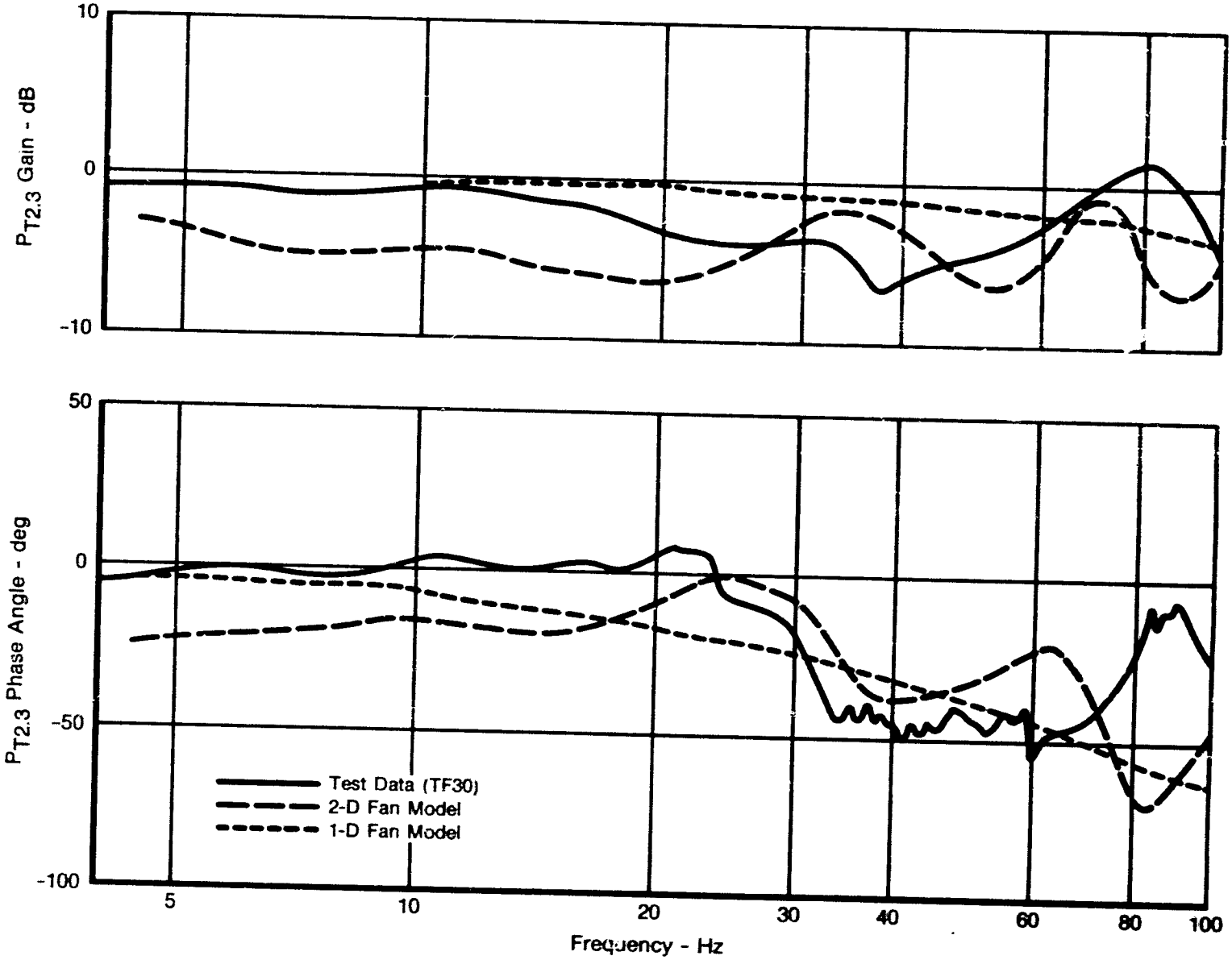

Figure 12. TF30 Engine Frequency Response of Fan Core (Sta. 2.3) to Inlet (Sta. 2.0) for One- and Two-Dimensional Models

PD 200583

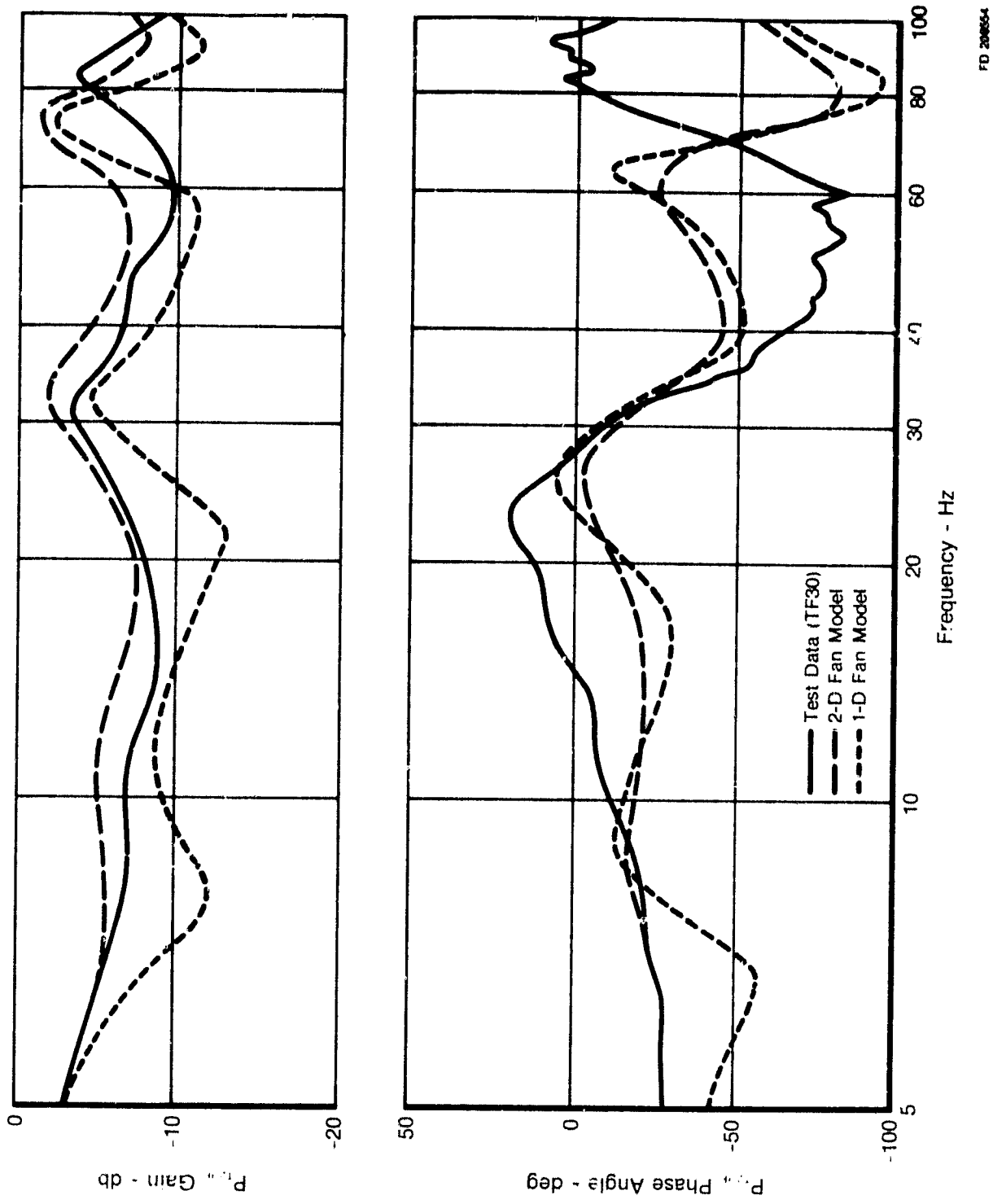

Figure 13. TF30 Engine Frequency Response of Fan Bypass (Sta. 2.3F) to Inlet (Sta. 2.0) for One- and Two-Dimensional Models

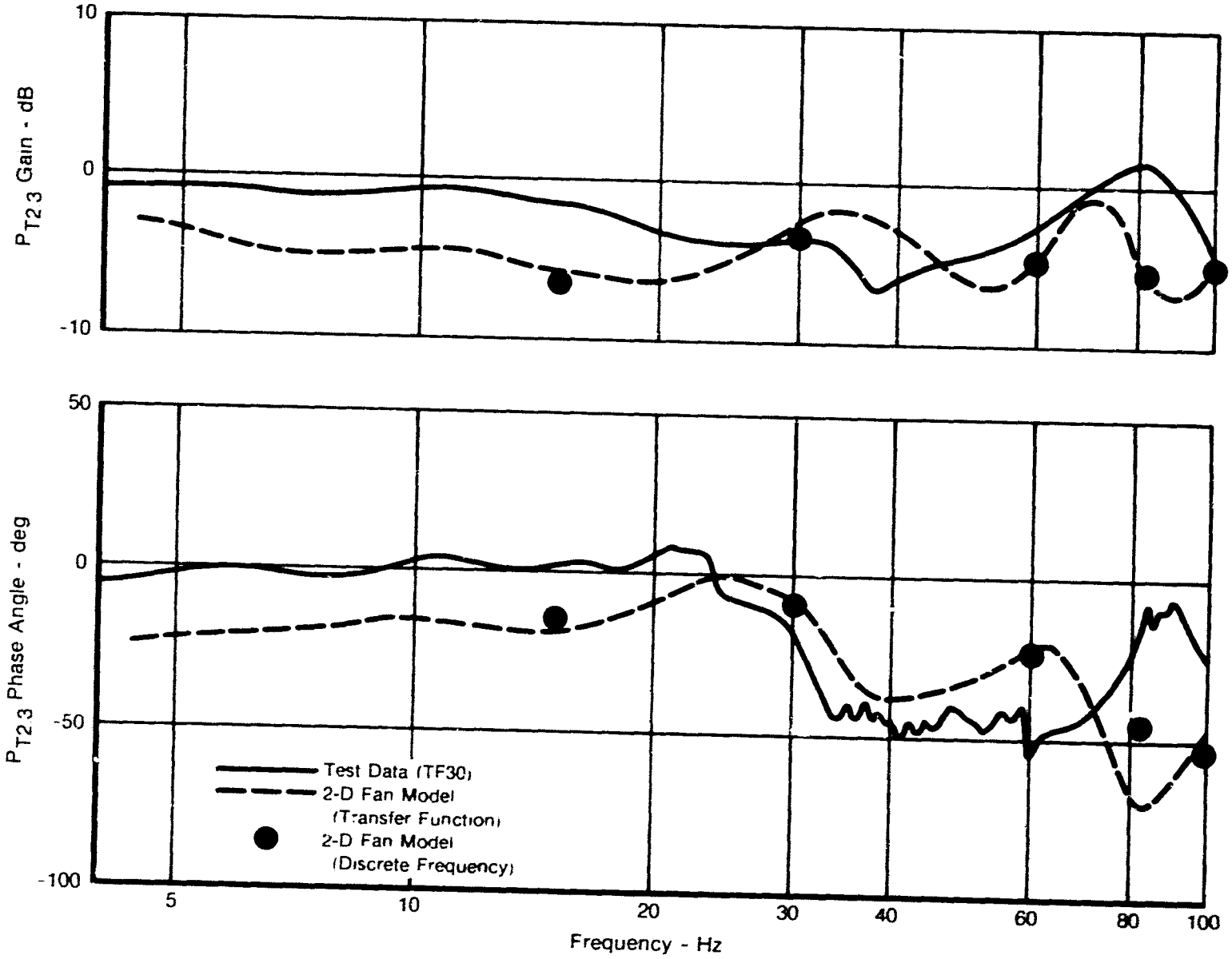

Figure 14. TF30 Engine Frequency Response of Fan Core (Sta. 2.3) to Inlet (Sta. 2.0) for Transfer Function and Discrete Frequency Methods

FD 208556

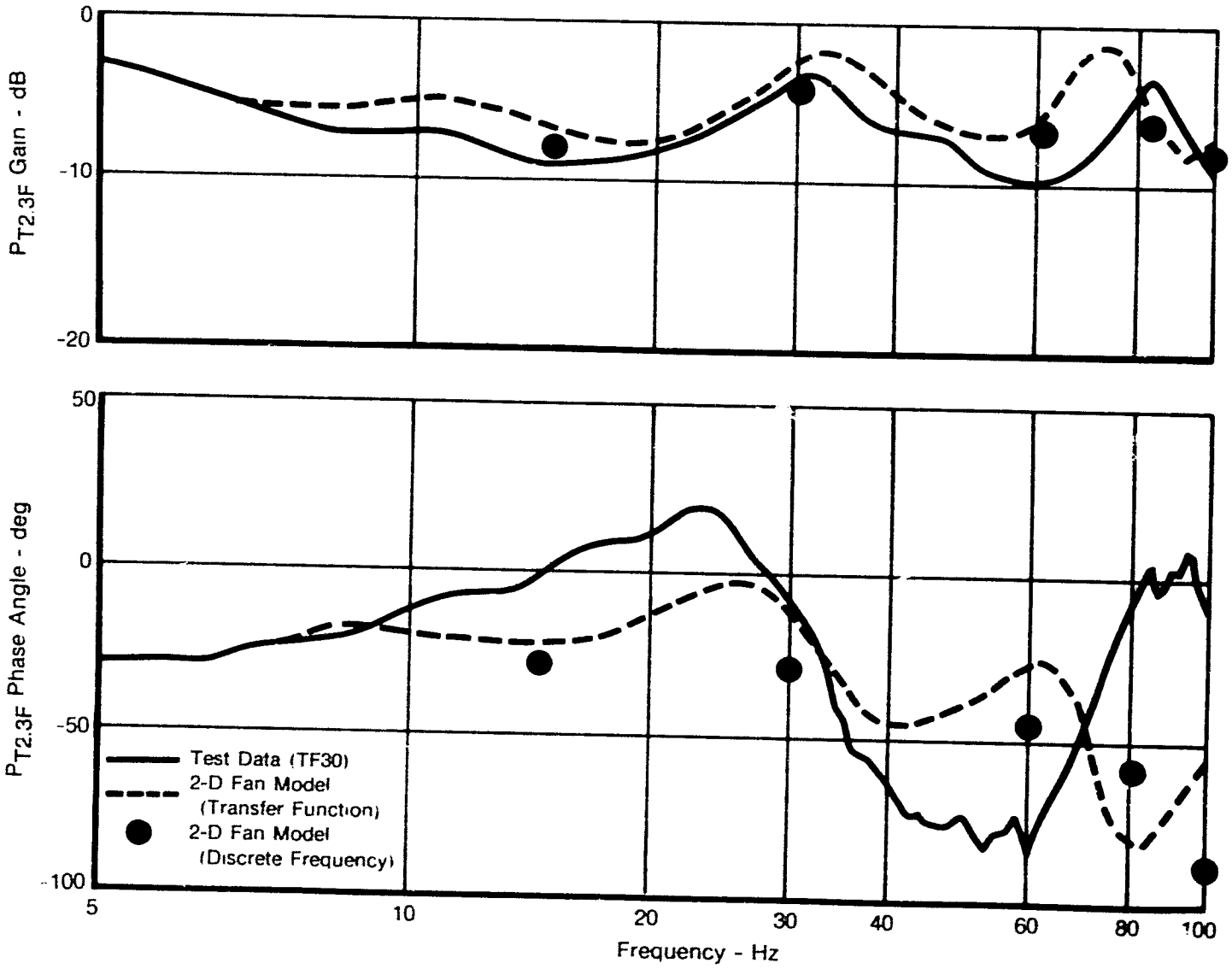

Figure 15. TF30 Engine Response of Fan Bypass (Sta. 2.3F) to Inlet (Sta. 2.0) for Transfer Function and Discrete Frequency Methods

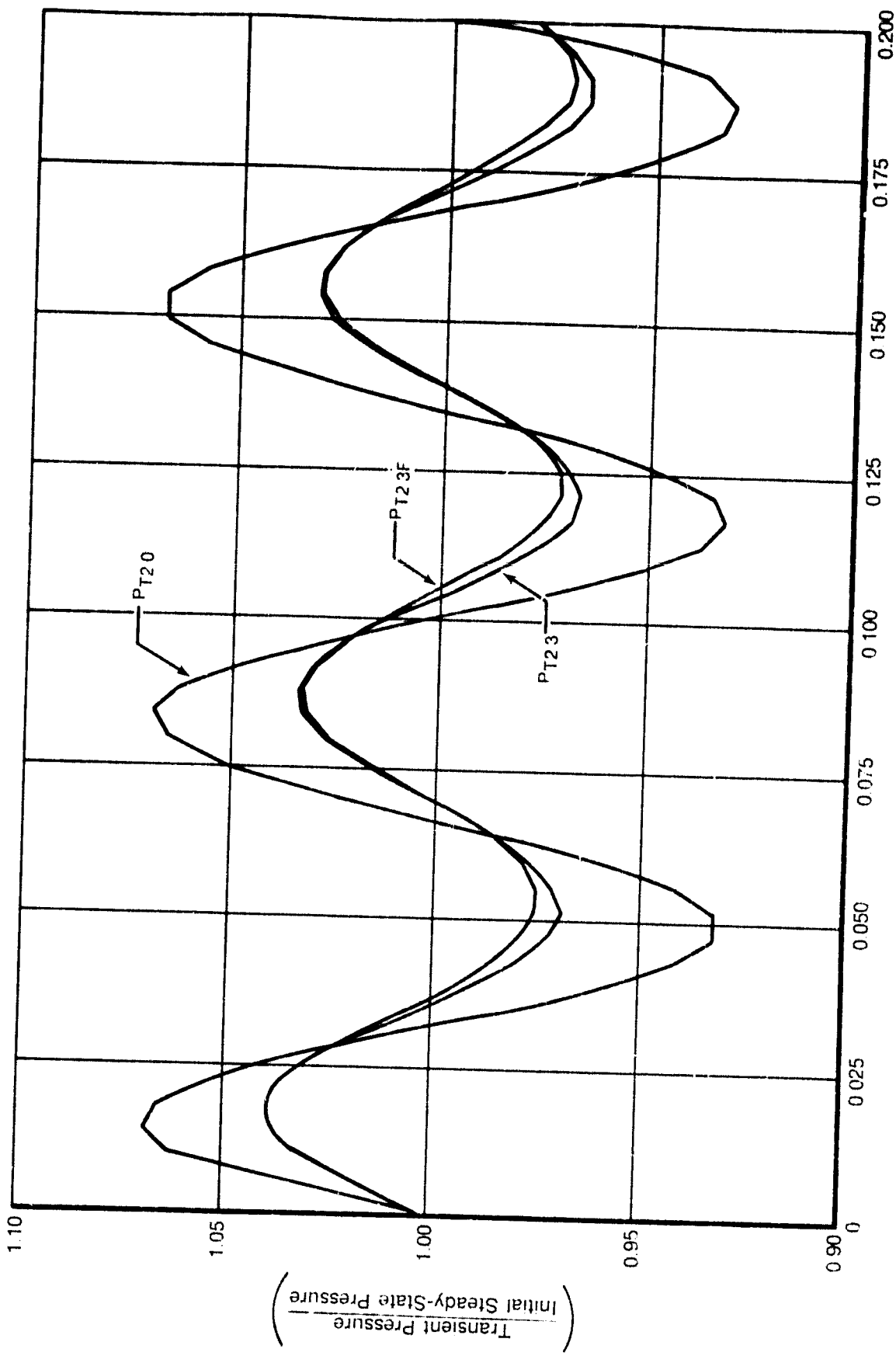

Figure 16. TF30 Simulation Fan Response to Inlet Pressure Cyclic Variation (15 Hz, 14% Amplitude)

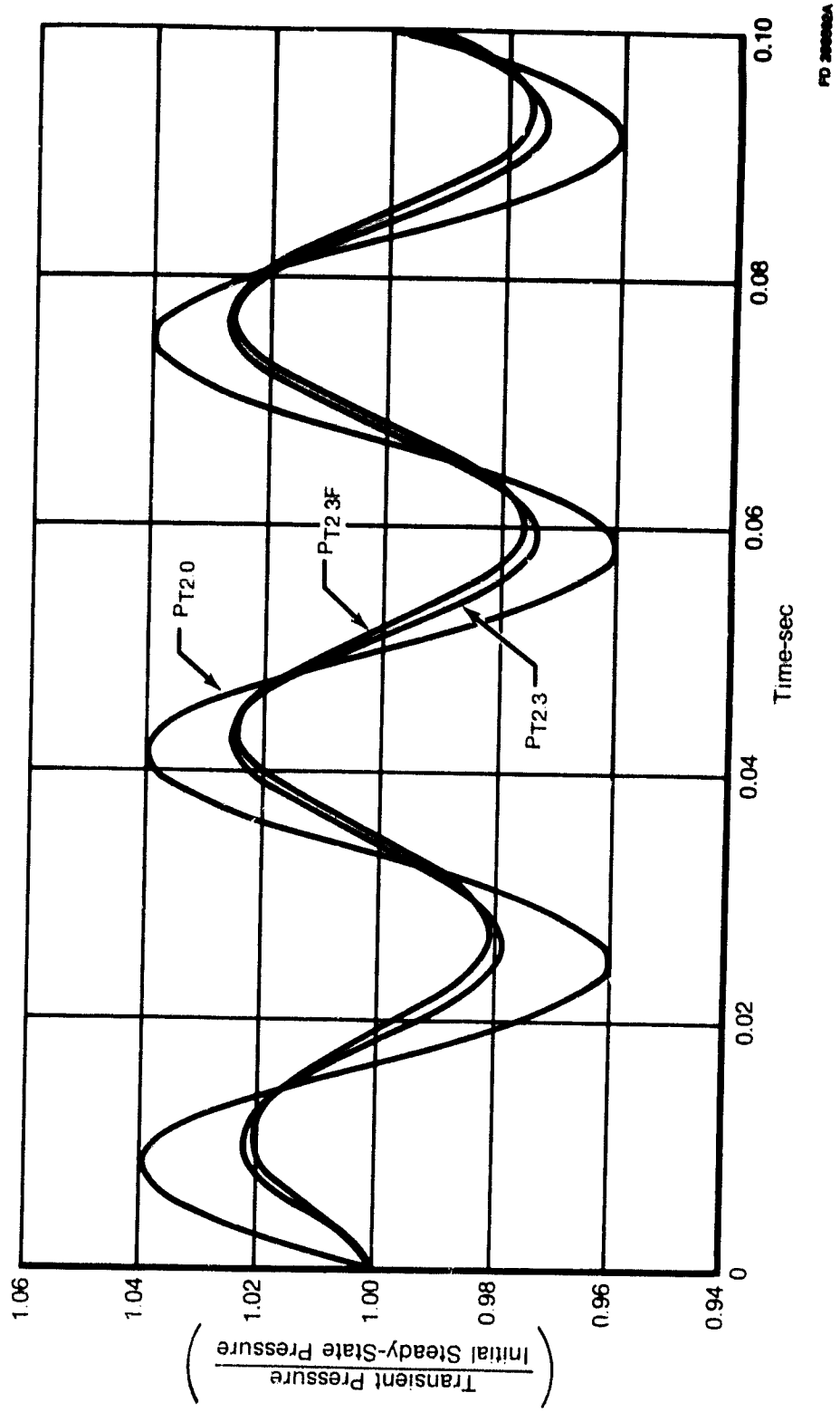

Figure 17. TF30 Simulation Fan Response to Inlet Pressure Cyclic Variation (30 Hz, 8% Amplitude)

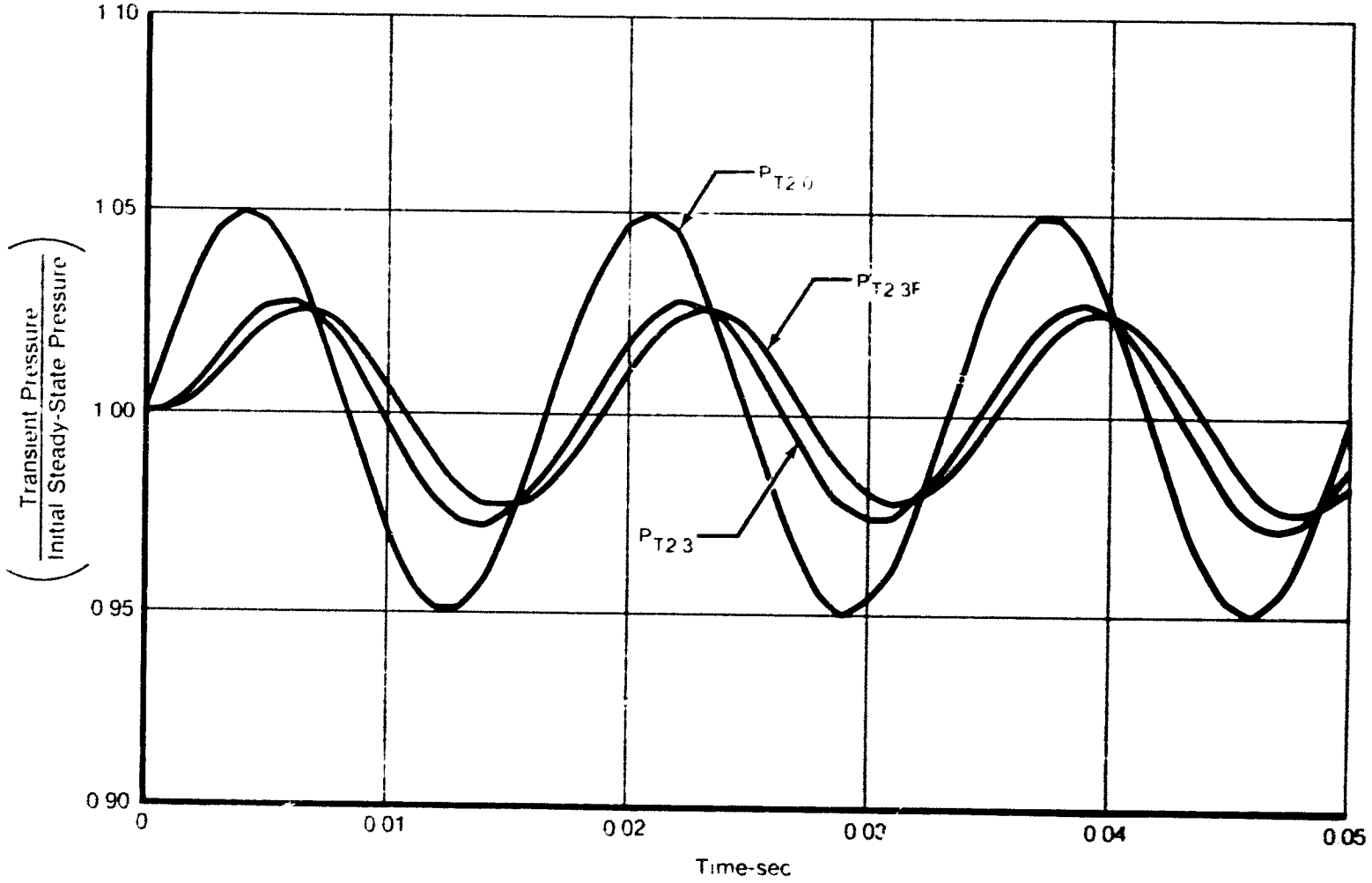

Figure 18. [illegible] Simulation Fan Response to Inlet Pressure Cyclic Variation (60 Hz, 10% Amplitude)

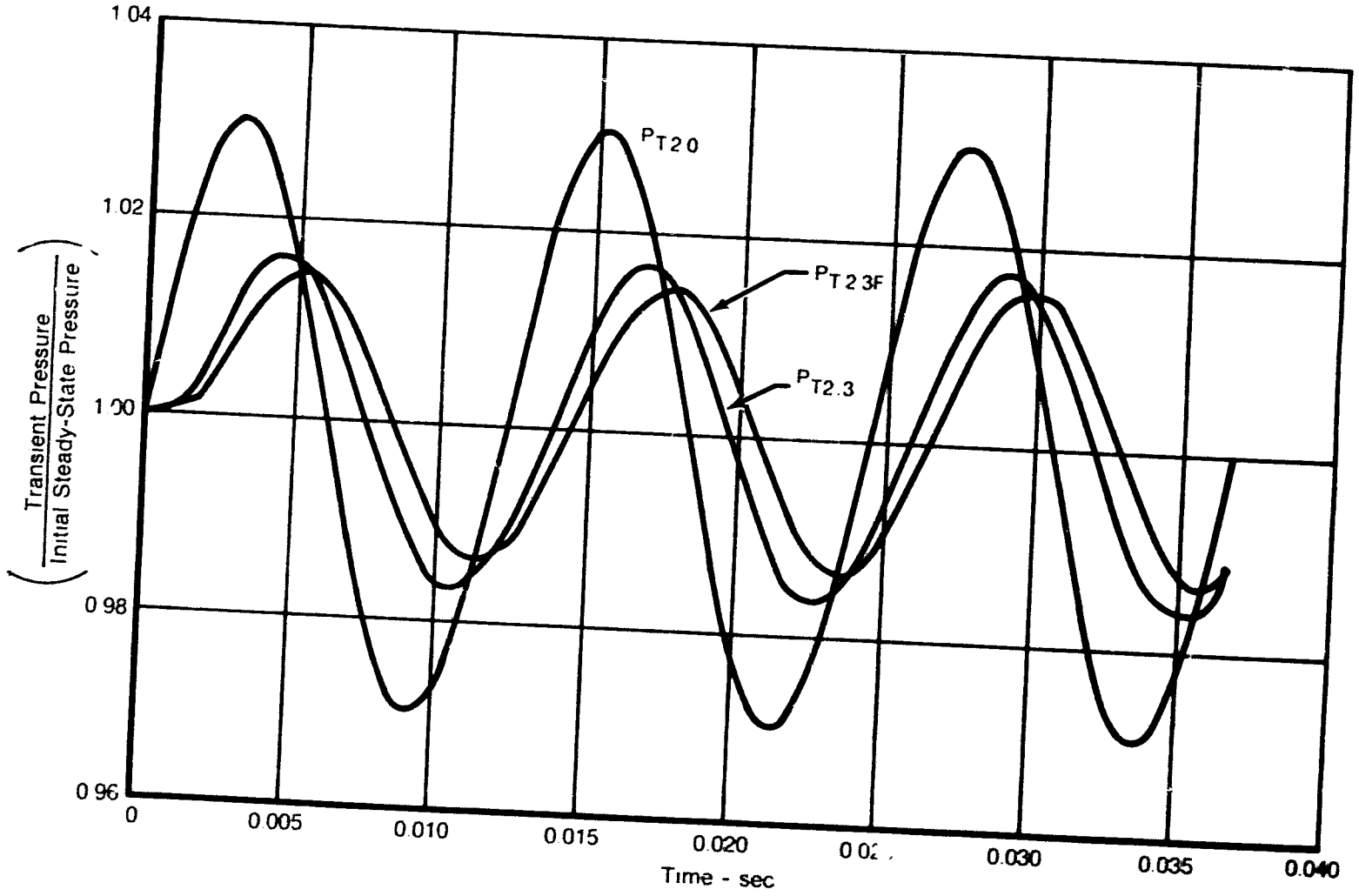

Figure 19. TF30 Simulation Fan Response to Inlet Pressure Cyclic Variation (82 Hz, 6% Amplitude)

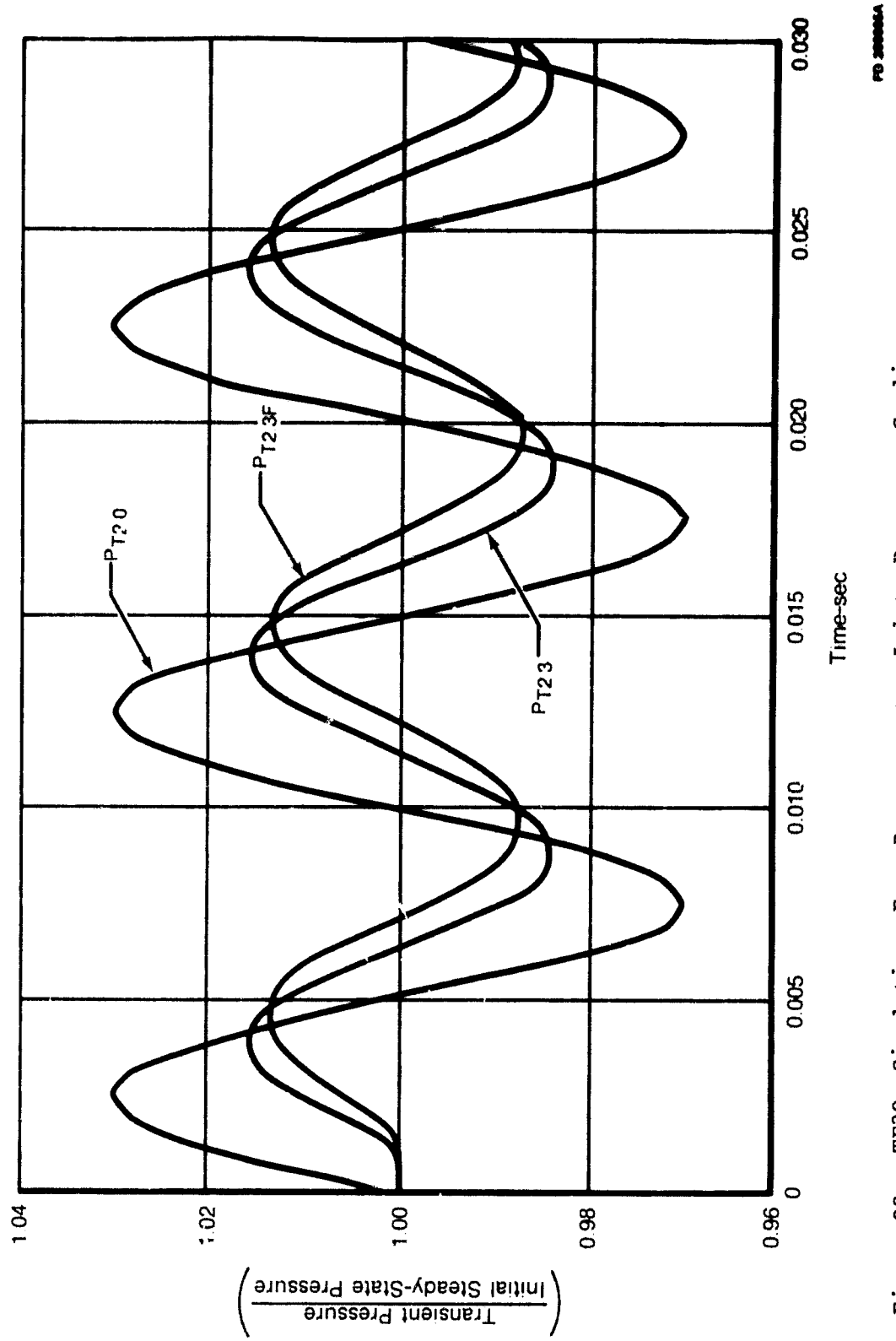

Figure 20. TF30 Simulation Fan Response to Inlet Pressure Cyclic Variation (100 Hz, 6% Amplitude)

Table 1. TF30 Response of Sta. 2.3 (Fan Core) to P_{t_2}

		Engine Data		Model Data	
Frequency	*Response*	*Frequency Sweep*	*Discrete Frequency*	*Transfer Function*	*Discrete Frequency*
15 Hz	Gain	-1.5 db	-3.5 db	5.8 db	-6.3 db
	Phase	2 deg	0 deg	19 deg	-15 deg
80 Hz	Gain	-3.6 db	4.2 db	2.5 db	3.4 db
	Phase	20 deg	7 deg	-8 deg	10 deg
60 Hz	Gain	2.7 db	4.4 db	5.0 db	5.0 db
	Phase	55 deg	52 deg	22 deg	23 deg
82 Hz	Gain	+1.5 db	0 db	4.2 db	5.2 db
	Phase	25 deg	67 deg	67 deg	41 deg
100 Hz	Gain	4.0 db	N/A	5.5 db	5.5 db
	Phase	25 deg	N/A	48 deg	54 deg

Table 2. TF30 Response of Sta. 2.3F (Fan Bypass) to P_{t_2}

		Engine Data		Model Data	
Frequency	*Response*	*Frequency Sweep*	*Discrete Frequency*	*Transfer Function*	*Discrete Frequency*
15 Hz	Gain	8.8 db	12.4 db	6.6 db	7.8 db
	Phase	4 deg	9 deg	29 deg	30 deg
80 Hz	Gain	3.4 db	5.7 db	2.7 db	3.9 db
	Phase	12 deg	28 deg	10 deg	30 deg
60 Hz	Gain	10.0 db	9.9 db	5.7 db	6.6 db
	Phase	85 deg	68 deg	25 deg	-46 deg
82 Hz	Gain	3.7 db	4.4 db	4.0 db	-6.6 db
	Phase	5 deg	70 deg	82 deg	-58 deg
100 Hz	Gain	10.0 db	N/A	6.5 db	8.0 db
	Phase	5 deg	N/A	58 deg	-92 deg

Stability Limits

The final evaluation of the improvement in dynamic response due to the radially coupled fan involved assessment of the stability limits of the fan. The evaluation was performed with a 15 Hz sinusoidal frequency on engine inlet pressure to determine the amplitude of pressure required to stall the engine. The results showed a dramatic improvement over the one-dimensional model, as detailed in figure 21. Core stream stall in the simulation occurred at an inlet pressure amplitude of 23% (peak to peak) compared to 28.5% for engine data, whereas the one-dimensional fan model required a 60% amplitude to stall the engine. Even then, the stall occurred in the bypass stream.

For this evaluation, pressure amplitude increased with transient simulated time, as shown in figure 22. This allowed phasing of the simulation to adjust before the large amplitudes were imposed to drive the turbomachinery pressure ratio over the stall limits. The gradual building of amplitude approximated engine testing. A slower rate might have produced an even closer correlation between model and engine data. The simulation produced a stall at the minimum inlet pressure, which duplicates the engine results reported in Reference 2.

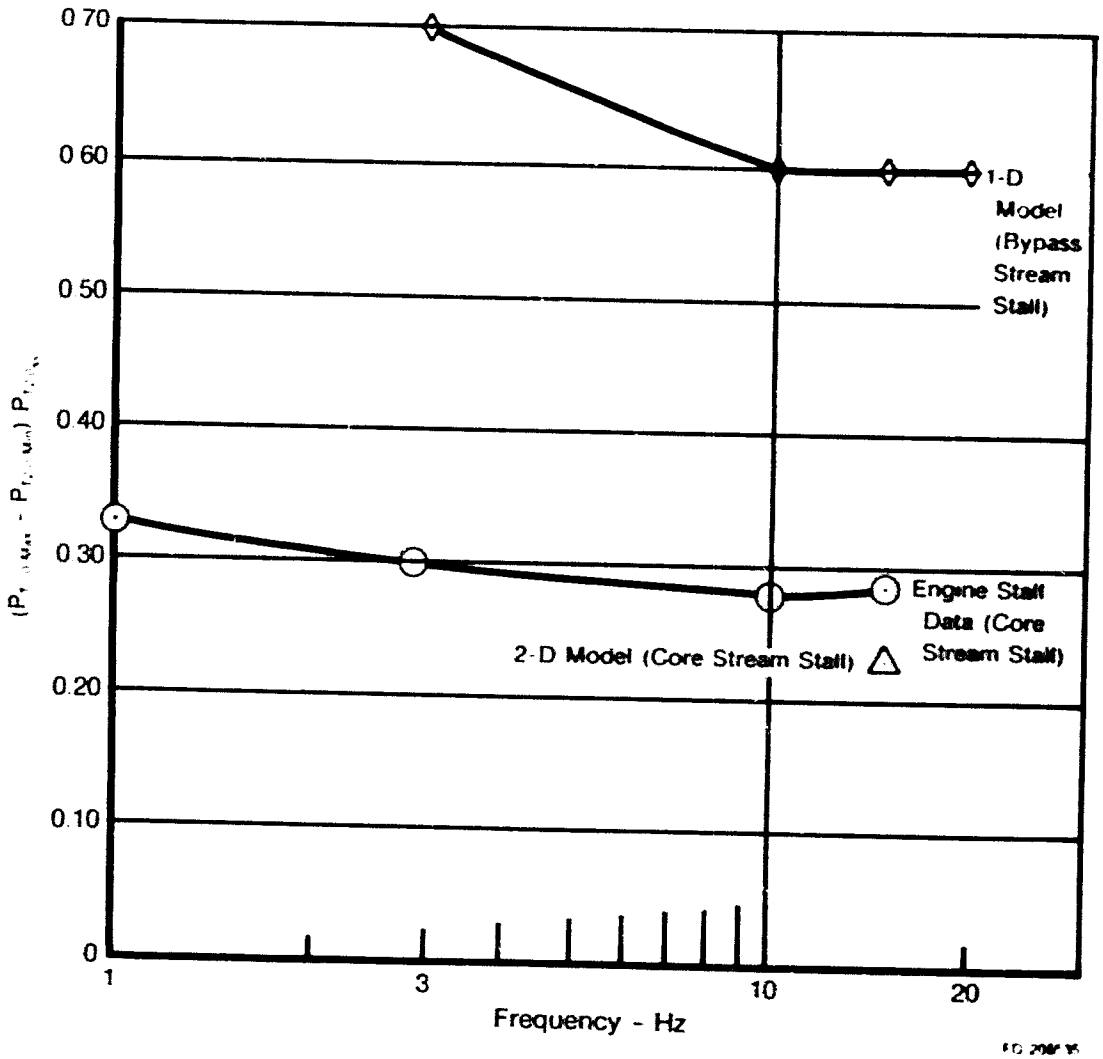

Figure 21. TF30 Two-Dimensional Simulation Stability Limit Agrees With Engine Data

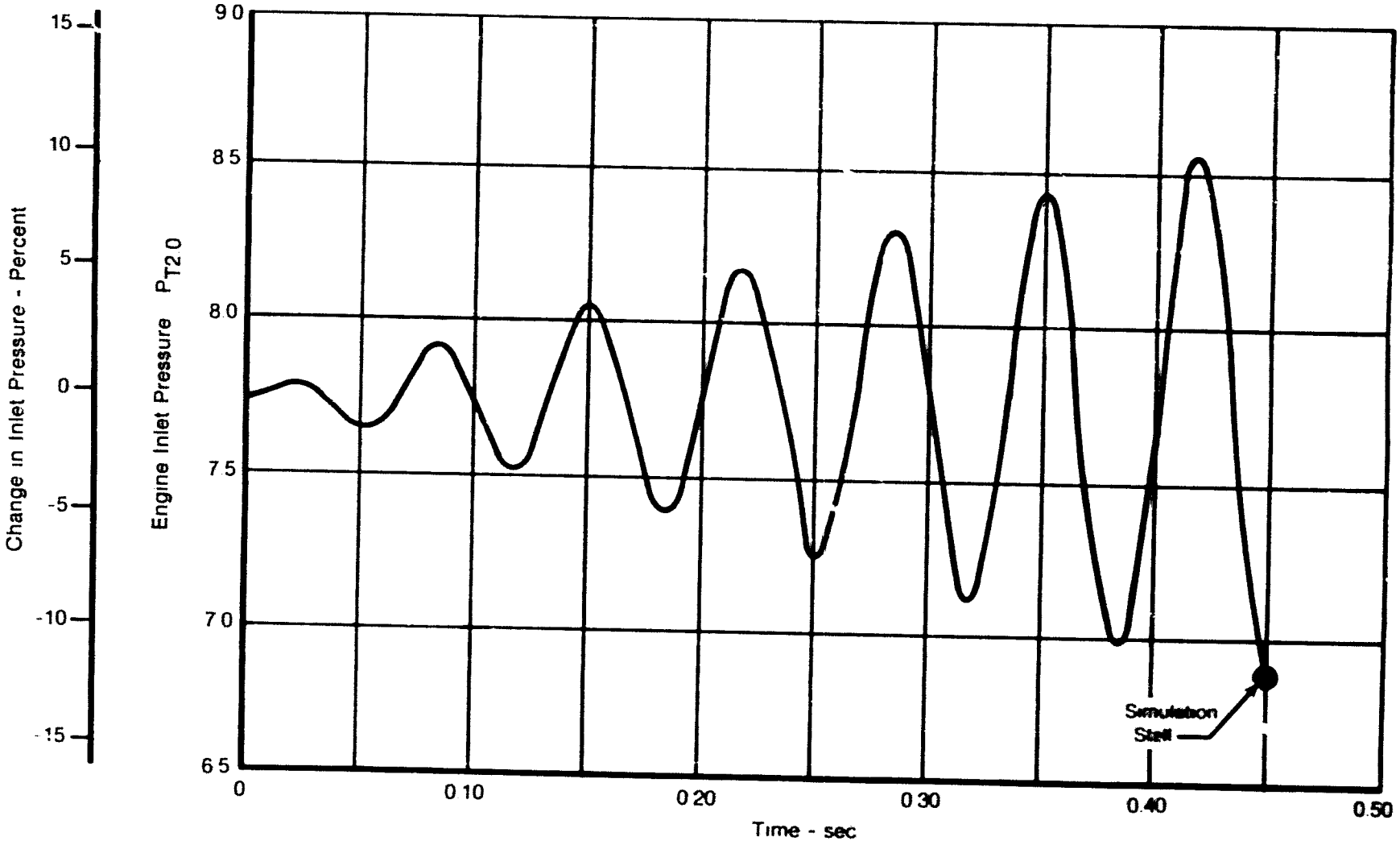

Figure 22. TF30 Simulation Driven to Stability Limit with a 15-Hz Cyclic Inlet Pressure Variation

Instability occurred in the fan core and low-pressure compressor when the combined pressure ratio and flow were driven beyond rig stall limits, as shown in figure 23. Figure 24 shows that the fan bypass stream is not near its rig stall line, although this was the stalling component in the one dimensional model evaluation (Reference 1).

Exceeding the stability limit of a component can be viewed as the transient pressure ratio exceeding some value for a finite amount of time. The transient pressure ratio during a sinusoidal disturbance can be analytically related to the discharge pressure response (gain and phase) to inlet pressure. Shown on figure 25-A are two examples of transient pressure ratio excursions as functions of exit pressure response. One example has 0 db gain, but 90° phase shift. Pressure ratio increase, which is proportional to percent exit pressure minus percent inlet pressure, reached a maximum value of 141%.

The second example has zero phase shift, but a -6.0 db gain and resulted in a 50% maximum increase in pressure ratio. Presented on figure 25-B is this pressure ratio relationship over a range of gain and phase where the increase in pressure ratio is normalized with inlet pressure ' amplitude. The frequency response values from the engine data, 2-D model, and 1-D model are also presented on figure 25-B for comparison.

The two-dimensional fan model very closely approximates engine data for both the fan bypass and fan core/low-pressure compressor streams. The lower attenuation encountered in the one dimensional model for the core stream, even though phase is close to engine data, results in lower pressure ratio increases, which prevents the core from reaching the stability limit.

Number of Fan Elements

Investigations included the dynamic configuration of the fan for further improvement in frequency response. The four-element baseline configuration consisted of two elements in the core stream and two elements in the bypass stream with the interface located between Stator 1 and Rotor 3. As shown in figure 26, two more configurations were evaluated consisting of six and eight elements, respectively. Both configurations were stage-by-stage representations with the eight element configuration possessing different pairings of rows and a separate element for the space between Rotor 3 and the splitter.

Figures 27 and 28 detail the frequency response results of the trades on element configuration. The fan discharge pressure response of the core stream (Sta. 2.3) and the bypass stream (Sta. 2.3F) appear on the same plot for each of the configurations with a reference plot of engine test data. The pressure gain as shown in figure 27, of the engine data shows much less attenuation in the core stream for the low frequency (less then 30 Hz) region than the bypass stream. The baseline four-element configuration produced about the same attenuation for both streams. The six-element configuration shows separation of the two streams with the bypass stream exactly matching engine data. The eight-element configuration shows further separation, but because the bypass stream indicated too much attenuation. The resonant frequencies of 30 and 82 Hz for the engine and 33 and 70 Hz for the model remain about the same for the different fan configurations, except that the eight-element fan configuration 70 Hz peak is very attenuated.

Similar trends existed for phase response between the different fan model configurations, as shown in figure 28. Again, the six element configuration more closely approximated engine data than the other configurations.

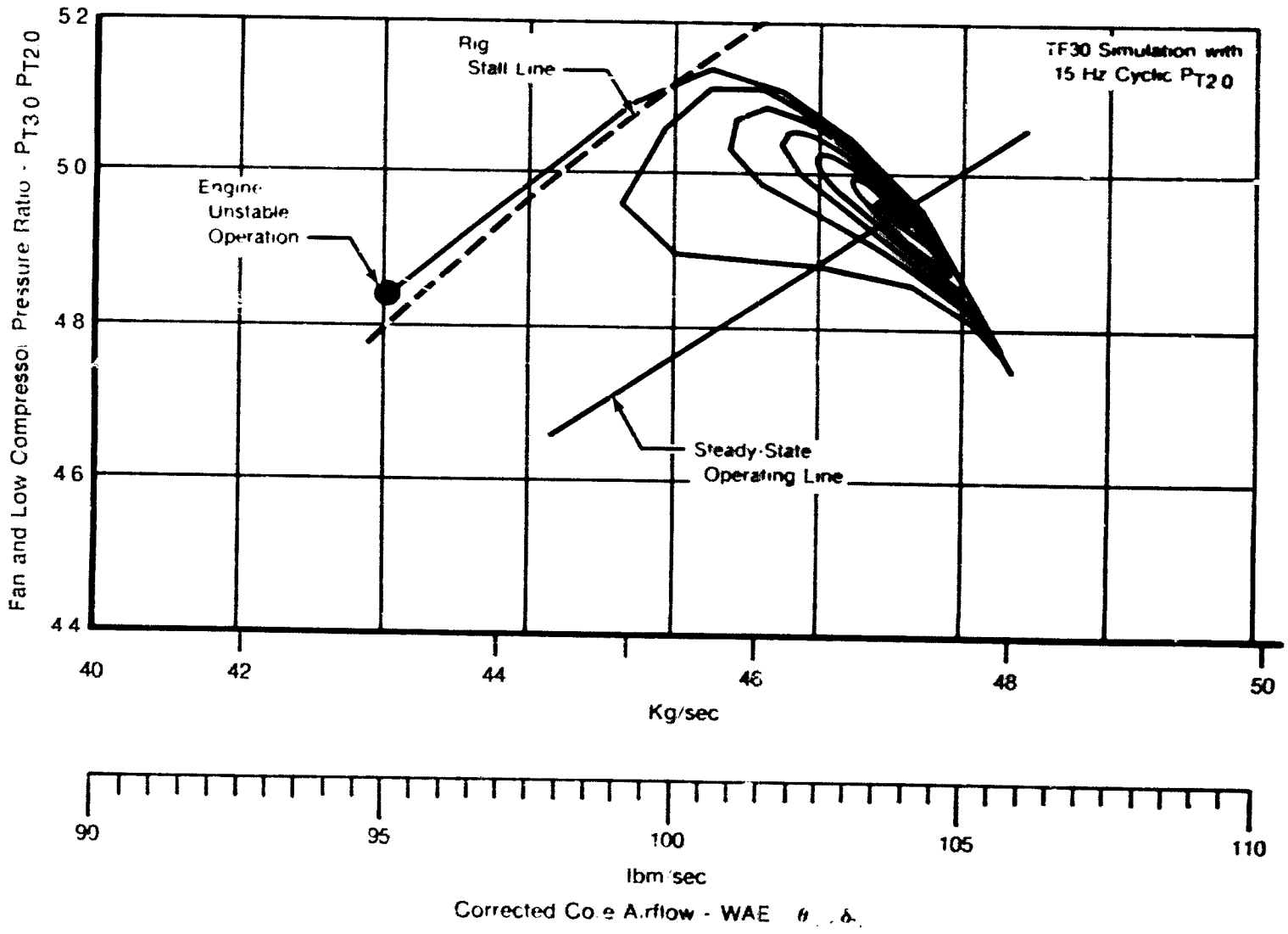

Figure 23. TF30 Simulation Stability Limit in Core Stream

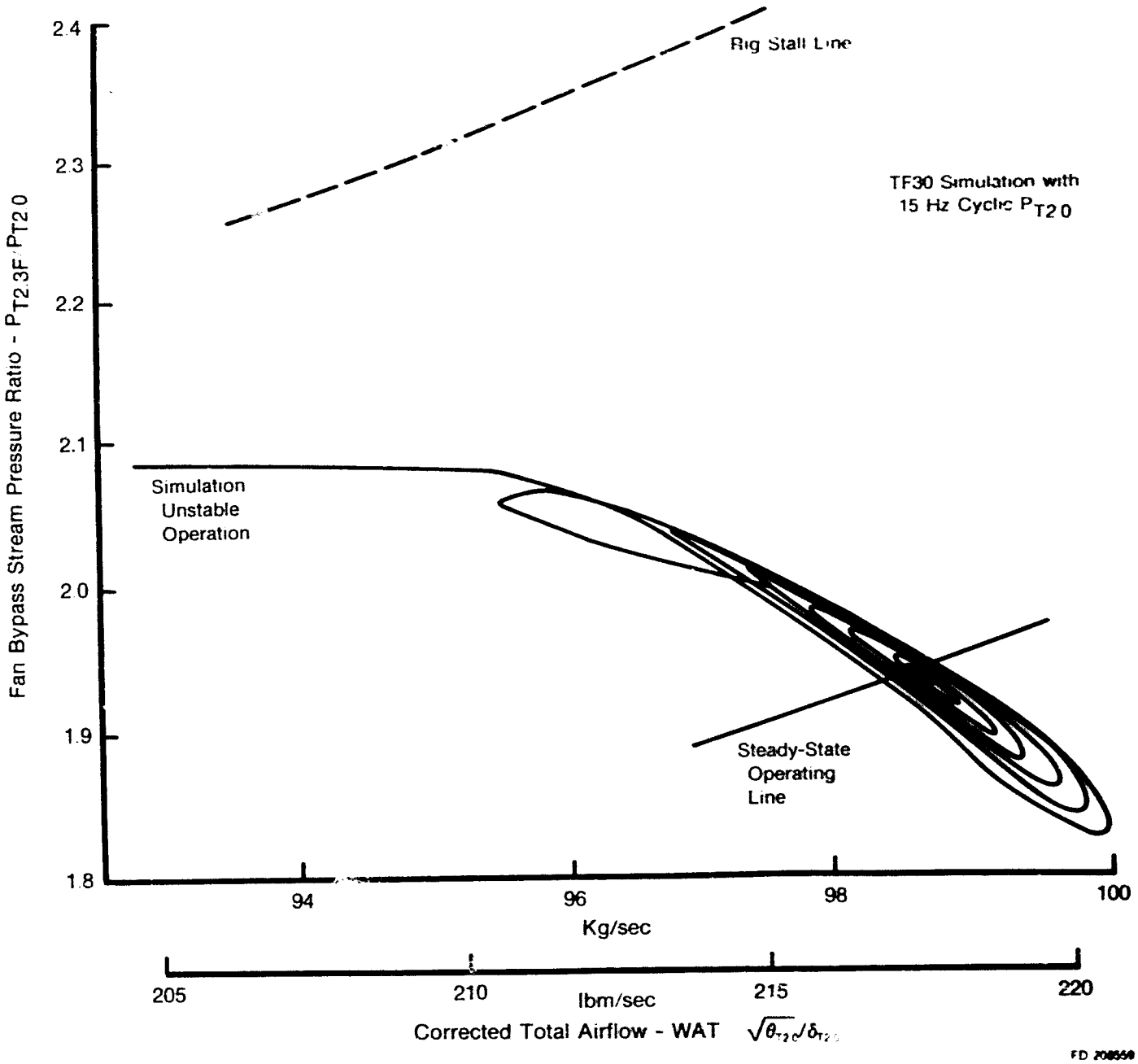

Figure 24. TF30 Simulation Stability Limit is Not in Bypass Stream

A. Two Theoretical Examples

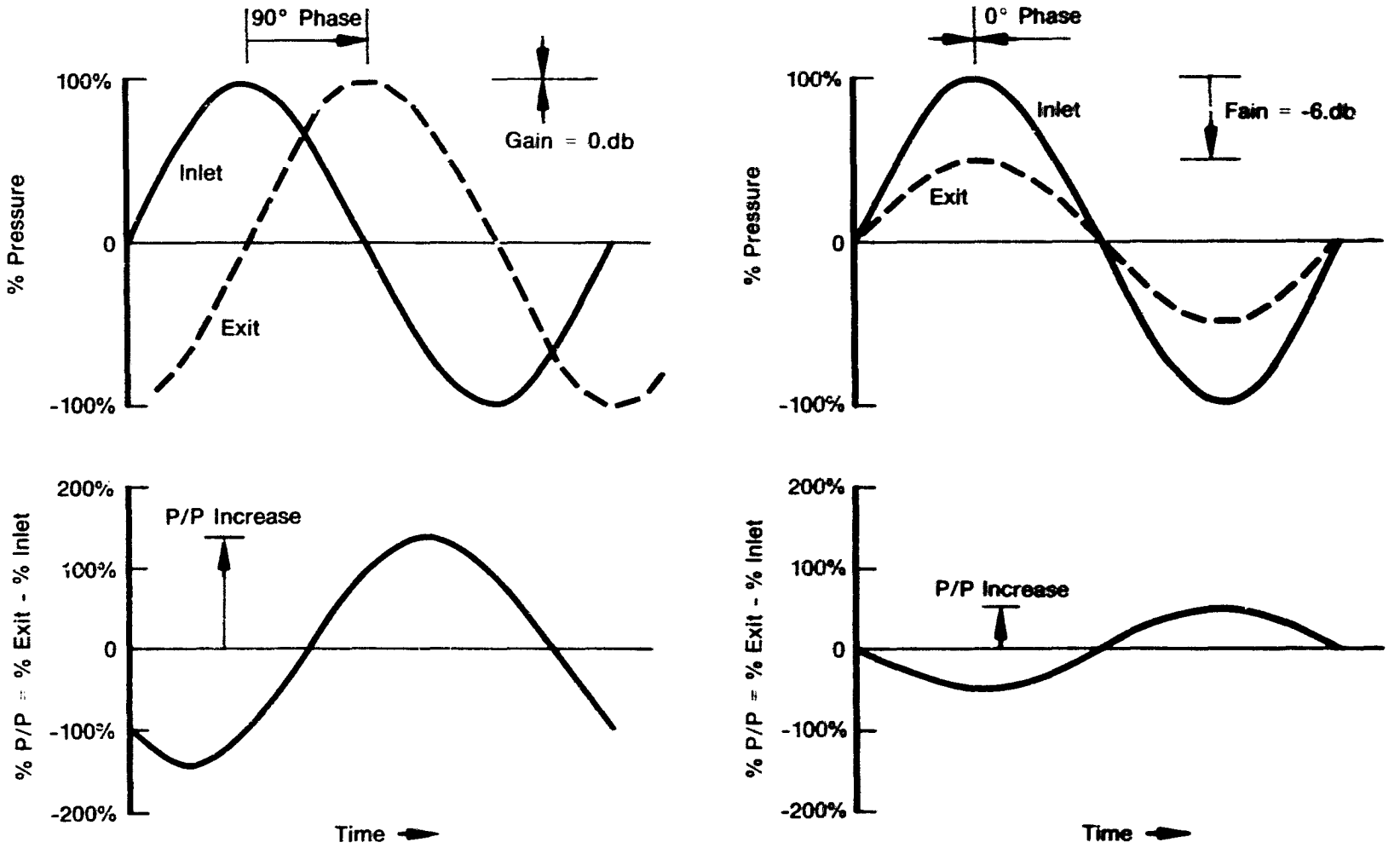

Figure 25. Transient P/P as a Function of Exit Pressure Response to Inlet Pressure (Page 1 of 2)

B. Comparison at 15 Hz Between Engine, One-Dimensional, and Two-Dimensional Models

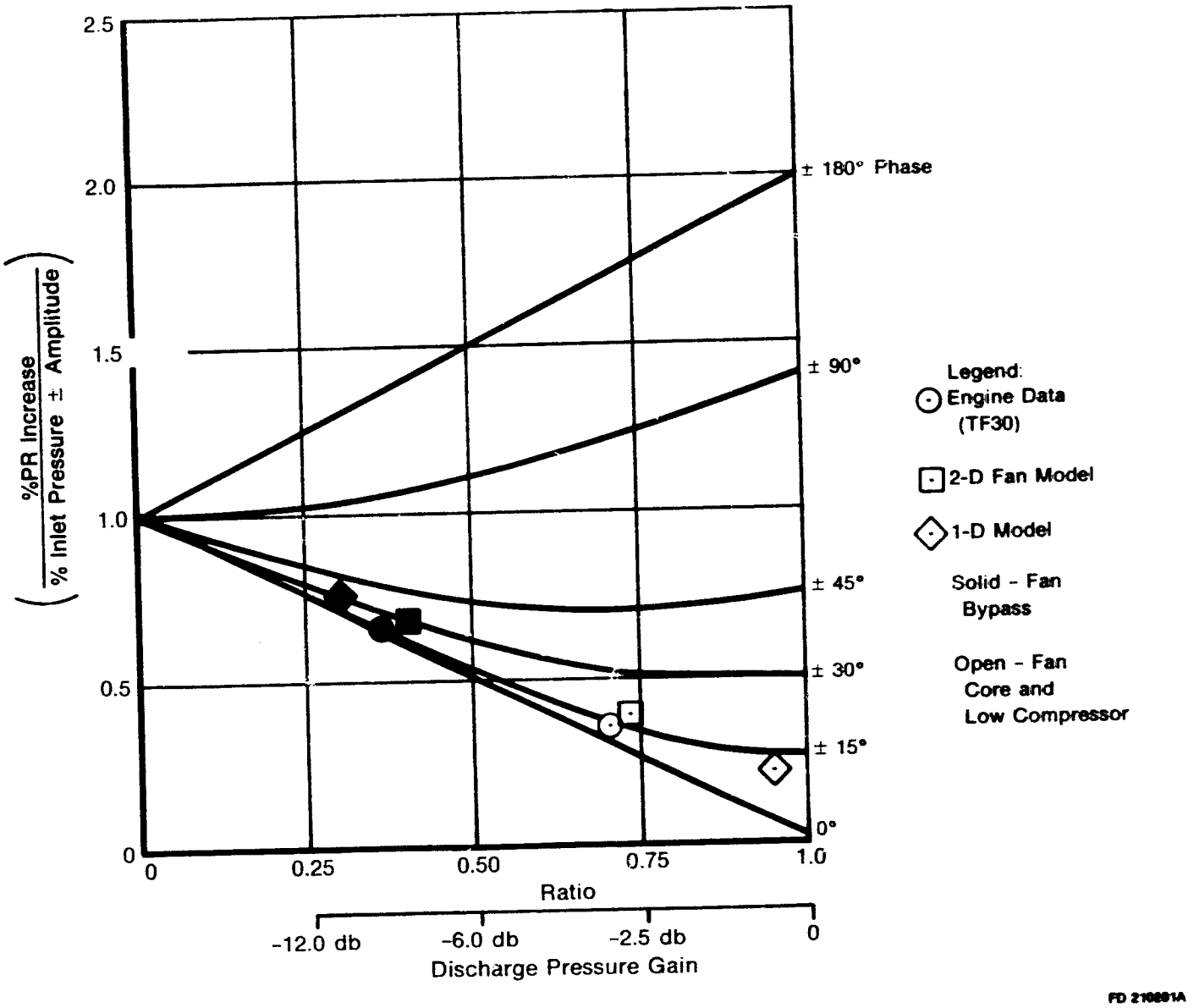

Figure 25. Transient P/P as a Function of Exit Pressure Response to Inlet Pressure (Page 2 of 2)

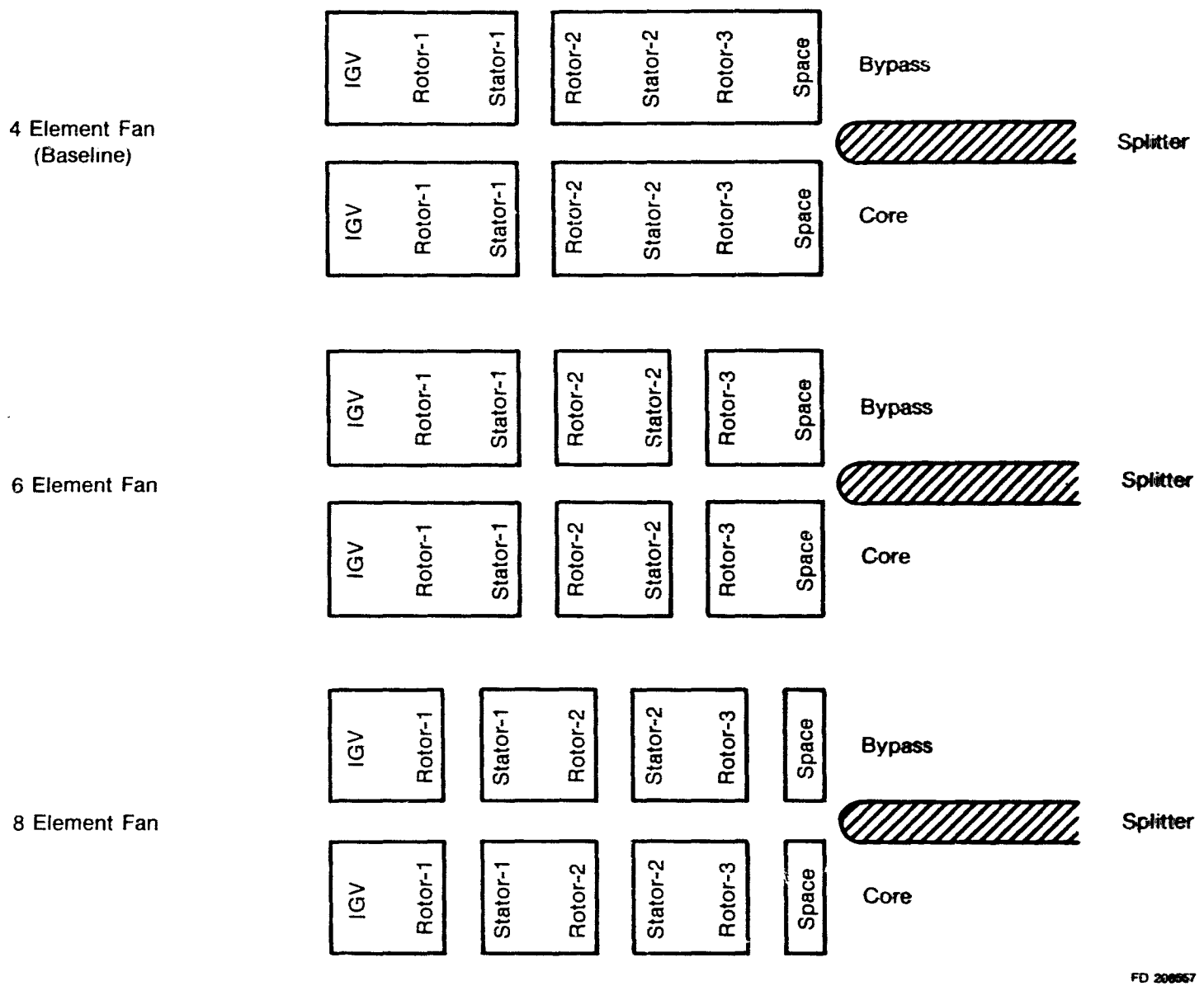

Figure 26. Fan Dynamic Element Breakup Configurations Investigated (TF30 Engine Simulation)

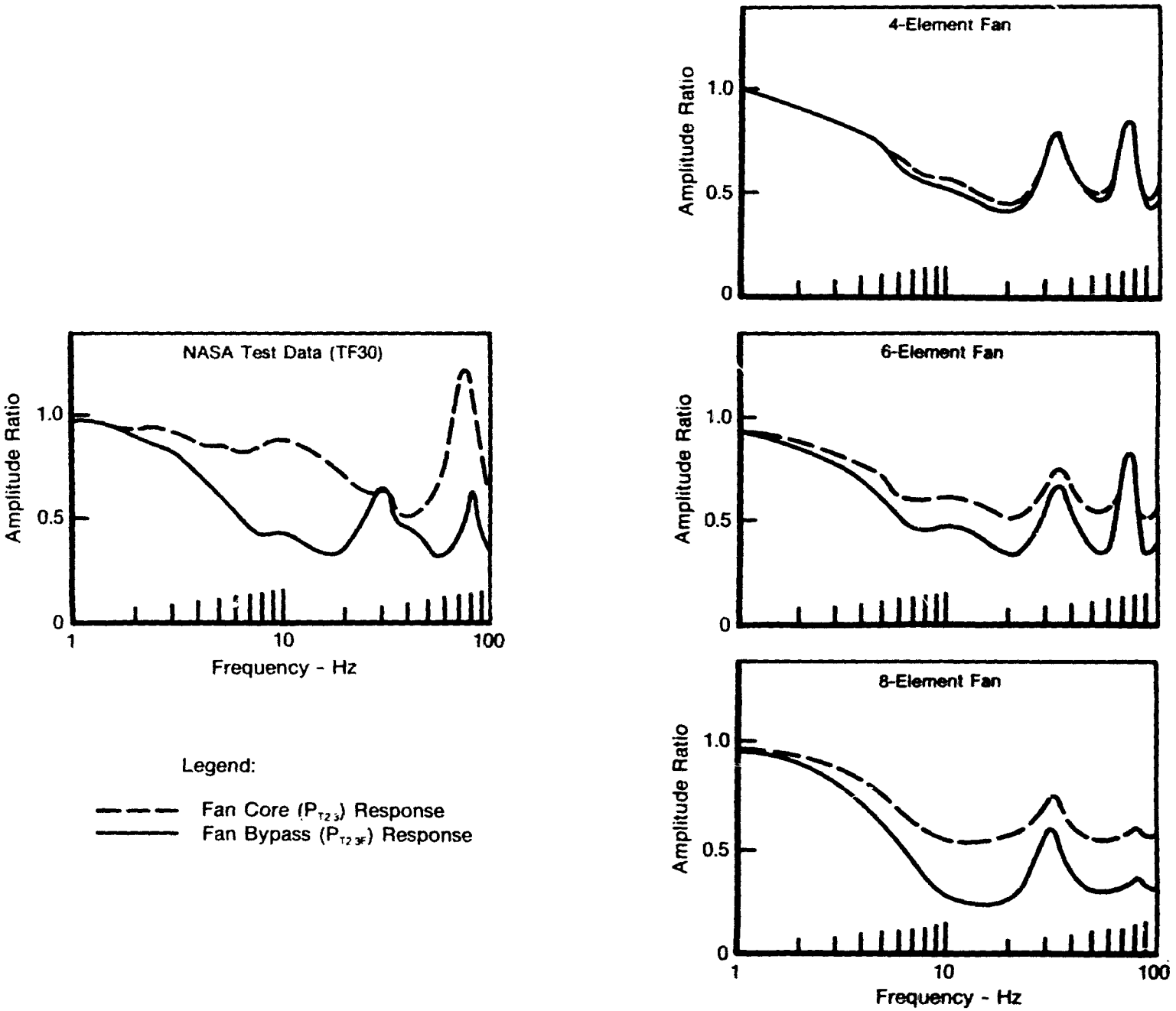

Figure 27. Fan Response (Gain) Changes with Dynamic Element Breakup (TF30 Engine Simulation)

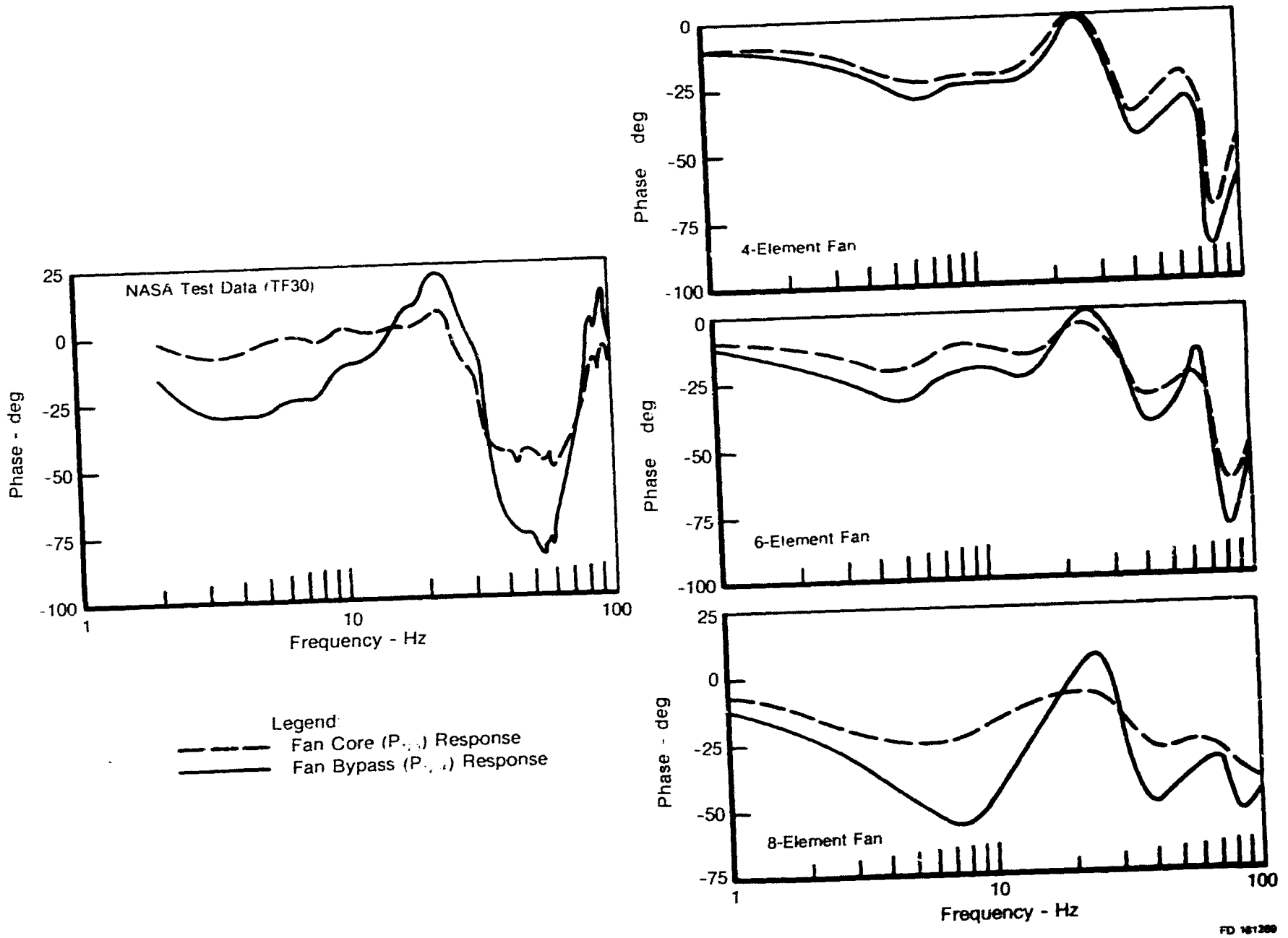

Figure 28. Fan Response (Phase) Changes with Dynamic Element Breakup (TF30 Engine Simulation)

The dynamic element configuration trade study reached the conclusion that the six-element stage-by-stage fan configuration is best suited for this application. It matched engine data except for the fan core stream in the low-frequency region, and in the magnitude of the high-frequency response amplitude peak. The low-frequency differences could be explained by the low pressure and/or high pressure compressor representations.

F100 ENGINE (REMOTE SPLITTER FAN) MODEL

The F100(3) is an augmented, mixed-flow twin-spool turbofan similar in the arrangement of components to the TF30 engine, as shown in figure 29, Compression system differences from the TF30 engine include a three-stage fan without a low-pressure compressor, and a ten-stage high-pressure compressor. Variable inlet guide vanes are on the fan and the first three stages of the high-pressure compressor. The physical splitter between the core and the duct bypass streams is located 14 cm (5.5 in.) aft of the last fan rotor (remote splitter configuration). Another version of the F100(3) engine locates the physical splitter 1.3 cm (0.5 in.) aft of Rotor 3 (proximate splitter configuration).

Element Configuration

The dynamic element configuration of the F100 engine model duplicates the TF30 engine model, except for the compression system. The high-pressure compressor was divided into five elements, which represents the same number utilized for the combined low- and high-pressure compressors in the TF30 model. The fan was configured with eight elements, four in each stream as shown in figure 30. This fan configuration duplicated the best staged configuration of the TF30 model (six elements) with an additional element in each stream forward of the splitter to account for the increased axial length of 14 cm (5.5 in.).

Fan Characteristics

The F100 remote splitter fan model was matched at the fan steady-state operating condition for a 0.9 Mach number and 50,000 ft altitude (0.9/50k) flight condition. The dividing streamline parameters (AREA and r, as described in Appendix B) were fixed at a bypass ratio condition equal to 0.67. This configuration was operated transiently by slowly increasing and decreasing bypass exhaust pressure in order to verify fan steady-state performance characteristics during the dynamic mode. These very slow transients resulted in essentially steady-state performance. As noted in figure 31, the fan warpage characteristic matched exactly with rig and engine data.

The resulting model radial and axial physical flows after these slow transients to higher and lower bypass ratios appear in figure 32. The trend of radial flow in the fan rows indicates rapidly increasing physical flows progressing through the fan, but the corrected flow variation is much less. At first observation, the direction of radial flows in the turbomachinery rows appears to be in the wrong direction. The radial flows for the higher bypass case progress toward the ID. However, this direction is correct in order to represent the movement of the dividing streamlines, as shown schematically in figure 33. The OD row performance characteristics represent a function of corrected flow per unit area (ϕ/A). With the area fixed from the initial steady-state splitting streamline location, the OD stream diverts flow in the radial direction to obtain the (ϕ/A) required to produce the correct pressure rise for this increased bypass ratio condition of figure 33. This diverted radial flow represents the movement of the dividing streamline toward the ID. Downstream of Rotor 3, the radial pressure warpage generated by the row characteristics produces a radial flow toward the OD, which represents the direction of the bending of the splitting streamline in relation to the initial steady-state splitting streamline location.

Therefore, the following observations were made concerning this radial flow model:

- The direction of the radial flows in the turbomachinery rows is the direction that the splitting streamline moves.
- The direction of the radial flows in front of the splitter is the direction of streamline bending relative to the steady-state location.

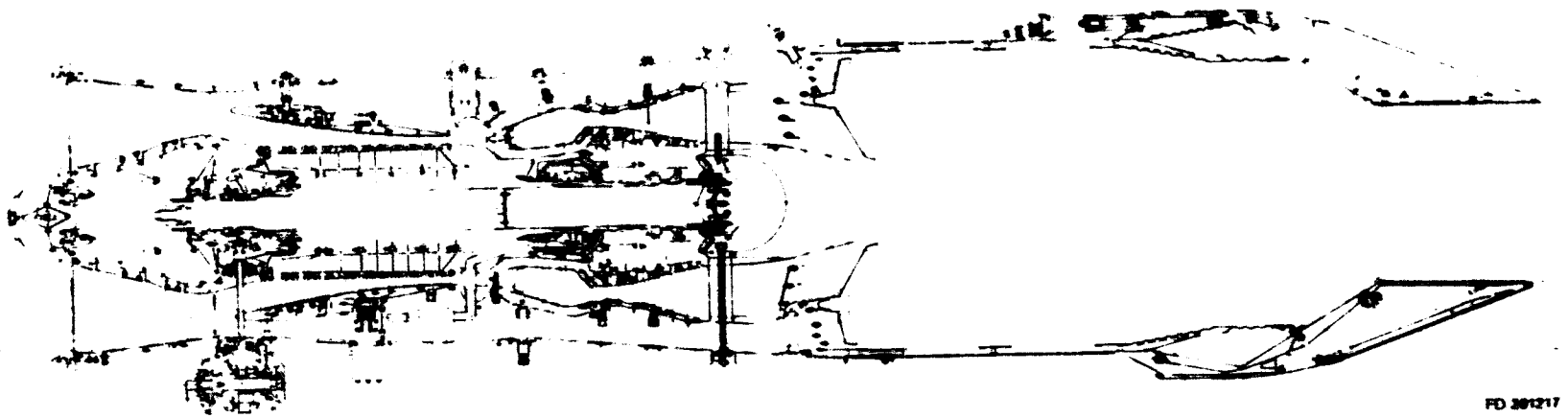

Figure 29. F100(3) Engine with Remote Splitter Fan

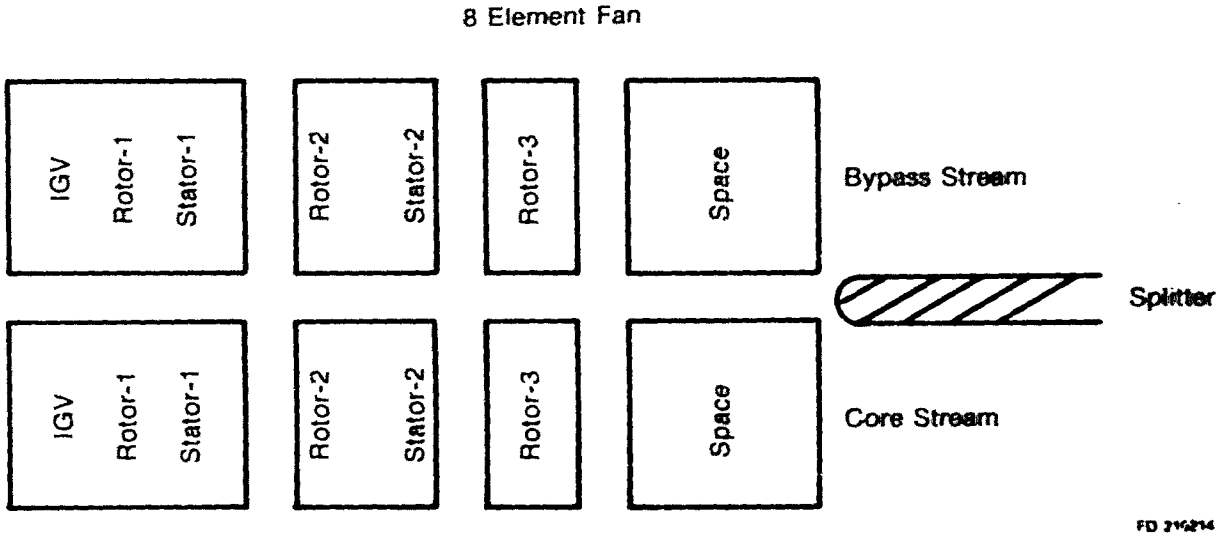

Figure 30. Fan Dynamic Element Configuration for F100 Fan

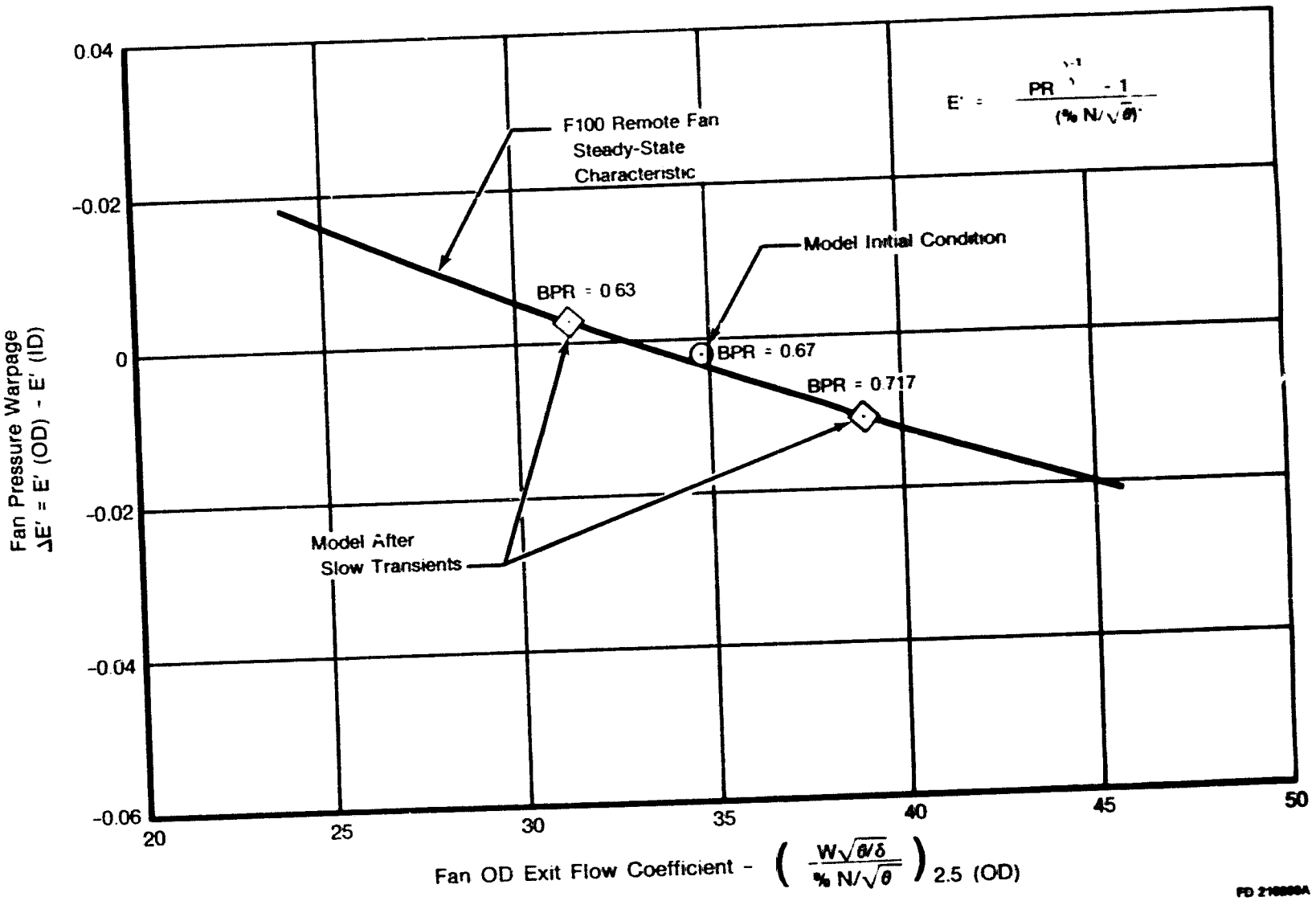

Figure 31. Dynamic F100 Remote Fan Model Matches Steady-State Data After Slow Transient

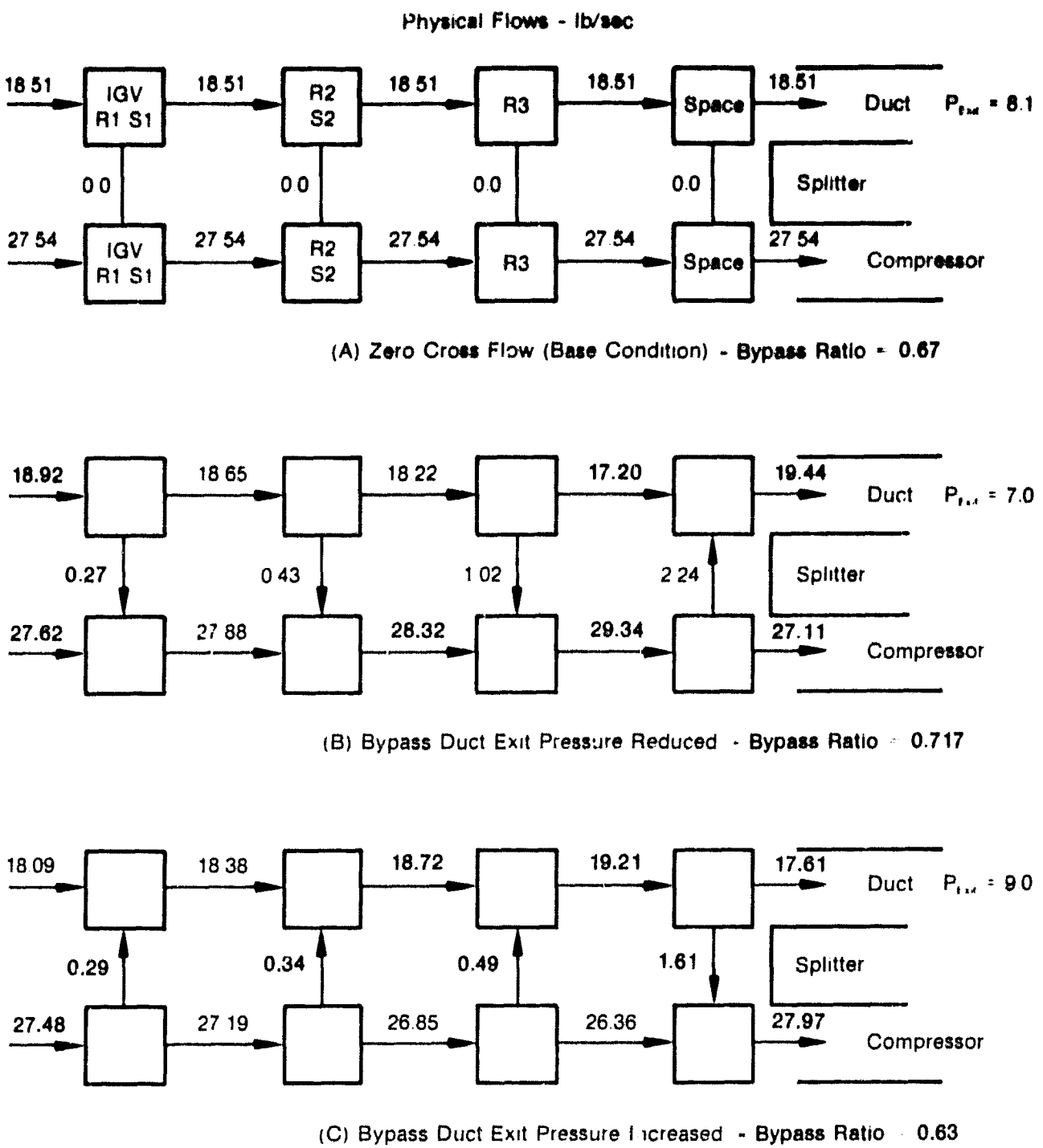

Figure 32. Physical Flows through Fan as Bypass Duct Exit Pressure is Changed (F100 Remote Splitter)

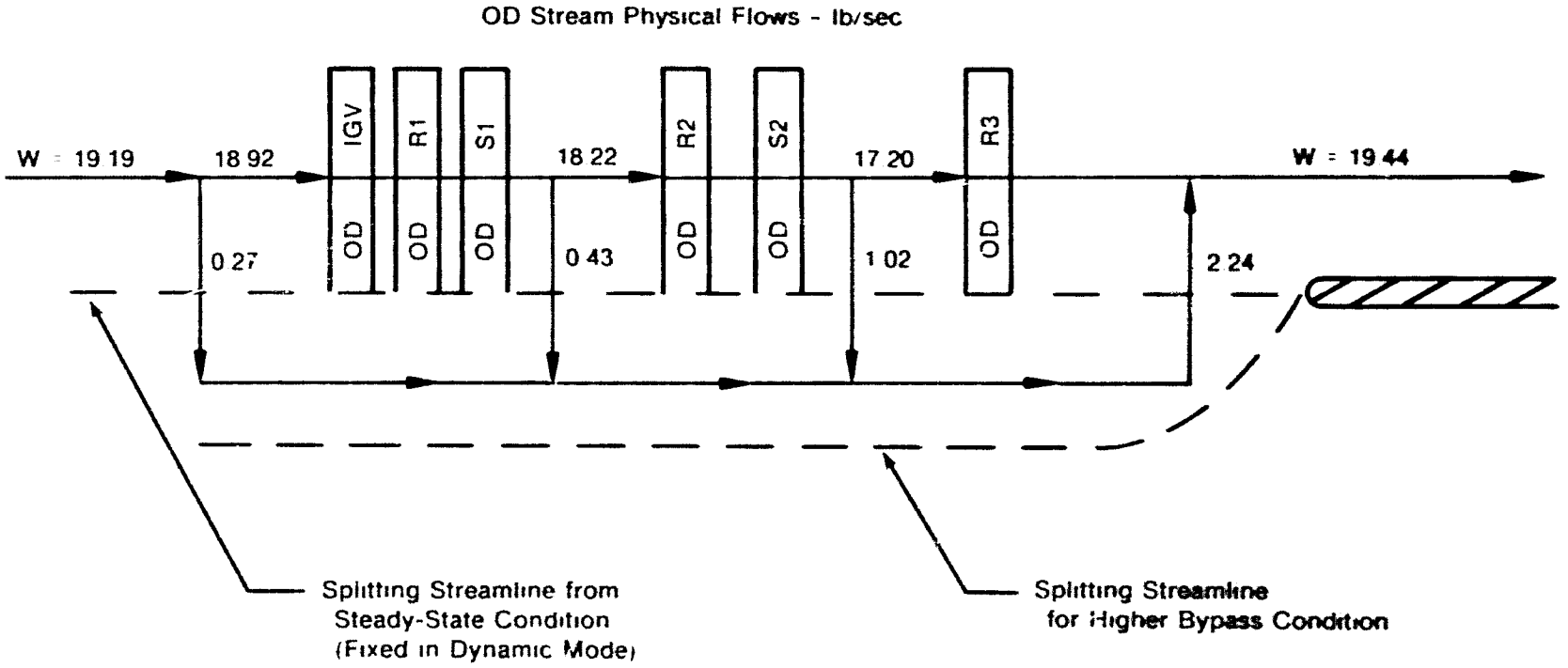

Figure 33. Dynamic Radial Flows Represent Movement of Dividing Streamline Between Fan OD and ID Streams - Bypass Ratio = 0.717

The fan representation with radial flows matched steady-state characteristics (figure 31) when the derivatives of the dynamics were very small (slow transient) This points out the potential of using radial flow representations in steady-state modeling to obtain accurate bypass ratio effects.

High Frequency Comparison

This portion of the investigation compared the F100 engine model to high frequency rumble (50 Hz) transient data generated on engine FX219-13 at the Arnold Engineering Development Center (AEDC) in 1974. Available high-response instrumentation data traces included augmentor pressure, fan exit OD and ID pressures, and main-burner pressures. Engine model evaluation proceeded by creating a model interface at the augmentor location to accept the rumble pressure oscillations of engine data as model input.

The resulting model response in terms of fan discharge pressures and mainburner pressure to the input augmentor pressure rumble of 52 Hz at a flight condition of 0.9/50k appears in figure 34. The fan discharge pressures of the model, particularly the OD stream, show good correlation in phase, but amplitudes are too large indicating less attenuation of the input augmentor pressure.

This study reached the conclusion that the lower attenuation of the fan discharge pressures resulted from an inadequate bypass duct model between the fan and augmentor. The engine model duct representation consisted of four axial elements with a constant area, whereas a large cross sectional area variation exists in the real engine down the length of the ducts.

When the F100 fan model was first assembled, it operated in a compression system "rig" mode consisting of F100 fan and compressor row characteristics and a duct module identical to the TF30 engine duct to verify model operation with augmentor pressure inputs. Operation of this rig model with identical augmentor rumble oscillations resulted in fan discharge pressures shown in figure 35. As can be observed, the amplitude of model fan discharge pressures closely approximated engine data, although slightly more attenuated, while an approximately 55° additional phase angle existed. It was anticipated that a complete F100 engine model with a more representative F100 duct (length, pressure losses, and average area) would correct this phase angle error. As noted in the engine model version depicted in figure 34, the phase improved, but at the expense of a large change in gain. Other differences between the rig and engine models included fan exit guide vanes and an increased number of fan dynamic elements from four in the rig to eight in the engine model. However, the duct representation change produced the largest influence. An adequate duct model for this frequency band width should include a variable area with more than four dynamic elements.

Model compression system parameters appear in figures 36 through 41 during the engine simulated 52 Hz rumble transient. The large (26%) variation in fan bypass ratio at the splitter reflects the excursions of the fan OD flow stream relative to the ID flow stream, as shown in figure 36. Excursions of this magnitude at this high frequency point out the need for aerodynamic coupling of the two streams.

Figures 37, 38, and 39 show the transient on fan maps for mass averaged, OD, and ID pressure ratios, respectively. The average pressure ratio moved toward the stall line with a maximum pressure ratio increase of 9.2% and a 2% reduction in flow. OD pressure ratio increased by a maximum of 9.9%, while the ID pressure ratio increased by 8.9%. The transient of the high-pressure compressor basically paralleled the stall line with an approximate ±1.25% flow excursion, as shown in figure 40.

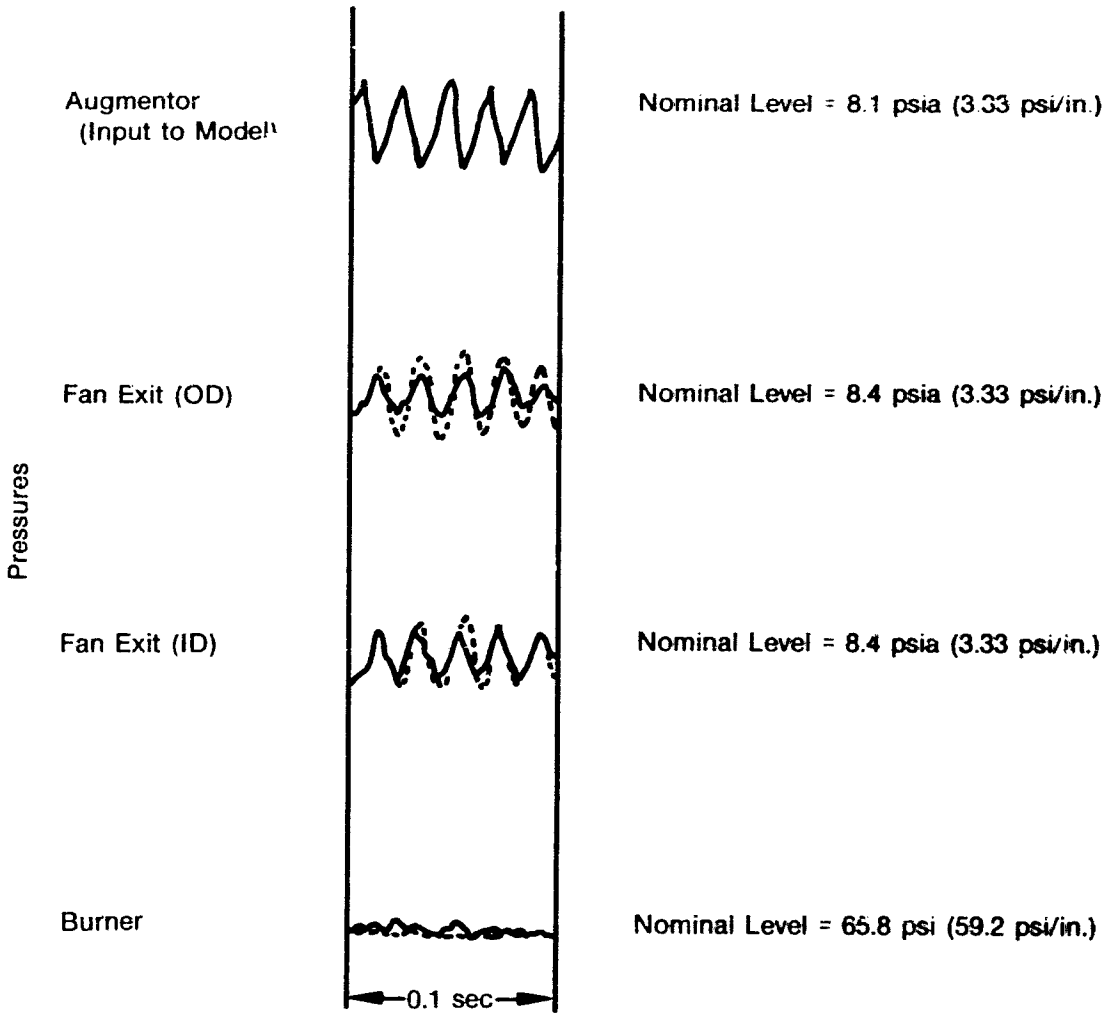

Solid Line - Engine FX219-13 52 Hz Rumble Data
Dashed Line - Model Response

FD 216 97

Figure 34. F100 with Remote Splitter Fan Model Response to 52-Hz Rumble at 0.9/50k Flight Condition

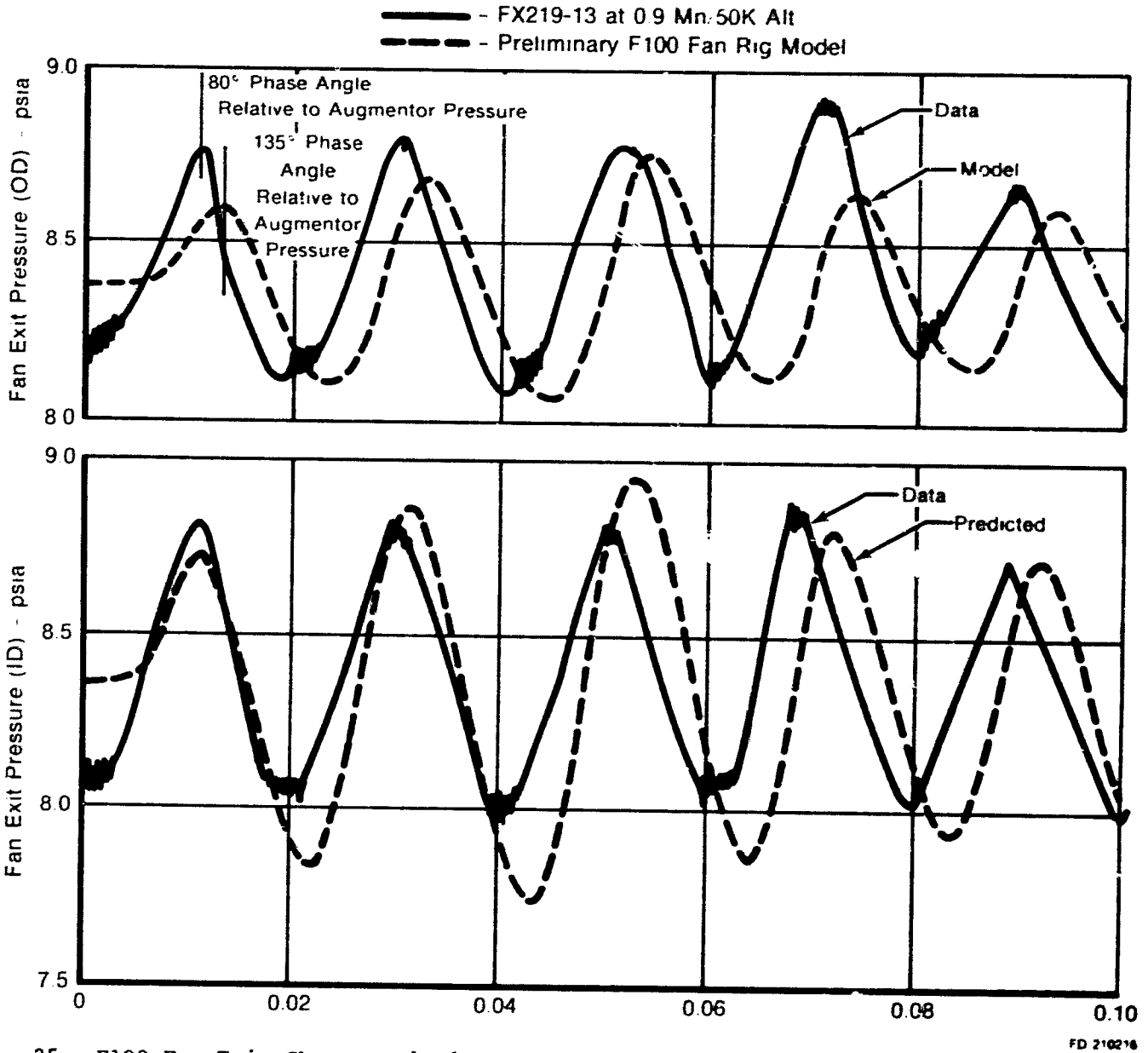

Figure 35. F100 Fan Exit Characteristics During 52-Hz Rumble

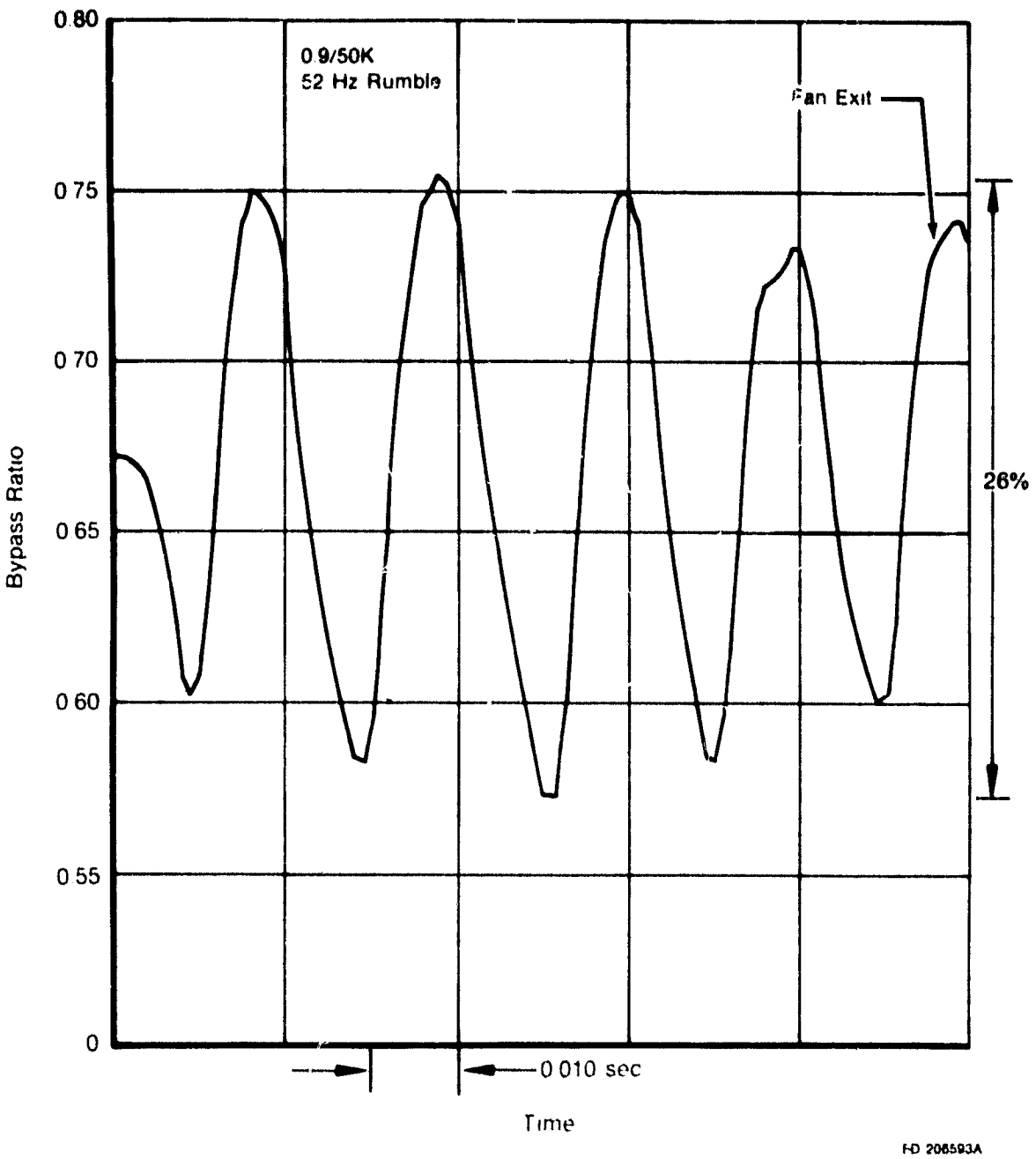

Figure 36. F100 Remote Splitter Fan Bypass Ratio Transient During A/B Rumble

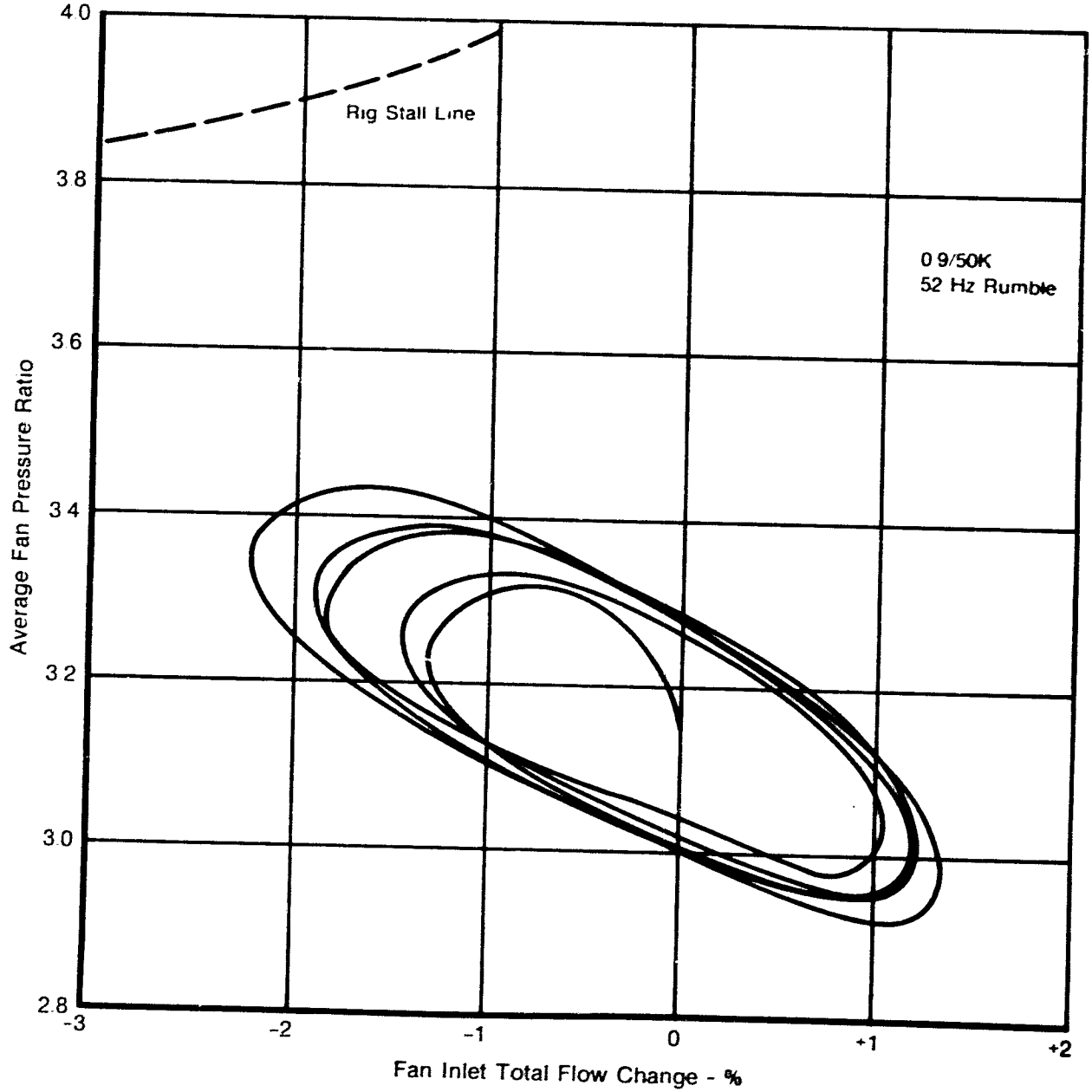

Figure 37. F100 Remote Splitter Fan Average Pressure Ratio Transient During A/B Rumble

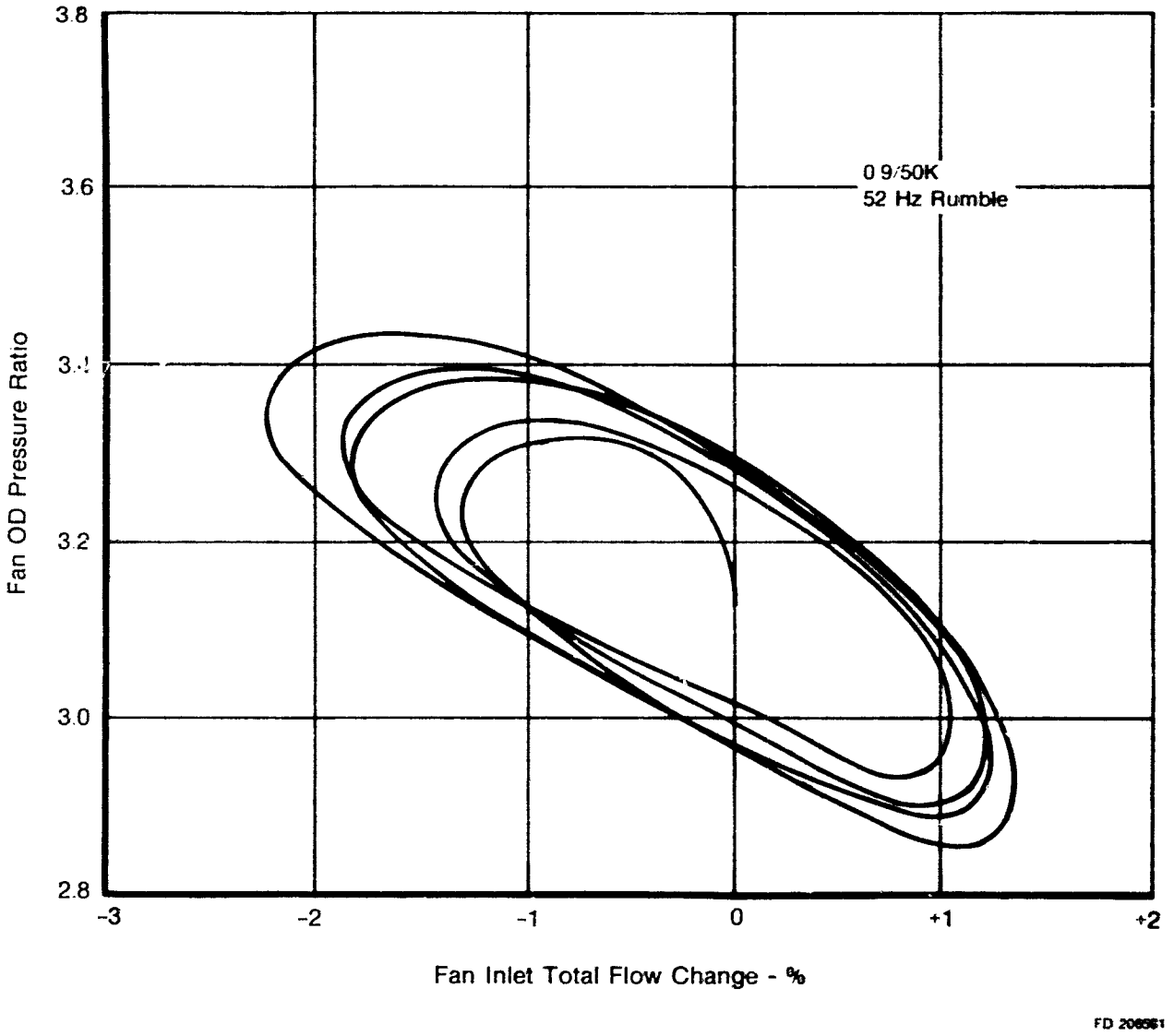

Figure 38. F100 Remote Splitter Fan OD Pressure Ratio Transient During A/B Rumble

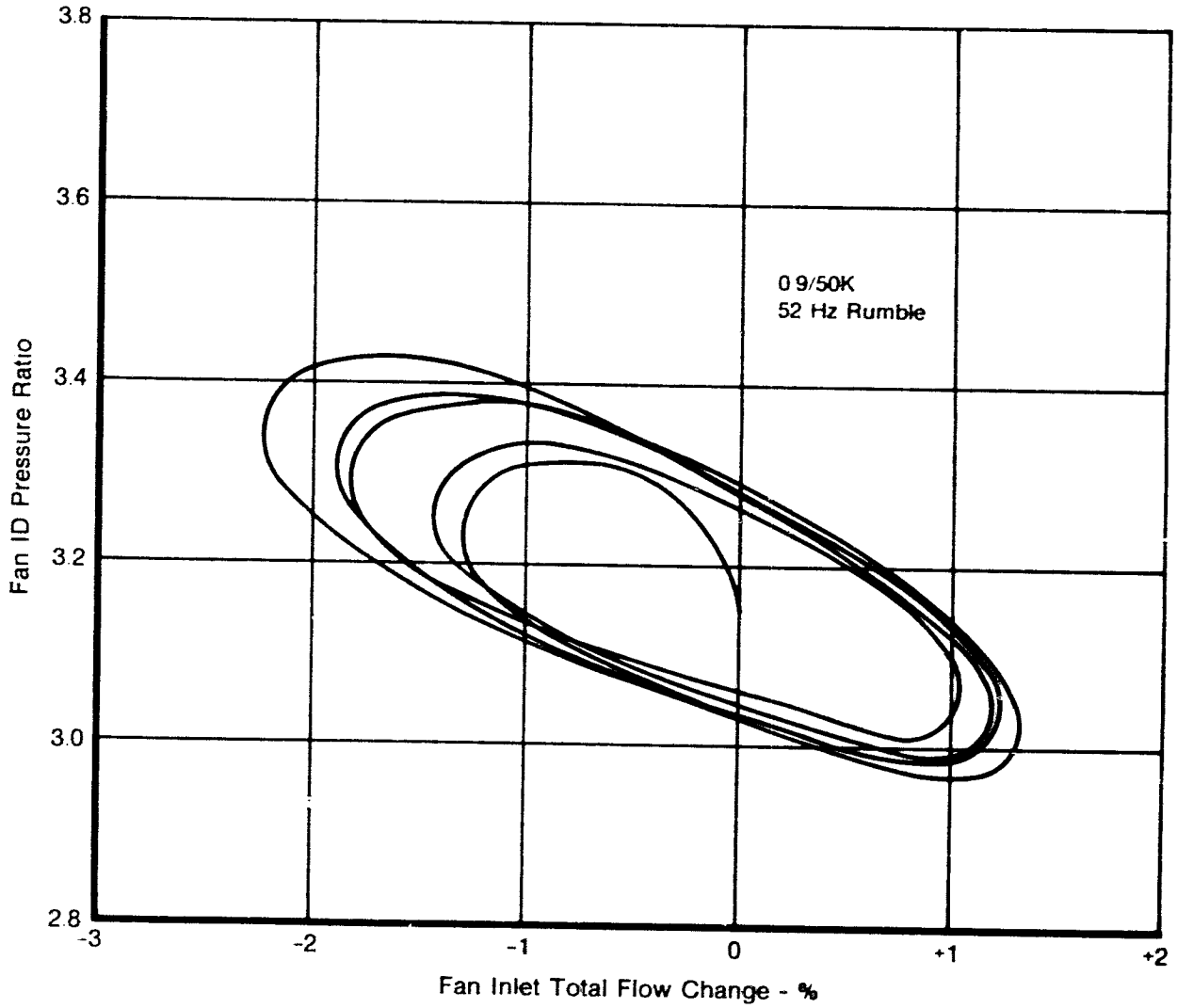

Figure 39. F100 Remote Splitter Fan ID Pressure Ratio Transient During A/B Rumble

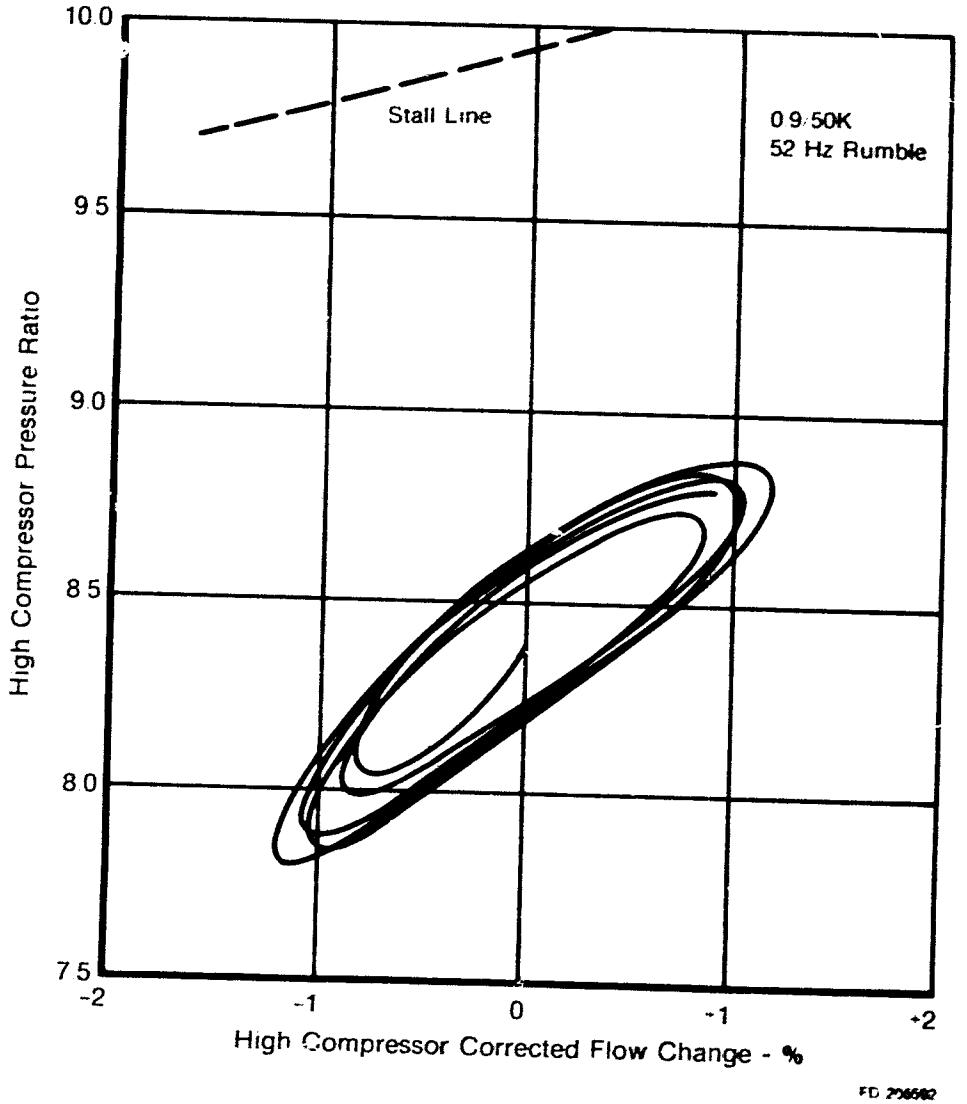

Figure 40. F100 High-Pressure Compressor Transient During A/B Rumble (Remote Splitter Fan)

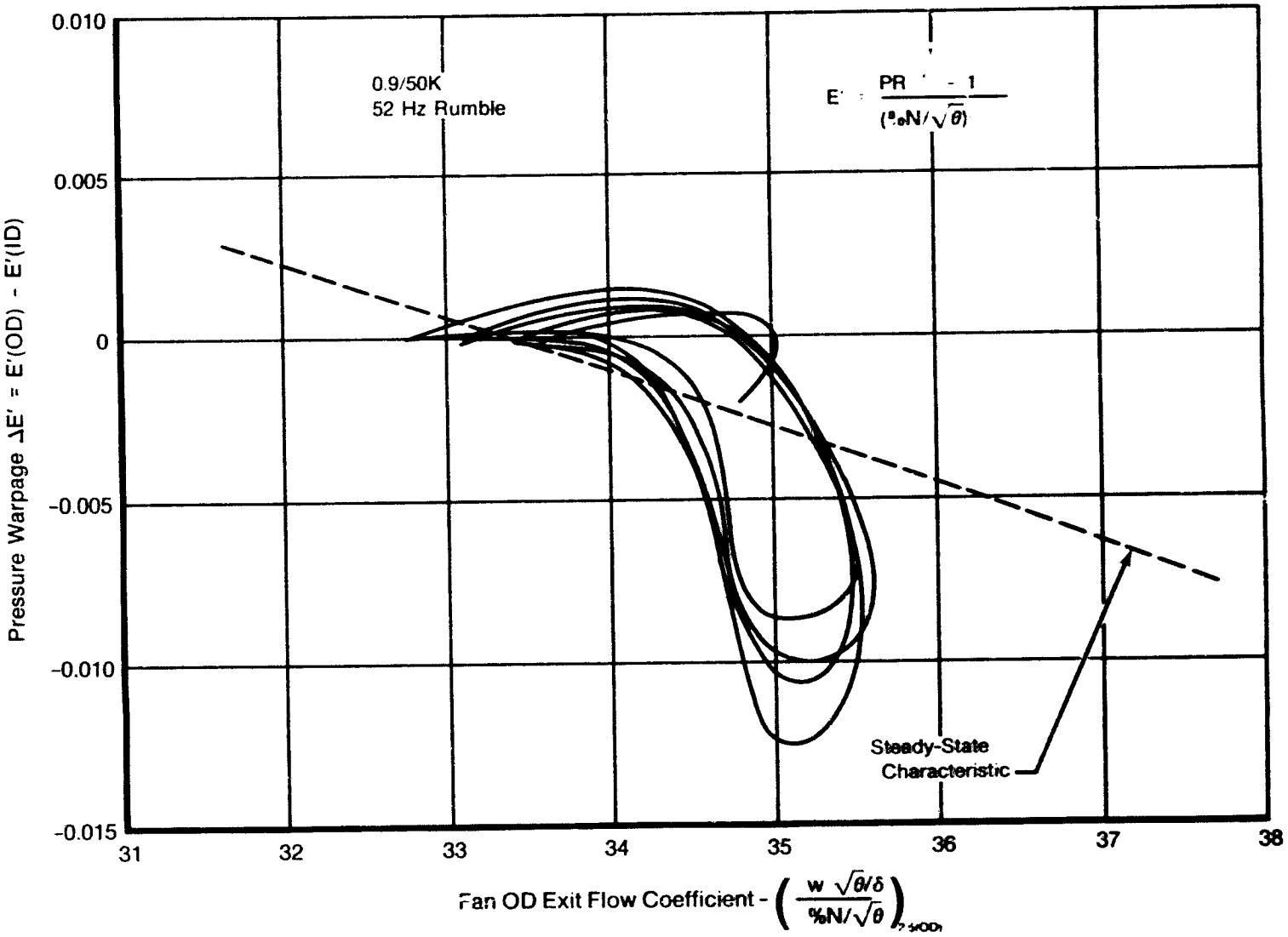

Figure 41. F100 Remote Splitter Fan Warpage During A/B Rumble

Figure 41 illustrates the model fan pressure transient warpage characteristics along with the steady-state characteristic. As shown previously, steady-state model performance matched engine data over a much wider excursion than this rumble transient. Therefore, model response was different with the two-dimensional fan than if fan performance during the transient had been forced to match this warpage (bypass ratio) correlation.

This investigation also compared the model with the same engine (FX219-13) during an additional augmentor rumble transient. A flight condition of 1.6/64K was selected because the fan operates at a lower operating point than at the 0.9/50K flight condition. The comparison between model fan discharge pressures and engine data appears in figure 42. As in the other remote splitter rumble comparison, model fan discharge pressures were less attenuated than engine data.

Stability Limits

A final evaluation induced low-frequency sinusoidal inlet pressure waves into the F100 engine with remote splitter model to determine the model stability limit. At a simulated flight condition of 0.7/30K, 8-Hz sine waves on P_t were input at four different amplitudes. As would be expected, the larger input amplitudes produced larger transient fan pressure ratios until the stability limit was obtained, as shown in figure 43. The condition with an amplitude of ±21.3% (42.5% peak to peak) resulted in model stall very close to the rig fan stall line detailed in figure 44.

The frequency response (gain and phase) listed below represent fan discharge pressure responses to the 8-Hz discrete frequency inlet pressure disturbances.

	Gain	*Phase*
Fan ID	-0.72db	-20°
Fan OD	-0.42db	-13°

The combined effect of gain and phase on transient pressure ratio increase appears in the analytical relationship of figure 45 and shows good correlation with the model maximum pressure ratios seen in figure 43 before the model stall occurs.

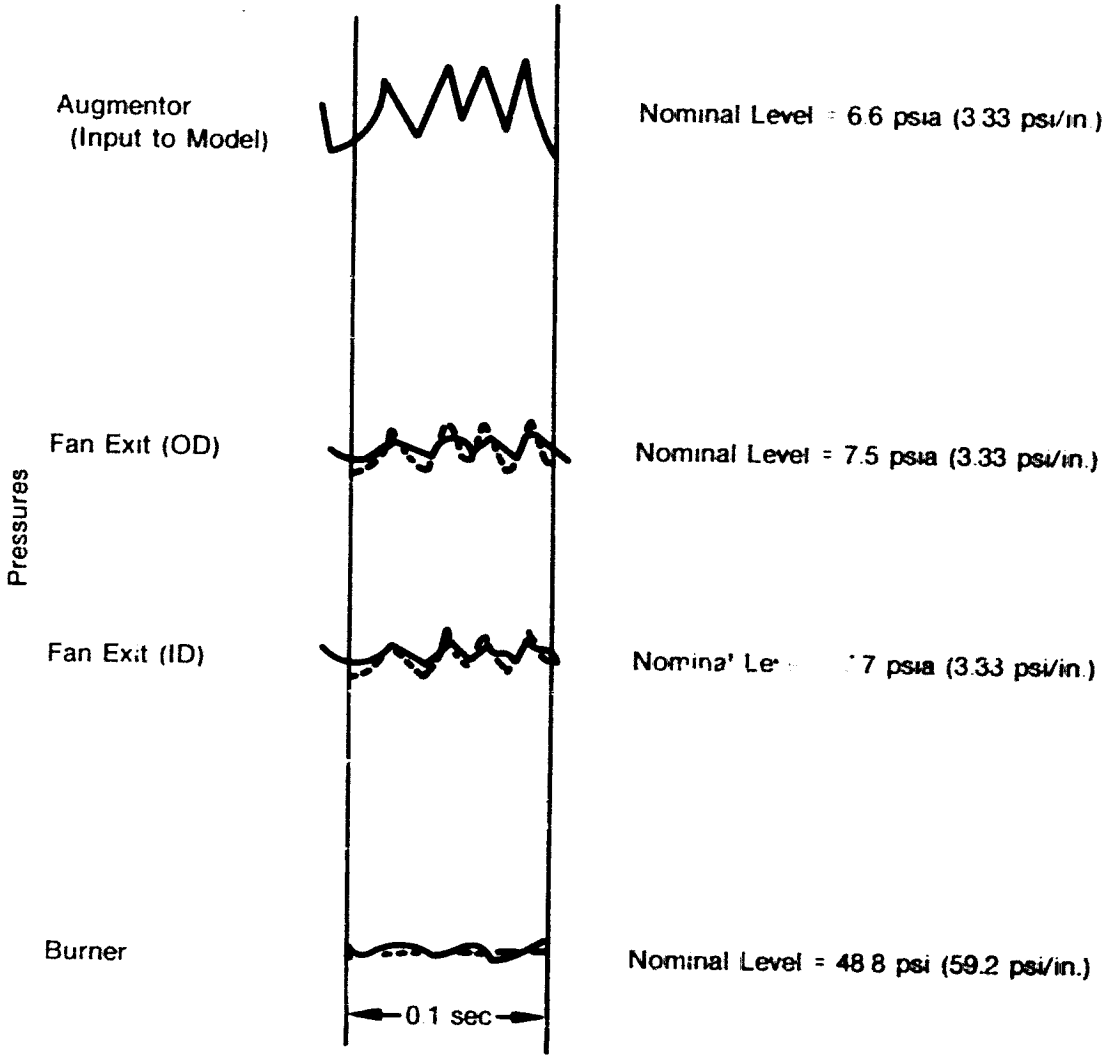

Solid Line - Engine FX219-13 53 Hz Rumble Data
Dashed Line - Model Response

FD 210196

Figure 42. F100 with Remote Splitter Fan Model Response to 53-Hz Rumble at 1.6/64k Flight Condition

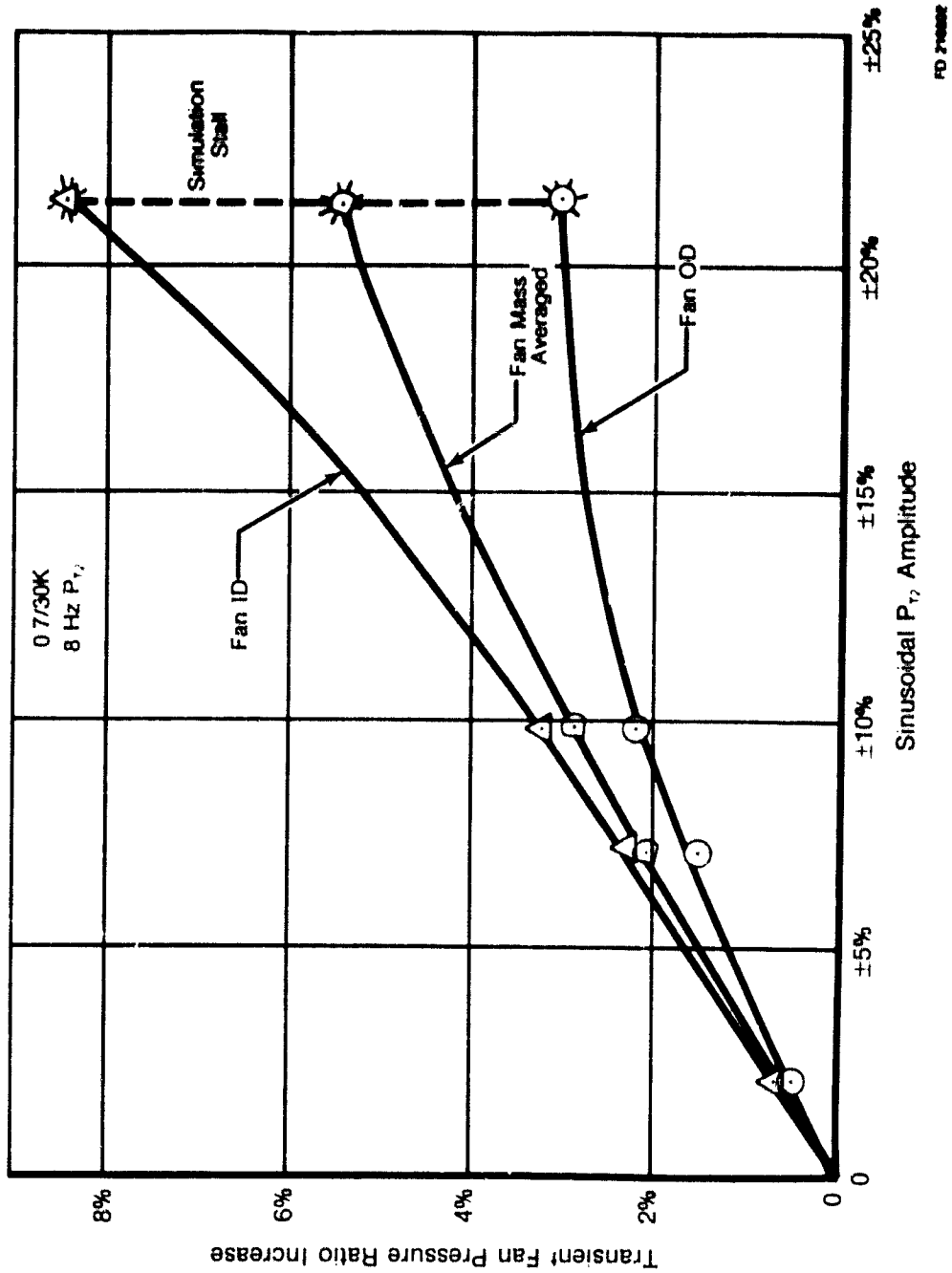

Figure 43. F100 Remote Splitter Fan Transient Pressure Ratio Response to 8-Hz P_{T2}

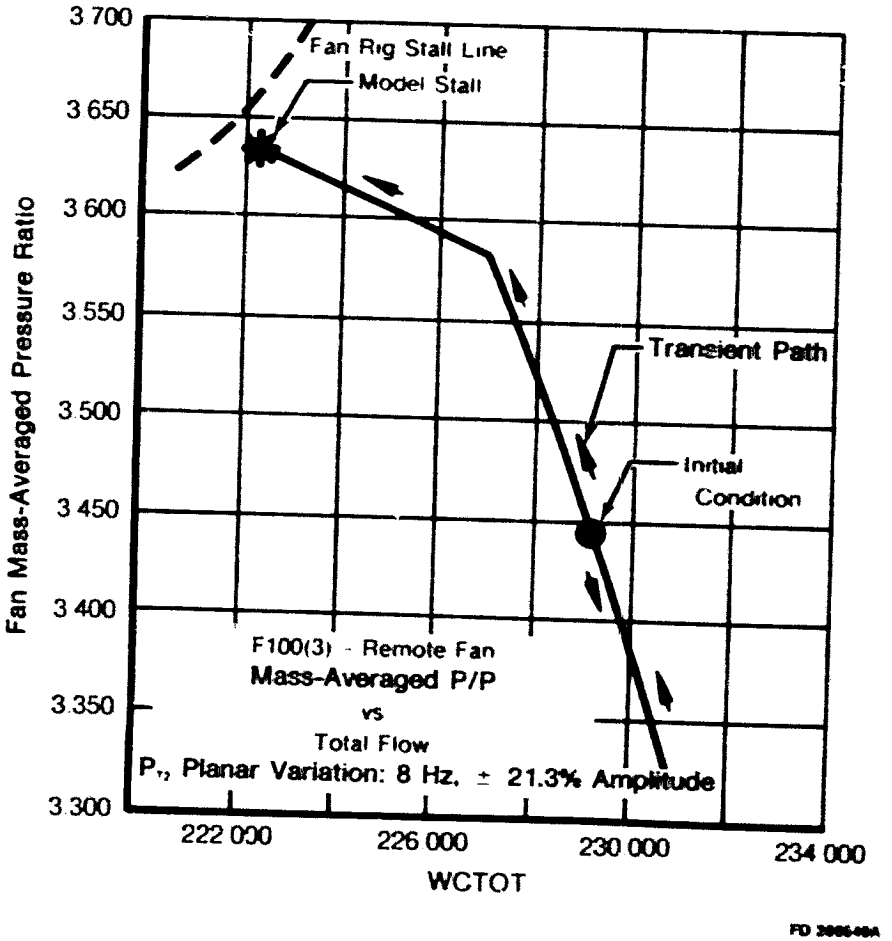

Figure 44. F100 Remote Splitter Fan Model Stability Limit Showing Agreement with Rig Data

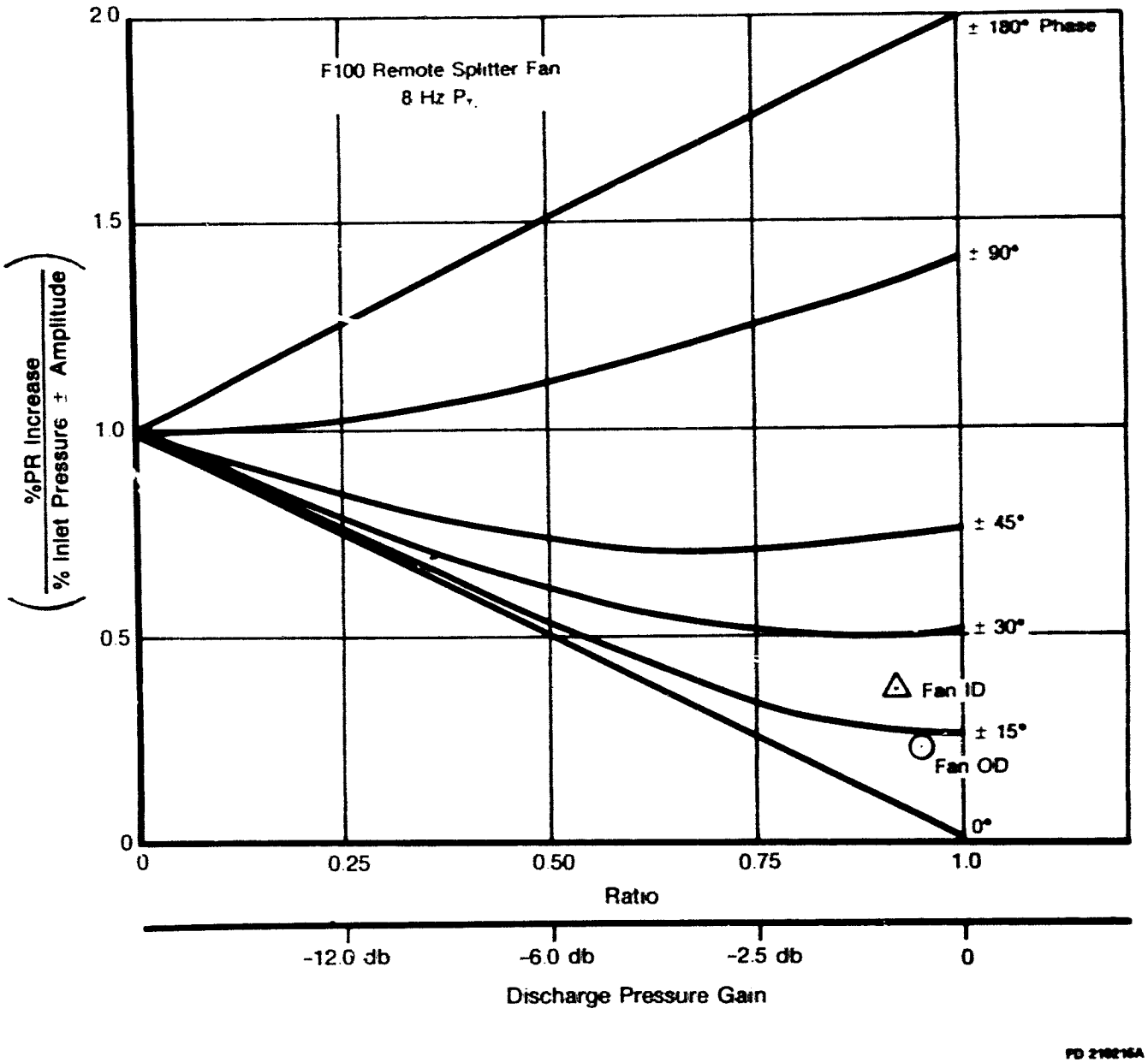

Figure 45. Combined Gain and Phase Effects on Maximum PR Increase - F100 Remote Splitter Fan

F100 ENGINE (PROXIMATE SPLITTER FAN) MODEL

Fan Characteristics

The F100 fan model underwent two modifications to simulate the engine with a proximate splitter. The physical splitter extended forward to within 0.5 in. of Rotor 3. First, the "space" element between Rotor 3 and the splitter was reduced from an axial length of 5.5 to 0.5 in. Second, a pressure calculation due to expansion/ contraction between Rotor 3 and the splitter was added. The area ratios for this expansion/contraction represent the difference between dividing streamline location on Rotor 3 and the nose of the splitter. This calculation procedure was included in the correlation of the empirical characteristics of the TF30 proximate splitter fan, but was not required to correlate the F100 remote splitter fan data.

The F100 proximate splitter fan data exhibits a steeper warpage characteristic than the remote splitter, as indicated in figure 46. The added area ratio calculation in the model moved the steady-state level of warpage to match the proximate data level. The smaller space between Rotor 3 and the splitter provides a stiffer resistance that accounts for the steeper warpage slope, but the verification of this characteristic after a slow transient (as done for the remote splitter) was not performed due to schedule and resource limitations.

High Frequency Comparison

This evaluation compared the F100 engine model with simulated proximate splitter to rumble data from engine P969 with close-coupled instrumentation. This instrumentation utilized Statham transducers mounted on the engine ("close") but some distance from the probe. The lower frequency response of the Statham transducer (compared to a kulite for high-response instrumentation) coupled with the dynamics of the "close" connecting tube resulted in some attenuation and phase shift in the recorded rumble signals. Rumble data for a proximate splitter F100 with high-response instrumentation was not available. A comparison of the 57-Hz rumble data of this engine to model response at a flight condition of 0.4/28k appears in figure 48. The comparison appears much closer than for the remote splitter engine, but because of the close-coupled instrumentation which attenuated actual amplitude excursions, no valid conclusions can be made between the proximate and remote splitter models.

The compression system transient excursions shown in figures 46 through 53 are larger than the remote splitter rumble, even though the augmentor rumble amplitudes for each were both about 25% peak to peak. The fan bypass ratio transient shown in figure 49 is 32% peak to peak, but includes a 19% change in the reduced bypass direction. The slow transient performance characteristics of the model were not verified. The fan map transients of pressure ratio versus flow shown in figures 51, 52, and 53 show the stall line being approached due to a 3% decrease in flow with only a 1.5% flow increase. This trend results from the steep (choked) pumping characteristic of the fan. The transient in the high-pressure compressor shown in figure 47 basically parallels the stall line.

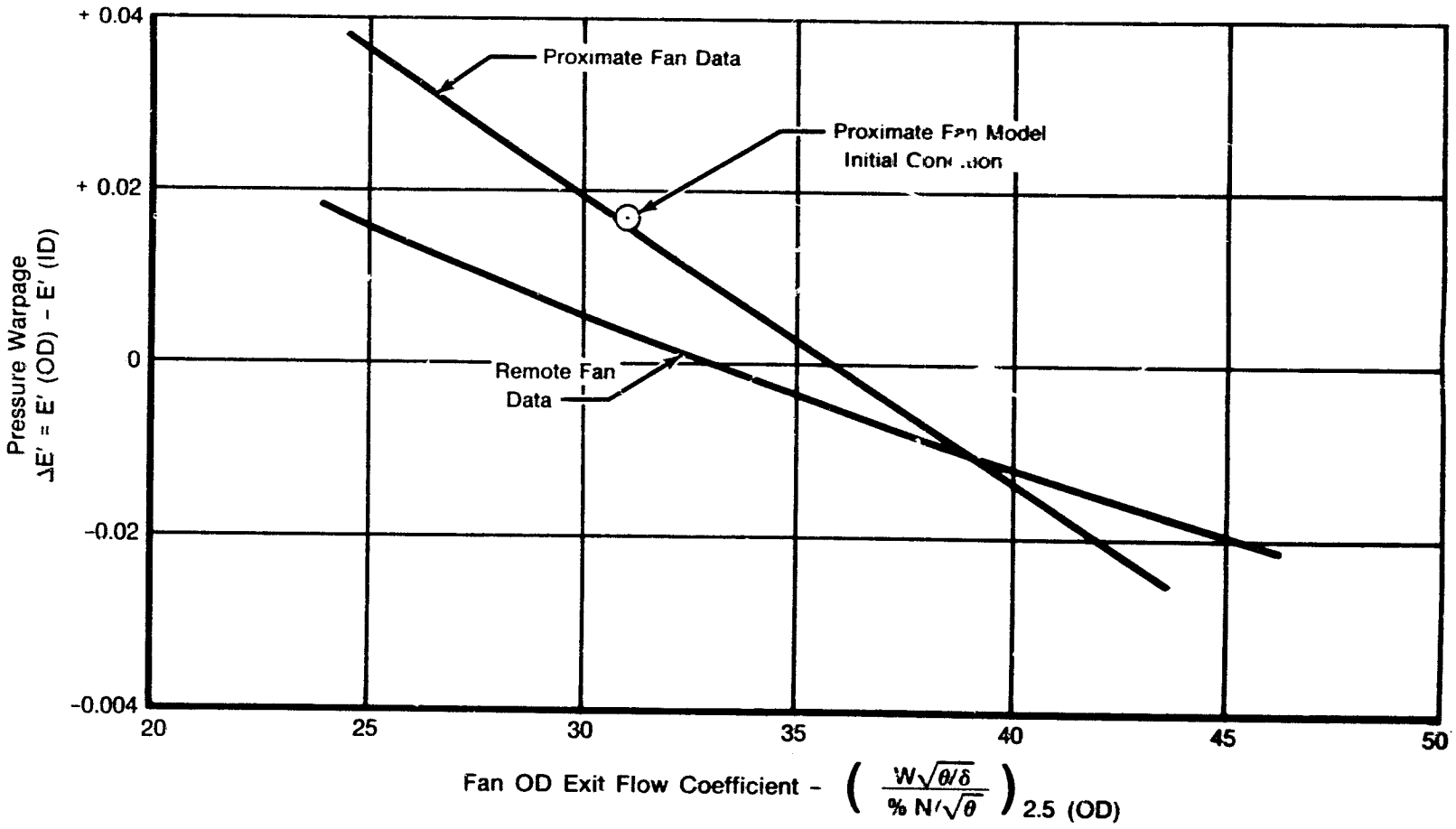

Figure 46. F100 Proximate Splitter Fan Model Matches Data Warpage Characteristics

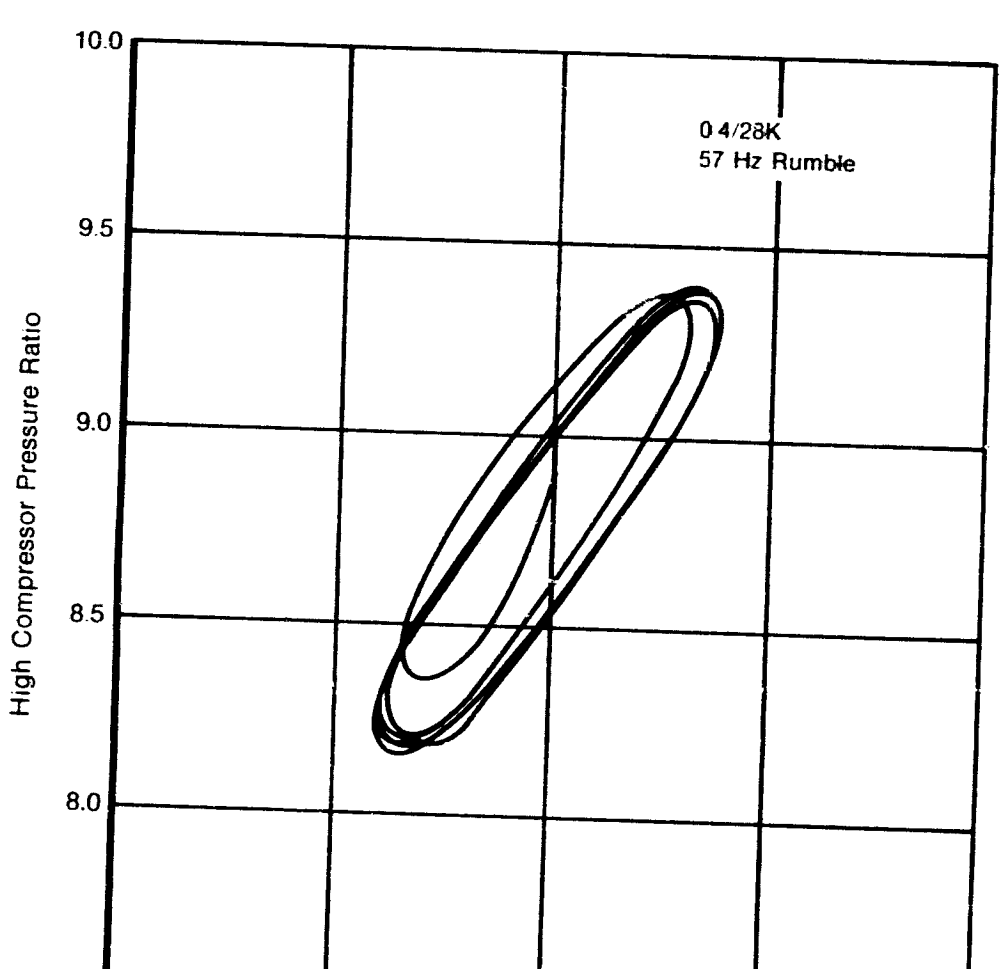

Figure 47. F100 High-Pressure Compressor Transient During A/B Rumble (Proximate Splitter Fan)

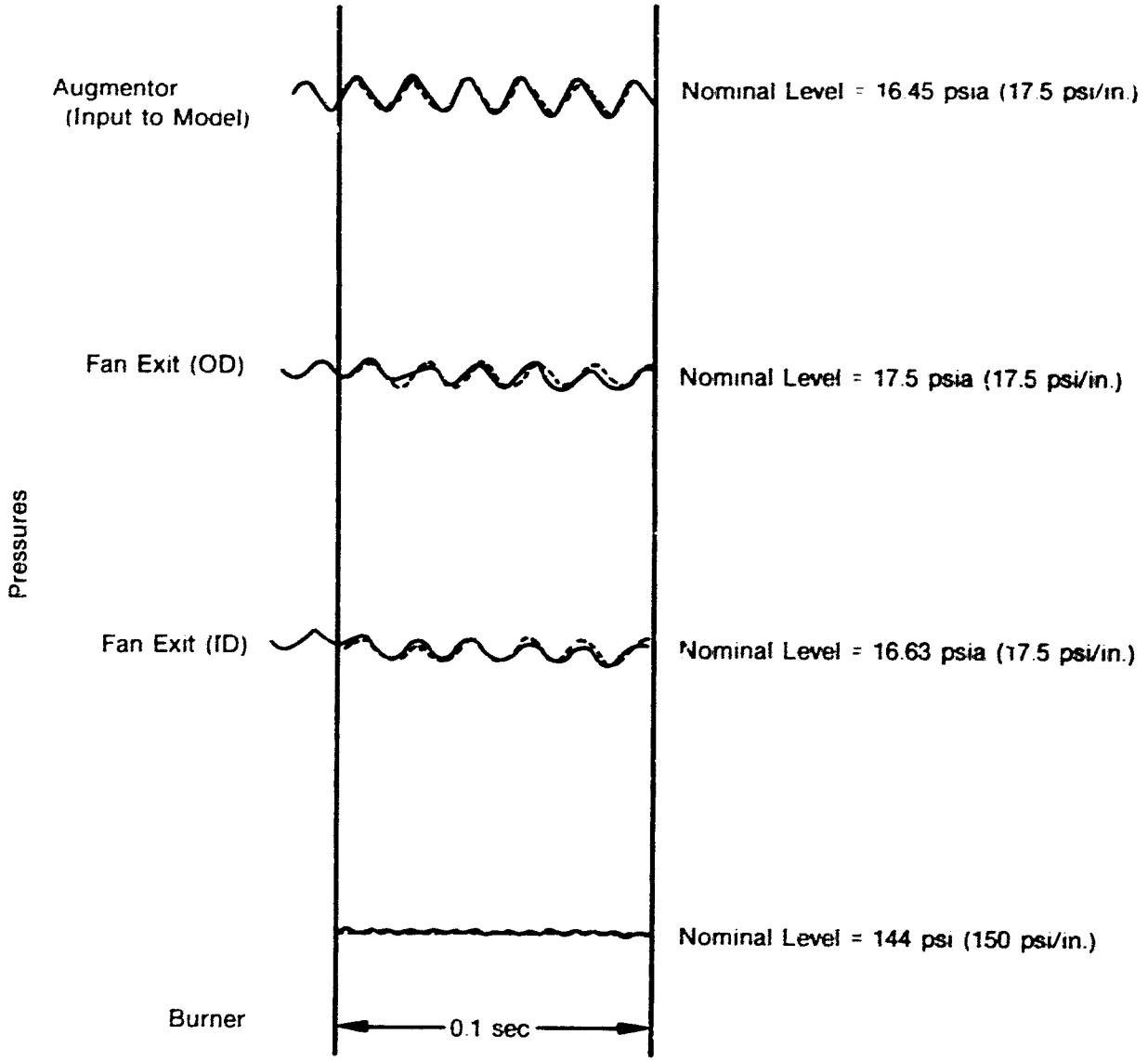

Figure 48. F100 Proximate Splitter Fan Model Response to 57-Hz Rumble at 0.4/28k Flight Condition

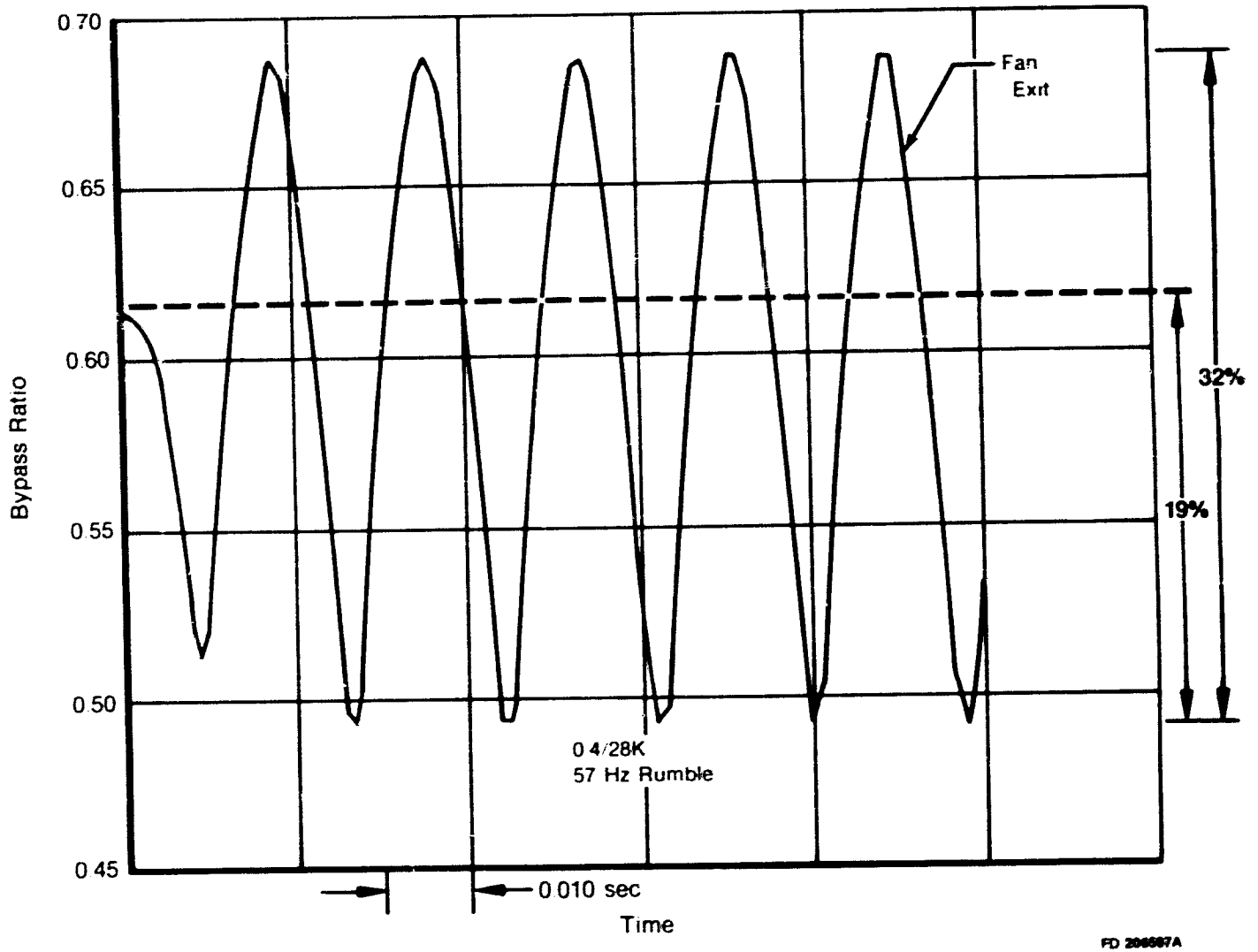

Figure 49. F100 Proximate Splitter Fan Bypass Patio Transient During A/B Rumble

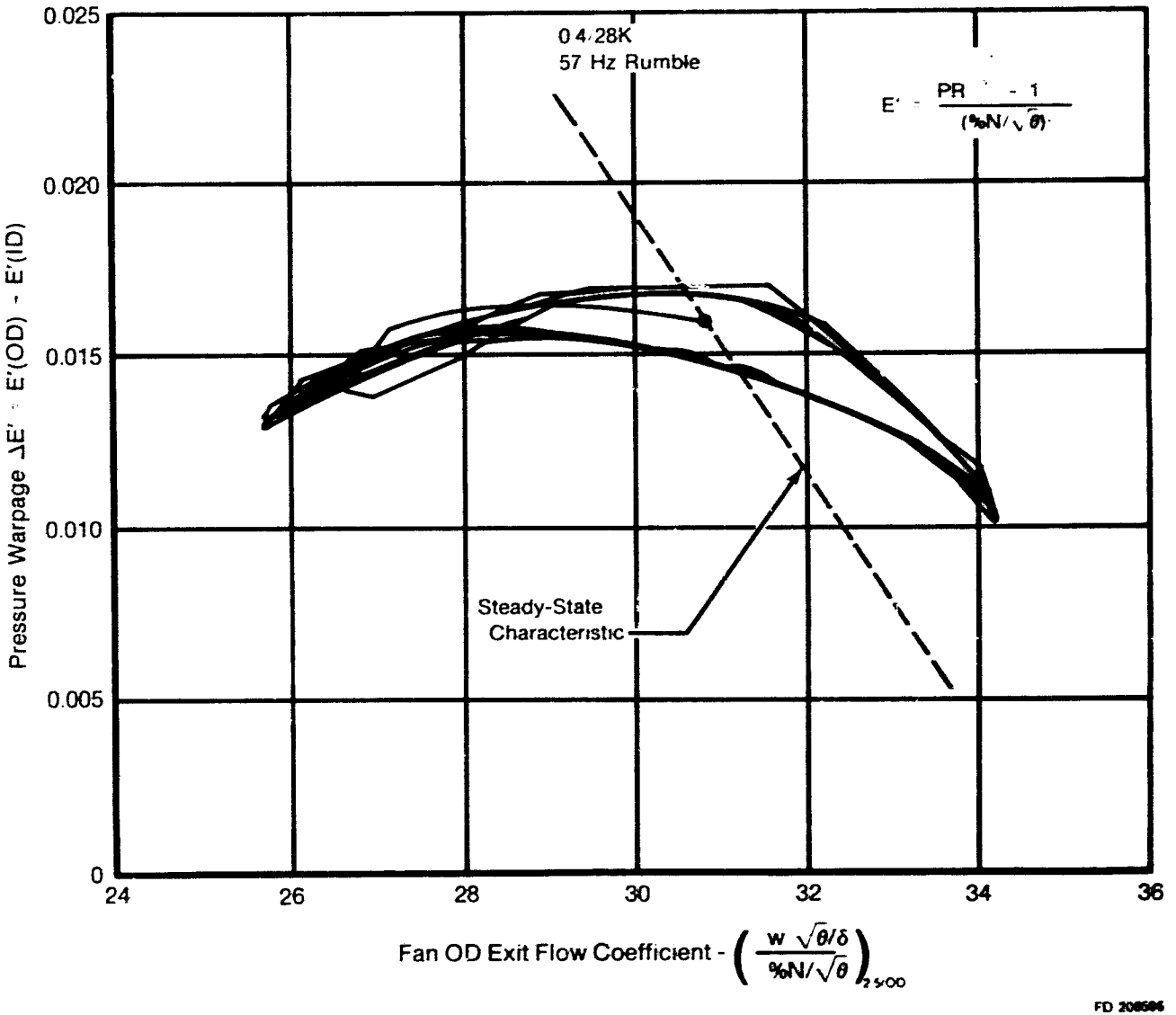

Figure 50. F100 Proximate Splitter Fan Warpage Transient During A/B Rumble

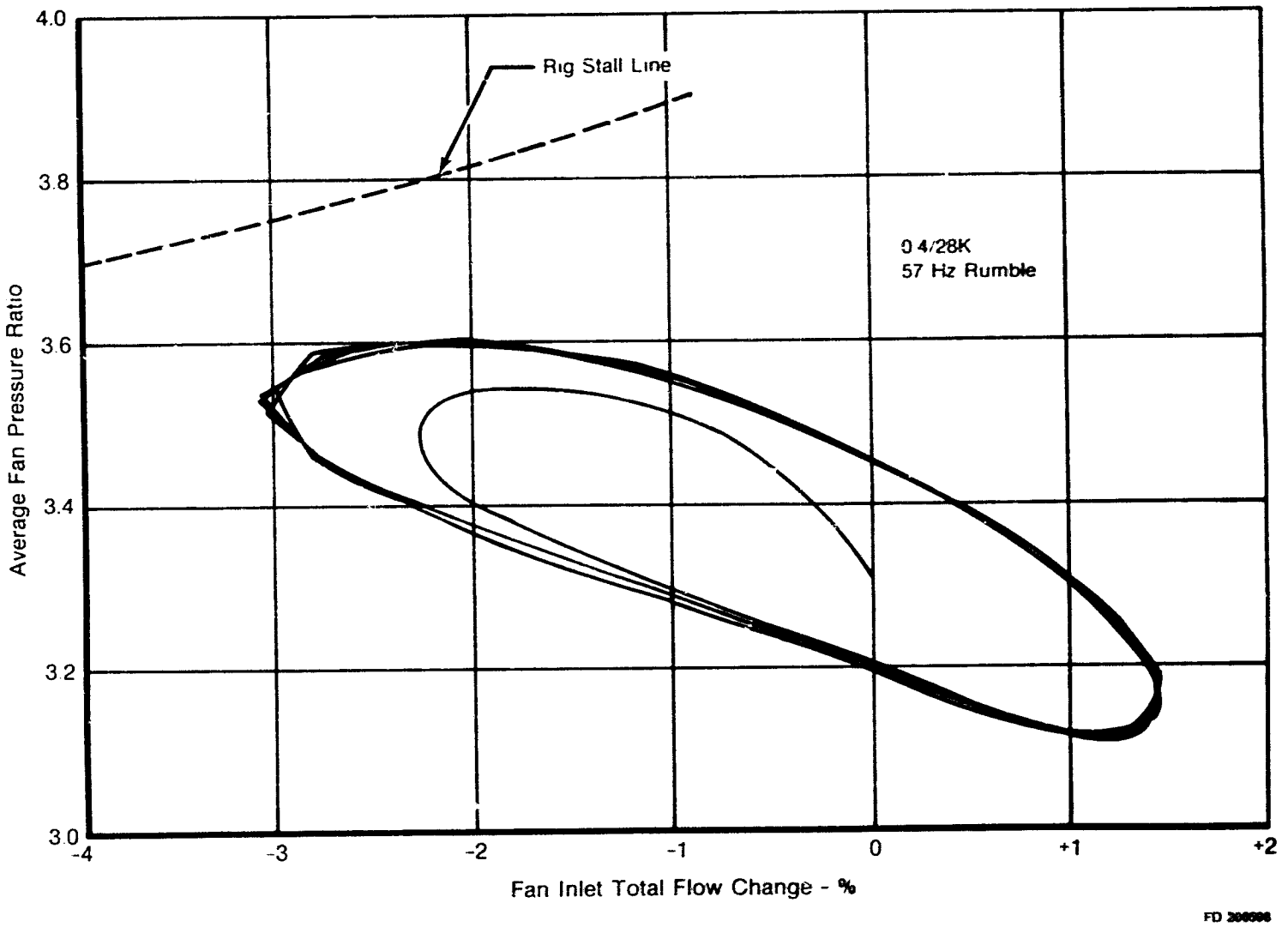

Figure 51. F100 Proximate Splitter Fan Average PR Transient During A/B Rumble

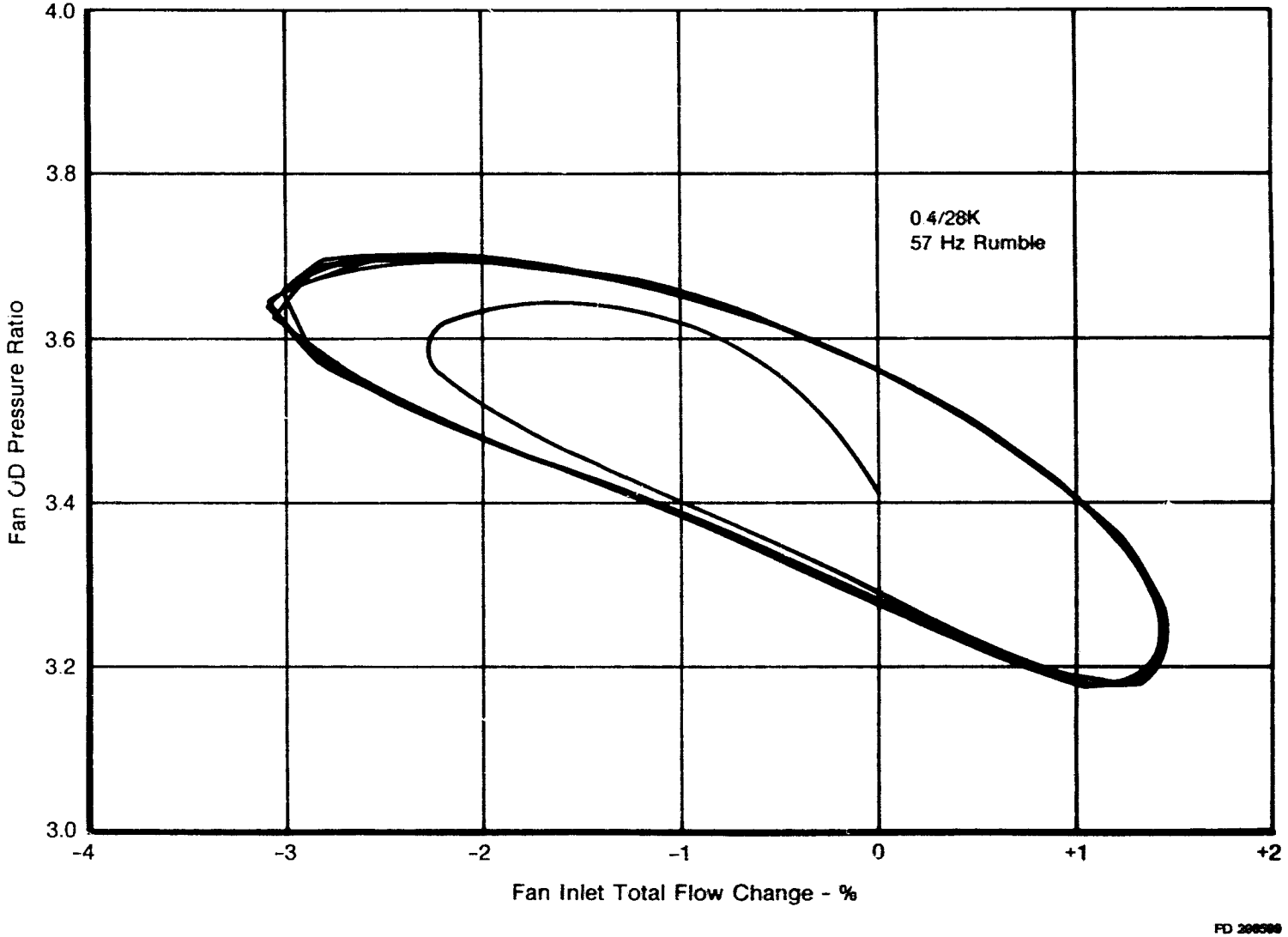

Figure 52. F100 Proximate Splitter Fan OD Pressure Ratio Transient During A/B Rumble

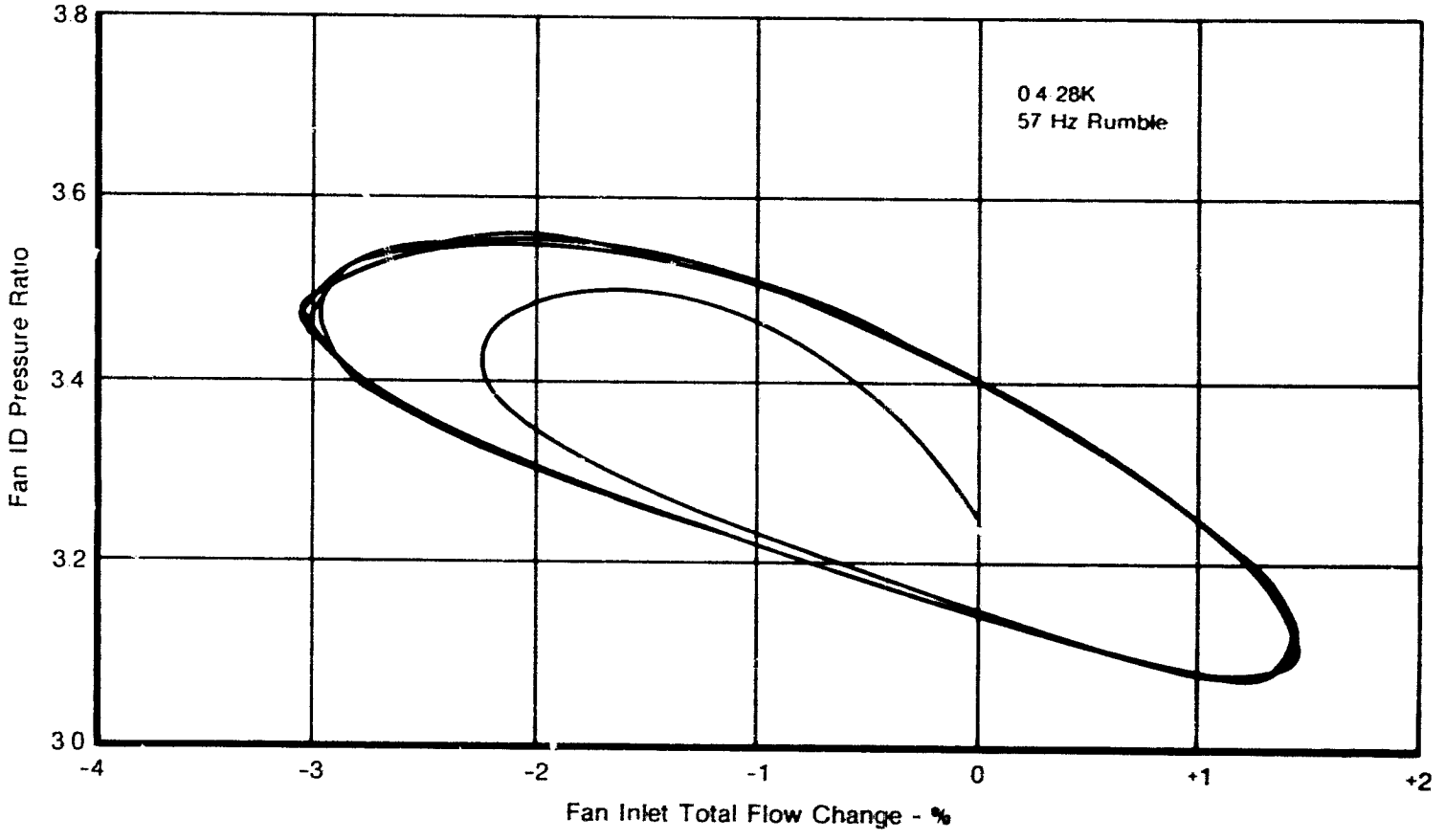

Figure 53. F100 Proximate Splitter Fan ID Pressure Ratio Transient During A/P Rumble

SUMMARY OF RESULTS

This program created a fan model using two-dimensional modeling equations to add dynamic radial coupling between the core stream and the bypass stream of the fan. When incorporated into a twin-spool, mixed flow turbofan engine simulation, this model improved frequency response up to 100 Hz. This modeling technology improvement was verified through comparison with NASA TF30 engine high-frequency data. The new fan model also matched engine stability limits at low frequency (15 Hz), whereas the one-dimensional fan model required twice the inlet pressure amplitude to stall the simulation.

With this verification of the improved fan model, a high-frequency F100 engine simulation was constructed using row-by-row compression system characteristics. In addition to the baseline F100(3) remote splitter fan, the model fan characteristics underwent modification to simulate the F100 proximate splitter fan. Upon comparison, the F100 models showed good correlation with high-frequency (50 to 60 Hz) rumble data. The F100 remote splitter model fan stability limit was verified by imposing inlet planar pressure variations at a low frequency (8 Hz).

Specific highlights of these results include:

TF30 Simulation:

- The improved baseline two-dimensional fan model in the engine simulation compared to the one-dimensional fan model and NASA engine data for frequencies up to 100 Hz appear in the frequency response bodie plots in figures 11 and 13. The new model did show resonant frequencies in both the fan core and bypass streams, even though the absolute magnitudes of these resonant frequencues were in slight error.

- The baseline four element dynamic fan could be improved slightly by use of a stage-by-stage six-element configuration as shown in figures 26, 27, and 28.

- Operating the simulation with discrete, cyclic inlet pressure variations of the same amplitude as engine data resulted in close agreement in response to the more cost-effective transfer function method of model frequency response, as shown in figures 14 and 15.

- The stability limit of the new fan model agreed well with engine data at 15 Hz, as shown in figure 21. Core stream stall occurred in the simulation at an inlet pressure amplitude of 23% peak to peak compared to 28% for engine data, whereas the old model with the one-dimensional fan required a 60% amplitude to stall, and the stall occurred incorrectly in the fan bypass stream.

- An analytical relationship of maximum fan pressure ratio increases due to variations in gain and phase of fan discharge pressure was generated. This relationship can be used to quantify the combined effects of discharge pressure gain and phase on stability (maximum pressure ratio) limits of turbomachinery, as shown in figure 25 for the stability limits of the TF30 models.

F100 Remote Splitter Fan Simulation

- The two-dimensional fan model with radial flows matched engine data characteristics when allowed to reach steadystate operation after a transient, as shown in figure 46.

- Augmentor pressure variations (rumble) at 50 Hz were imposed on the model and resulting fan discharge pressures compared with engine data at 0.9/50k and 1.6/64k flight conditions, as shown in figures 34 and 42, respectively. Phase compared well and the higher gain of the model probably resulted from an inadequate duct model.

- Transient fan bypass ratio variations during a 52 Hz rumble transient appear in figure 36. The large magnitude (28%) variation points out the need for dynamic coupling between the two fan streams in high-frequency simulations.

- Increasing amplitude on engine inlet pressure (P_{t_2}) cyclic variations resulted in good agreement between the model fan stability limit and the fan rig data, as shown in figure 44.

F100 Proximate Splitter Fan Simulation

- The remote fan splitter was changed to simulate the proximate fan splitter configuration characteristics. The change amounted to an additional expansion/contraction pressure calculation term downstream of Rotor 3 that represented an area variation between the location of the splitting streamline on Rotor 3 and the nose of the splitter. The initial steady-state condition before the rumble transient matched proximate splitter fan warpage data, as shown in figure 46, but other off design conditions were not verified. A more accurate representation of the proximate fan splitter would require new Rotor 3 characteristics that include radial flow effects on warpage, but this was beyond the scope of this contract.

- Comparison of the proximate fan splitter simulation with 57-Hz rumble data at a flight condition of 0.4/28k appears in figure 50. Although the gain of the fan discharge pressures appear much better than the remote splitter model, the proximate engine instrumentation was close-coupled, not high-response instrumentation as in the remote engine. Therefore, because the close coupled instrumentation clipped off the maximum and minimum pressure amplitudes, the exact model fidelity could not be determined.

CONCLUSIONS AND RECOMMENDATIONS

The following conclusions and recommendations were drawn from the modeling technology improvements acquired under this investigation of remote and proximate fan splitter model simulations:

- The two-dimensional fan model using radial, dynamic coupling between the fan ID and OD axial flow streams produced significant improvements in frequency response.
- High-frequency (greater than 10Hz) dynamic simulations of mixed flow turbofan engines require dynamic coupling between fan ID and OD axial flow streams to approach the correct frequency response.
- The TF30 and F100 engine models developed under this contract exhibit sufficient frequency response accuracy to help plan high-frequency engine testing and assist in data analyses.
- Technology improvements in duct and augmentor models should be pursued for turbofan engine model applications where accurate resonant frequencies are required.
- Additional modeling technology might be required, such as separating the variable area flow path effect from the row "actuator disk" characteristic.
- The potential of steady-state fan characteristics using radial flow for the bypass variation should be explored.

APPENDIX A
DYNAMIC EQUATIONS AND SOLUTIONS

Dynamic Equations

This appendix describes the equations used to simulate dynamic operation of an engine and to calculate frequency response. The equations express the dynamics of rotor speed transients, unsteady compressor aerodynamics, and gas path fluid flow.

Rotor Dynamics

Simulation of engine transient operation requires accounting for the effects of rotor dynamics. Acceleration or deceleration of the rotors occurs when turbine horsepower exceeds or becomes less than compressor horsepower requirements. The basic formula used to calculate rotor speed changes is

$$\frac{dN}{dt} = \frac{\Delta Q}{I_r} \tag{A1}$$

where:

ΔQ = rotor torque unbalance
I_r = rotor polor moment of inertia
N = rotor speed

Unsteady Compressor Aerodynamics

Incorporating unsteady aerodynamic effects accounts for the deviations from quasi-steady lift characteristics that an airfoil exhibits in a transient flow environment. Inlet airflow incidence angle changes require a finite period of time to propagate to the trailing edge of the airfoil. This effect on airfoil performance appears in figure 54. The difference in airfoil lift coefficient translates into deviations in blade and vane loss characteristics for compressor operation, as illustrated in figure 55. The net effect on compressor operation is an effective modification of compressor map characteristics in a high-frequency operating environment.

The unsteady effects are computed by applying a first-order lag to the quasi-steady entrophy change across the rotor or stator. The quasi-steady entrophy change comes from the equation

$$\Delta s = \left(\frac{\gamma}{\gamma - 1}\right) R \ln TR_r - R \ln PR_r \tag{A2}$$

where, TR_r and PR_r are the total temperature and total pressure ratios defined by the rotor or stator characteristics. A time constant modifies the quasi-steady entrophy change that represents a function of the rotor or stator chord length and the axial velocity at the stator or rotor exit, such that

$$\tau = \frac{\text{chord length}}{\text{axial velocity}} \tag{A3}$$

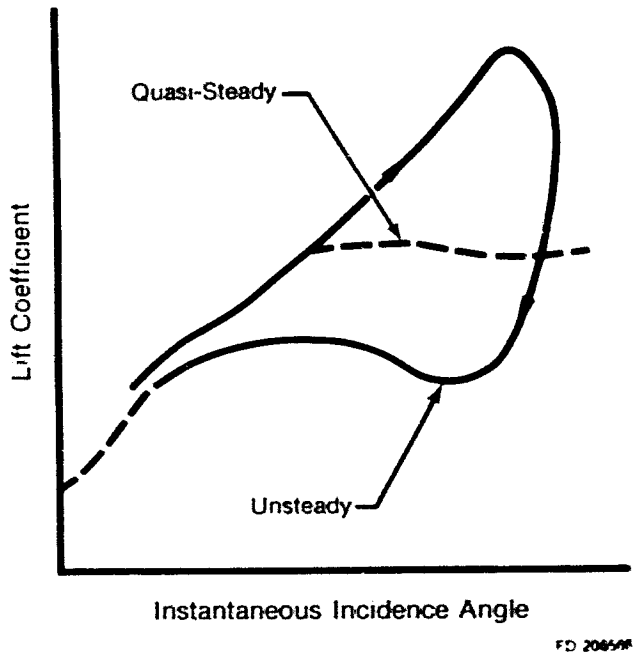

Figure 54. Airfoil Life Characteristics

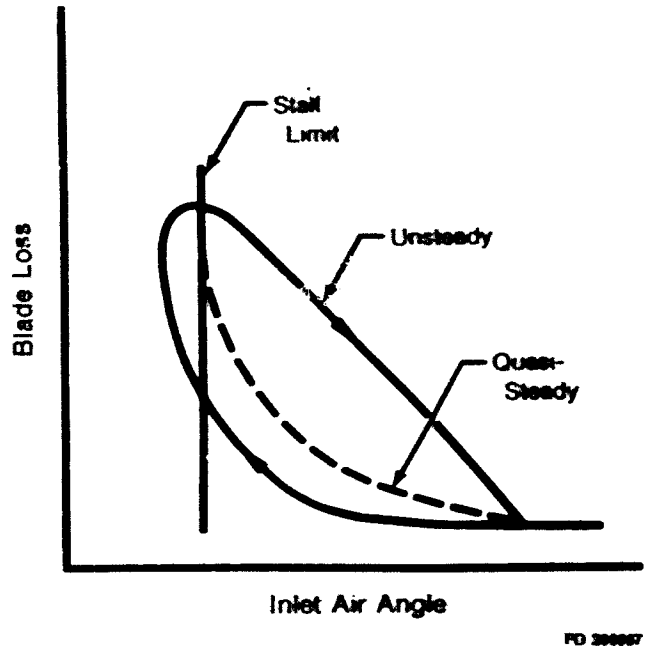

Figure 55. Compressor Airfoil Loss Characteristics

The dynamic entropy change is obtained by appling the time constant as shown below:

$$\Delta s \left[\frac{1}{\tau s + 1}\right] \Delta s' \tag{A4}$$

Equation A2 is rewritten to solve for dynamic pressure ratio

$$PR_t = \exp\left(\frac{\gamma}{\gamma - 1} \ln TR_t - \frac{\Delta s'}{R}\right) \tag{A5}$$

where temperature ratio is held constant at the quasi-steady value.

Fluid Flow Dynamic Equations

The general relationships that describe one-dimensional fluid flow phenomena recognize three basic properties: mass of the fluid, its momentum, and its energy. These represent conservation properties in that a change to any one of them within the boundaries of a system must be the result of quantities passing through the boundaries. In most basic terms, then, these relationships can be expressed as

$$\Delta Mass_{CV} = Mass_{in} - Mass_{out} \tag{A6}$$

$$\Delta Momentum_{CV} = Momentum_{in} - Momentum_{out} \tag{A7}$$

$$\Delta Energy_{CV} = Energy_{in} - Energy_{out} \tag{A8}$$

where, CV refers to a bounded system known as a control volume or finite element; "in" refers to quantities entering the finite element; and "out" refers to quantities leaving the finite element. The introduction of the independent variable time (t) allows the formulation of equations that describe the properties within the finite element at a particular value of time, such that

$$m \quad Mass \quad Mass_{t} + \frac{\Delta Mass_{in}}{\Delta t}\Delta t \quad \frac{\Delta Mass_{out}}{\Delta t}\Delta t \tag{A9}$$

$$P \quad Momentum \quad Momentum_{t} + \frac{\Delta Momentum_{in}}{\Delta t}\Delta t \quad \frac{\Delta Momentum_{out}}{\Delta t}\Delta t \tag{A10}$$

$$E \quad Energy \quad Energy_{t} + \frac{\Delta Energy_{in}}{\Delta t}\Delta t \quad \frac{\Delta Energy_{out}}{\Delta t}\Delta t \tag{A11}$$

As Δt approaches zero, the right-hand side of these equations represent integrals with respect to time of the time deviations of the incoming and outgoing quantities. These may be expressed as follows:

$$m = \int \partial m/\partial t \cdot dt \tag{A12}$$

$$P \quad \int \partial P/\partial t \cdot dt \tag{A13}$$

$$E \quad \int \partial E/\partial t \cdot dt \tag{A14}$$

At this point, recognize that the solutions obtained must be in terms of the parameters with which fluid systems are normally identified; i.e., pressure, temperature, density, and velocity. The first formulas presented represent time deviations of the three basic properties at the boundaries of the system. The formulas that follow represent quantities of the properties within the finite element at a particular time.

Figure 56 shows a representation of the geometry within a typical finite element. The time derivatives of the properties, either incoming or outgoing, may be represented by:

$$\frac{\partial m}{\partial t} = \rho A v = W \tag{A15}$$

$$\frac{\partial P}{\partial t} = \frac{\partial (mv)}{\partial t} = \frac{v \partial m}{\partial t} + \frac{m \partial v}{\partial t} = vW + \Sigma F \tag{A16}$$

$$\frac{\partial E}{\partial t} = h_i W \tag{A17}$$

where,

$$h_i = \int CpdT + 0.5\ \rho v^2 = \int CpdT_T \tag{A18}$$

The mass derivative (Equation A15) is density times the area normal to the flow direction times the distance traveled by the fluid per time differential. This latter quantity is the velocity of the fluid. Time rate of change consists of two terms, the first describing the change in momemtum due to mass transfer and the second consisting of the summation of forces on the fluid in the direction of the flow. This second term represents an application of Newton's Second Law to the finite element. The energy derivative, expressed in terms of total enthalpy, is the sum of the specific kinetic energy of the fluid and the specific potential, or thermal, energy contained in the fluid. The specific enthalpy is multiplied by flow to obtain the time rate of change in energy at the boundary.

At this point, the time derivatives of mass, momentum, and energy have been identified in terms of the parameters usually associated with fluid flow. In particular, these quantities have been defined at the boundaries of a finite element, or control volume, assuming that the flowfield is one-dimensional. Spatial integrals, which define the quantities of mass, momentum, and energy with the boundaries, are given by:

$$m = \int_{CV} \rho dV = \int \rho A dL \tag{A19}$$

$$P = \int_{CV} \rho v dV = \int \rho A v dL \tag{A20}$$

$$E = \int_{CV} 0.5\ \rho v^2 dV + \int_{CV} \rho CvT dV = \int [0.5\ v^2 + CvT]\ \rho A dL \tag{A21}$$

A basic assumption in the implementation of the finite element technique follows that the parameters of elements vary in a linear fashion from one side to the other. These formula for the spatial variations in the general parameter are:

$$p = p_{in} + \left(\frac{p_{out} - p_{in}}{\Delta L}\right) L \tag{A22}$$

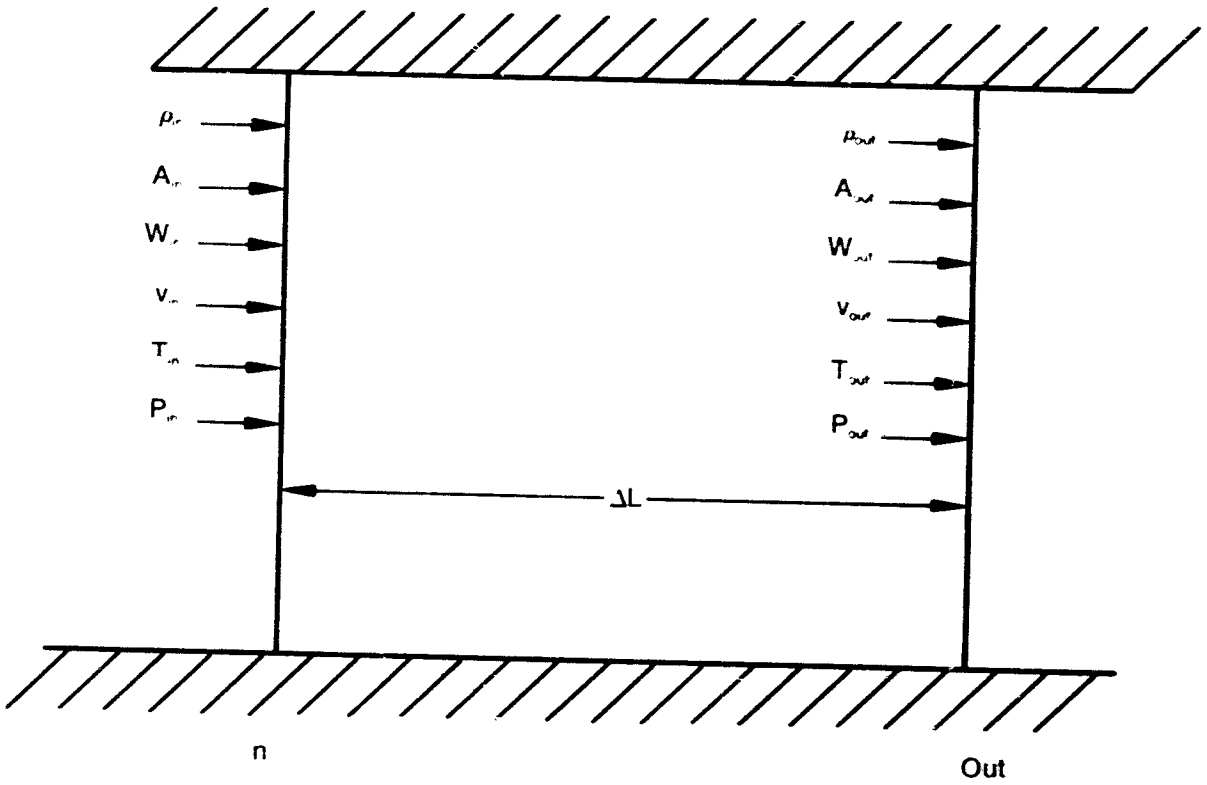

Figure 56. Finite Element Pepresentation

FD 210211

where, L varies from O to L across the element. This formula is applied to variations in pressure, temperature, density, area, and velocity across the element.

Substitution of these equations into the spatial integrals allows their evaluation and yields the following functions for the properties within the finite element:

$$m = f(\rho, A, \Delta L) \tag{A23}$$

$$p = f(\rho, A, v, \Delta L) \tag{A24}$$

$$E = f(\rho, A, v, T, \Delta L) \tag{A25}$$

One term still remains to be defined: the sum of the forces on the fluid exerted by its surrounding the flow direction (F), which appears in the equation for the time rate of change in momentum. Figure 56 shows that the geometry of the finite element plays a role in the assessment of the forces exerted in the fluid. The boundaries through which flow passes are assumed to be normal to the flow direction. The walls of the duct form the other boundary of the element. Total force consists of two parts: the force exerted by the fluid outside the element and the force exerted by the walls on the fluid inside the element. The first term is simply pressure times the flow area at the boundary. In the absence of friction or any area variation across the element, there are no body forces exerted by the walls in the flow direction.

The sum of forces on the fluid within the finite element then becomes:

$$\Sigma F = p_{in}A_{in} - p_{out}A_{out} \tag{A26a}$$

Up to this point, the discussion has been limited to one-dimensional flow in ducts without considering the changes to the properties imposed by external mechanisms; in particular, changes due to the forces on the fluid exerted by the turbomachinery and the rate of energy transfer to the fluid in the form of mechanical work, such that

F' = force on the fluid due to mechanical components (A27)
dW/dt = rate of mechanical work performed on the fluid by the mechanical components

The spatial integrals of Equations A19 through A21 define the three equations which govern fluid flow within a one-dimensional finite element. These equations may be written as:

$$m = (2\rho_{in}A_{in} + 2\rho_{out}A_{out} + \rho_{in}A_{out} + \rho_{out}A_{in})\ \Delta L/6 \tag{A28}$$

$$= \int (W_{in} - W_{out})\ dt \tag{A29}$$

$$P = [(3A_{in} + A_{out})\ \rho_{in}v_{in} + (A_{in} + 3A_{out})\ \rho_{out}v_{out} + (A_{in} + A_{out})\ (\rho_{in}v_{out} + \rho_{out}v_{in})]\ \Delta L/12 \tag{A30}$$

$$= \int (W_{in}v_{in} - W_{out}v_{out} + P_{in}A_{in} - P_{out}A_{out} + F')\ dt \tag{A31}$$

$$E = [\nu (A (\rho /5 + \rho /20) + A (\rho /20 + \rho /30)) +$$

$$V (A (\rho /30 + \rho /20) + A (\rho /20 + \rho /5)) +$$

$$v v (A (\rho /10 + \rho /15) + A (\rho /15 + \rho /10))] \Delta L/2 +$$

$$Cv](3A + A) \rho T + (A + 3A) \rho T +$$

$$(A + A) (\rho T + \rho T)] \Delta L/12 \quad \text{(A32)}$$

$$= \int \left[h W - h W + \frac{dW}{dt} \right] dt \quad \text{(A33)}$$

In evaluating external force and energy derivative inputs to a finite element, a concept known as the actuator disk is employed. In this model, a series of disks of negligible length, across which the total temperature and pressure change as a specific function of a specific component characteristic, represent the turbomachinery. The effect of these changes on the momentum and energy flux at the incoming boundary of the finite element become part of the calculations by utilizing the parameters that result from the component characteristics in the calculation of incoming momentum and energy derivatives. This concept appears schematically in figure 57. The "in" station represents the inlet of the component, while conditions that would exist at the component exit in the steady-state condition are assumed at the "in'" station. Momentum and energy derivatives computed as a function of conditions at this station include the effects of the turbomachinery components. On this basis, the expressions for the time derivatives of momentum and energy presented in Equations A28 and A29 can be modified in the following manner:

$$W 'v' + P 'A = W v + P A + F' \quad \text{(A34)}$$

$$h W' = h W + \frac{dW}{dt} \quad \text{(A35)}$$

The engine simulation describes compressor characteristics on a row-by-row basis. Dynamically, the model utilizes finite elements to describe compressor operation. The finite element configuration requires that row performance characteristics be combined algebraically to establish the properties associated with the finite element actuator disk.

Solution Technique

The previous section defined three ordinary differential equations (ODE) applicable to a single finite element within an arbitrary flowfield. This set can be applied to each of the elements of the system. The resulting set of equations, when solved simultaneously, describe the flowfield at any point in time, given the time history of the field up to that point and its current boundary conditions. The simulated response of the system consists of a series of solutions at the discrete values of time required by the particular problem being studied. It must commence with a steady-state solution which provides the required initial values of the properties.

The transient solution technique applies implicit solution methods directly to the ODE. A simple trapezoidal numerical integration scheme is applied to the time derivatives of the properties, as shown in Equations A15 through A17. This results in a set of non-linear algebraic equations which yield solutions at discrete values of time in an interative manner.

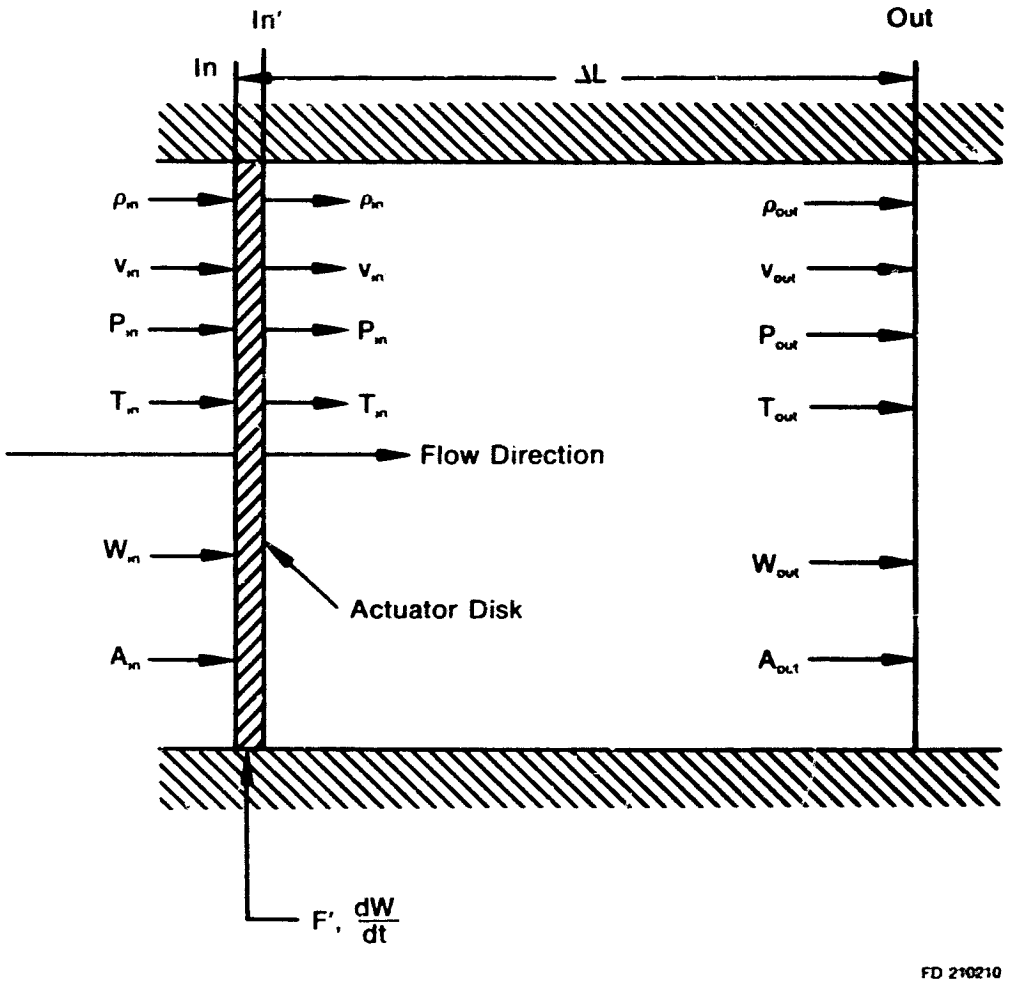

Figure 57. Finite Element Representation Showing the Actuator Disc Concept

The concept referred to above is generally known as a relaxative method. Relaxative methods rely on solving a set of implicitly defined relationships in an interative manner. This solution method uses a set of independent variables which permit computation of both the right-hand and left-hand sides of the set of governing equations (Equations A28 through A33). A solution is obtained when, for a particular set of boundary conditions, the values of all independent variables satisfy the equations.

In applying this method to the set of non-linear algebraic equations which are used to model the dynamic behavior of the flowfield described by an arbitary set of finite elements, a set of three variables describing conditions at the exit of each element must be chosen. Two of these must describe the state of fluid, while the third must describe its motion. Pressure and temperature, either static or total, are chosen for the first two, while mass flow or velocity is used for the third. This set of variables is sufficient to explicitly calculate both sides of the three equations and, hence, the three error terms associated with them. Additional pairs of independent variables and errors are used to implicity define boundary conditions or constraints of the system that cannot be expressed explicitly. These include the flow areas in the turbines and at the exhaust nozzle. A sophisticated non-linear equation solver, utilizing a modified Newton-Raphson approach, operates on this set of independent variables and errors to achieve the required solutions.

Frequency Response Calculation

Frequency response, defined as gain and phase versus frequency of the simulation was evaluated by two methods: (1) transfer functions and (2) amplitude and phase analysis of response to discrete frequency sine waves at P_t. The capability of these analytical methods was consolidated into the engine simulation and could be activated via input.

The transfer function combined a state-variable definition of the engine with the routines of Seidel, as reported in Reference 3. As described in Reference 4, the state-variable method provided a linear description of a system using first-order differential equations in the form:

$$\dot{x}(t) = Ax(t) + Bu(t) \qquad \text{(A36)}$$

where:

- x = state vector
- u = input vector
- A = system matrix
- B = input matrix

The output system is described by:

$$y(t) = Cx(t) + Du(t) \qquad \text{(A37)}$$

where:

- y = output vector
- C = output matrix
- D = output/input direct coupling matrix

The matrices in the above expressions consist of partial derivatives determined from the simulation of finite differences. Each state and input variable perturb individually with all others held constant.

The state variables used for the baseline simulation include mass, momentum, and energy of each dynamic element, core exhaust for dynamic mixing, and fuel flow for the engine fuel control. The input variable is $P_{T2.0}$ and the output variables are $P_{T2.2}$ and $P_{T2.5F}$. Formulation of these variables results in matrices of the following form for a 62nd-order system:

$$A = \begin{vmatrix} \frac{\partial \dot{x}_1}{\partial x_1} & \cdots & \frac{\partial \dot{x}_1}{\partial x_{62}} \\ \vdots & & \vdots \\ \frac{\partial \dot{x}_{62}}{\partial x_1} & \cdots & \frac{\partial \dot{x}_{62}}{\partial x_{62}} \end{vmatrix} \qquad B = \begin{vmatrix} \frac{\partial \dot{x}_1}{\partial u_1} \\ \vdots \\ \frac{\partial \dot{x}_{62}}{\partial u_1} \end{vmatrix}$$

$$C = \begin{vmatrix} \frac{\partial y_1}{\partial x_1} & \cdots & \frac{\partial y_1}{\partial x_{62}} \\ \vdots & & \vdots \\ \frac{\partial y_4}{\partial x_1} & \cdots & \frac{\partial y_4}{\partial x_{62}} \end{vmatrix} \qquad D = \begin{vmatrix} \frac{\partial y_1}{\partial u_1} \\ \vdots \\ \frac{\partial y_4}{\partial u_1} \end{vmatrix}$$

Using the computer routines of Seidel furnished by NASA-LeRC and reported in Reference 3, matrix algebra solved Equations A36 and A37 simultaneously to define the transfer function y(t)/u(t). The resulting gain and phase characteristics of the simulation were obtained from the transfer functions.

The second method for defining simulation frequency response utilized direct analysis of a transient induced by discrete frequency sine waves applied to inlet pressure. As shown in figure 58, direct measurement of input pressure and output pressure wave amplitude and phase lag were made from the time traces of the transient.

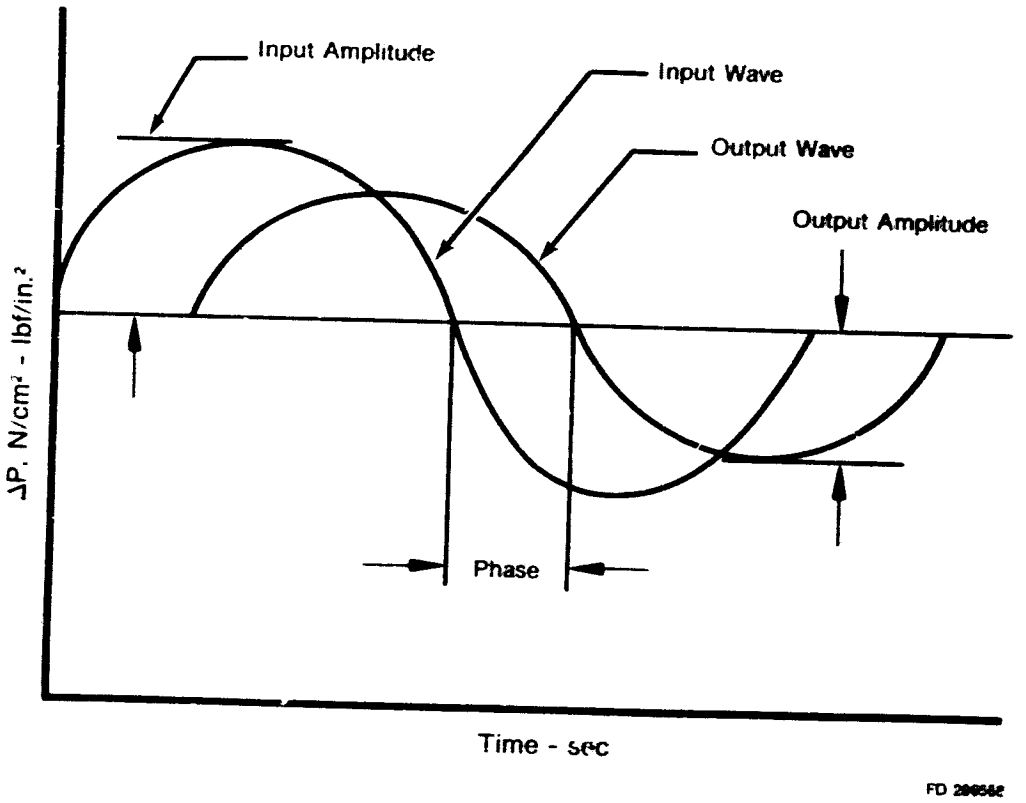

Figure 58. Wave Analysis for Evaluation of Gain and Phase

APPENDIX B
F100 FAN ROW CHARACTERISTICS

This appendix describes the blade row performance characteristics of the F100(3) fan, as modeled under this contract. These blade row characteristics (from Reference 5) are derived from empirical F100 fan rig data plus extrapolations based on cascade correlations. A static pressure rise characteristic simulates the stationary (stator) element, while a static pressure rise characteristic plus a total temperature rise characteristic represent the rotating (rotor) element. A "dividing" streamline separates the fan core (ID) flow from the fan bypass (OD) flow. A given location of the dividing streamline, which varies with bypass ratio, defines the flow areas in the ID and OD streams. The assumption made here is that flow per unit area across the span of the fan remains constant.

Figures 59 through 68 present the fan row characteristics for the ID flow stream and the OD flow stream. The performance parameters of (Ψ) for the static pressure rise and (λ) for the total temperature rise represent functions of the mass flow parameter (ϕ/A) and the speed parameter. These parameters are defined in the following manner for either the ID stream or the OD stream, where speed parameter accounts for variable guide vane effects:

$$\text{PSI} = \frac{\Delta P_s}{P_s}\left(\frac{(N/\sqrt{\theta})_D^2}{(N/\sqrt{\theta})^2}\right)\frac{r_B^2}{r^2} \tag{B1}$$

$$\text{LAMDA} = \frac{\Delta T_T}{T_T}\left(\frac{(N/\sqrt{\theta})_D^2}{(N/\sqrt{\theta})^2}\right)\frac{r_B^2}{r^2} \tag{B2}$$

$$\text{PHI/A} = \frac{W\sqrt{\theta}}{\delta}\left[\frac{1}{A}\left(\frac{(N/\sqrt{\theta})_D}{(N/\sqrt{\theta})}\right)\frac{r_B}{r}\right] \tag{B3}$$

$$\text{SPEED PARAMETER} = \frac{(N/\sqrt{\theta})}{K1 + (K2)\alpha} \tag{B4}$$

where:

A	= stream area (ID or OD) defined by location of dividing streamline
K1,K2	= empirical constants relating vane angle and speed
N	= rotor speed
P	= pressure
r	= radius to center of stream area (ID or OD)
T	= temperature
W	= physical flow rate
	= angle of inlet guide vanes
	= exit - inlet
	= pressure/standard pressure
	= temperature/standard temperature

Subscripts

B	= base radius at bypass ratio = 1.0
D	= design conditions
s	= static
T	= total

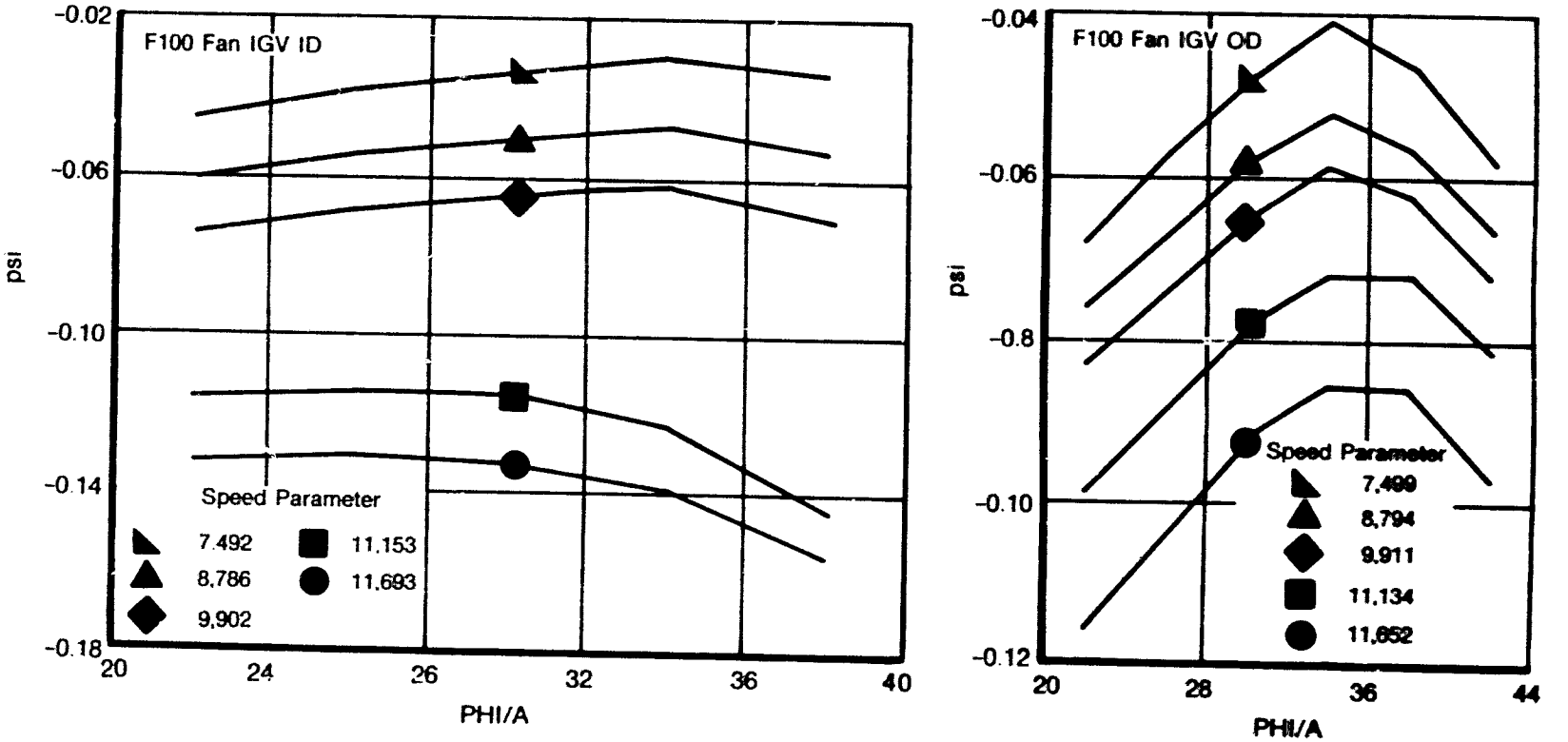

Figure 59. F100 Fan IGV Pressure Rise Characteristics

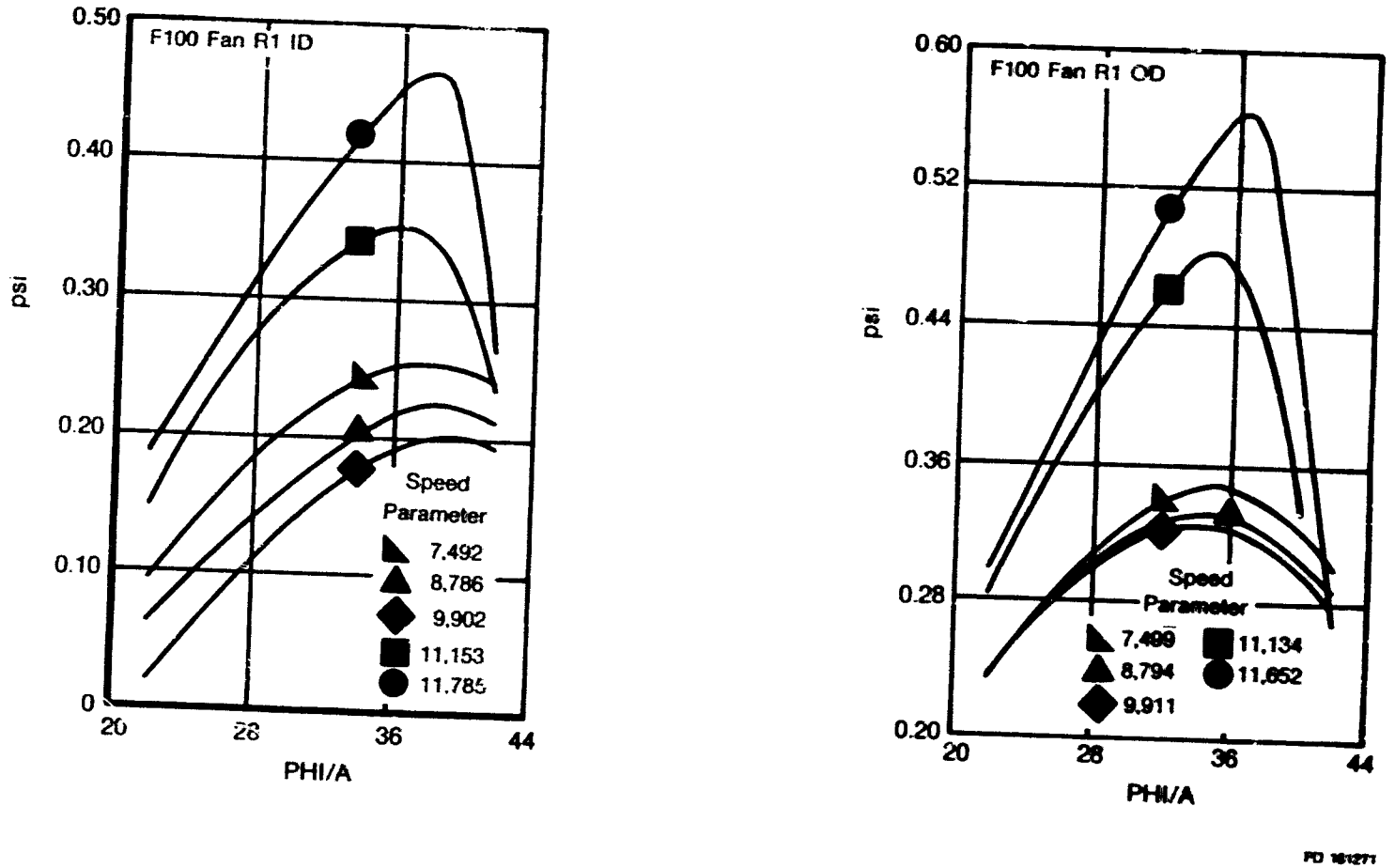

Figure 60. F100 Fan Rotor 1 Pressure Rise Characteristics

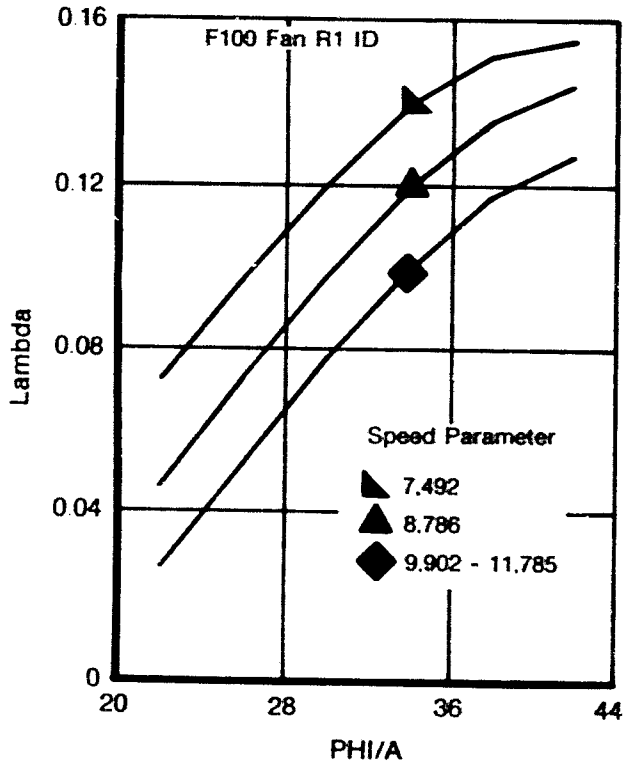

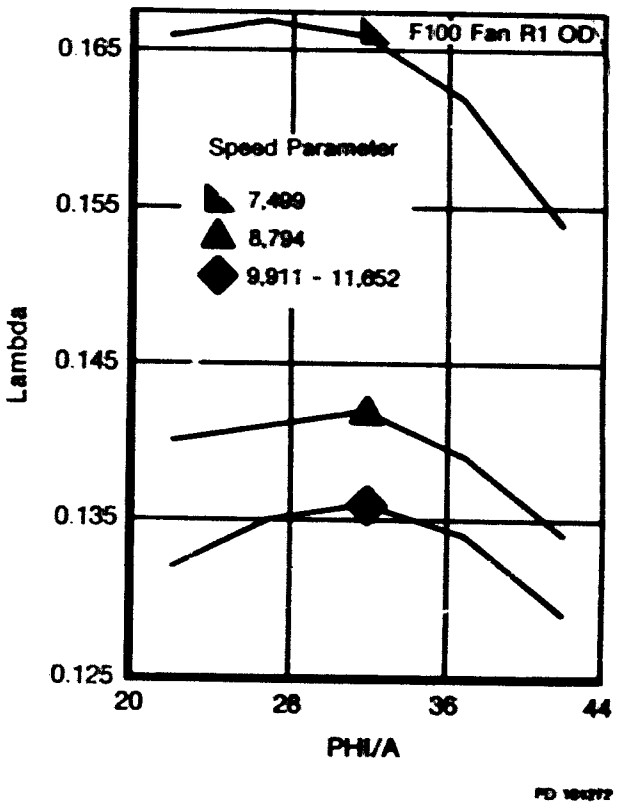

Figure 61. F100 Fan Rotor 1 Temperature Rise Characteristics

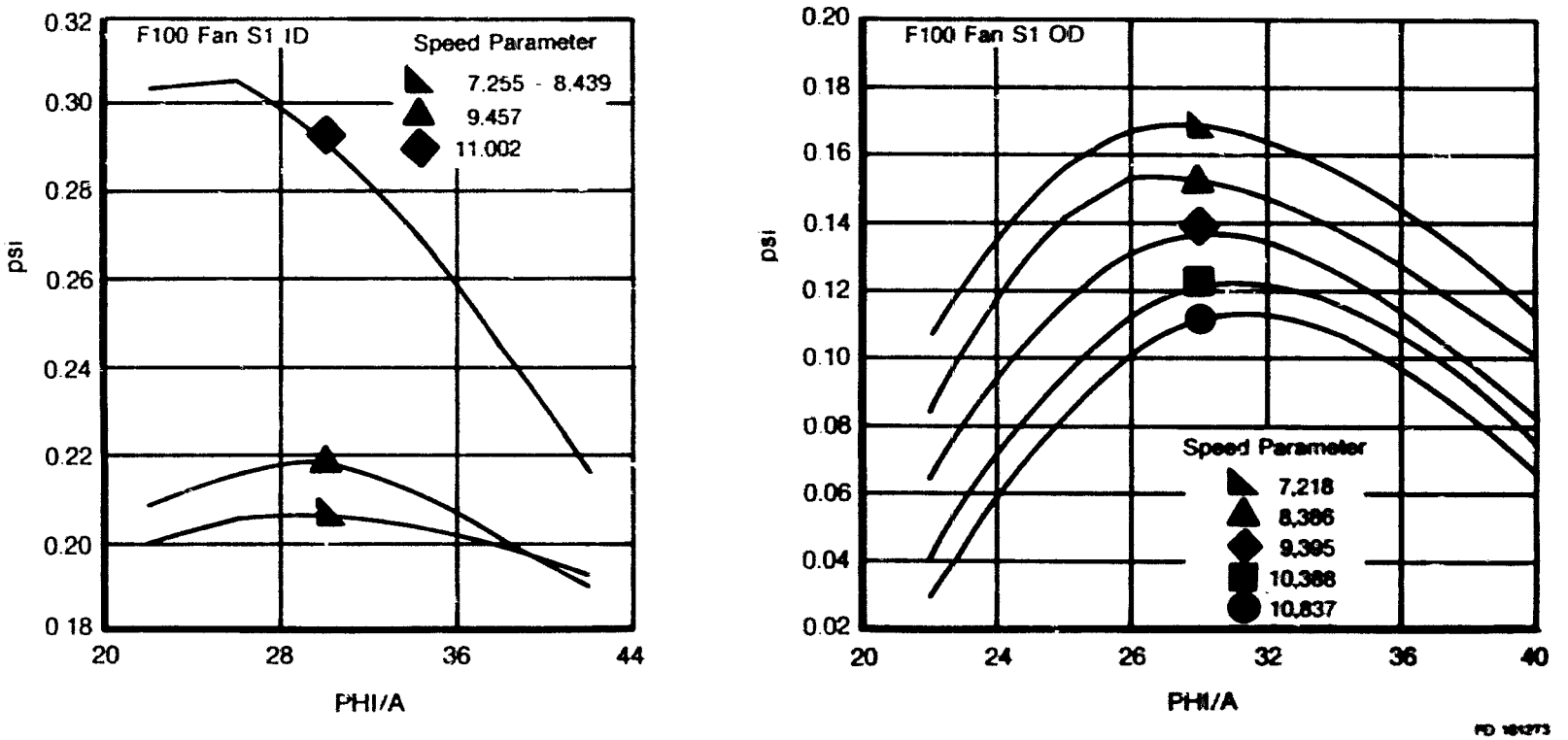

Figure 62. F100 Fan Stator 1 Pressure Rise Characteristics

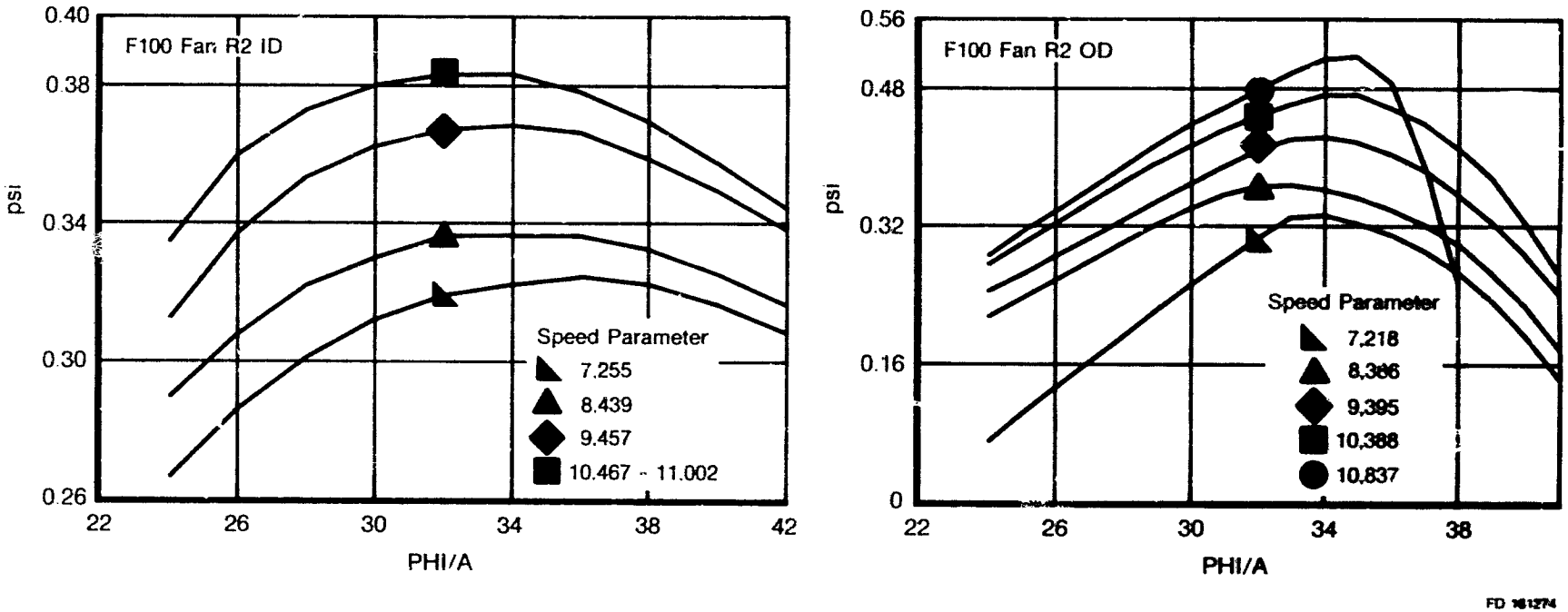

Figure 63. F100 Fan Rotor 2 Pressure Rise Characteristics

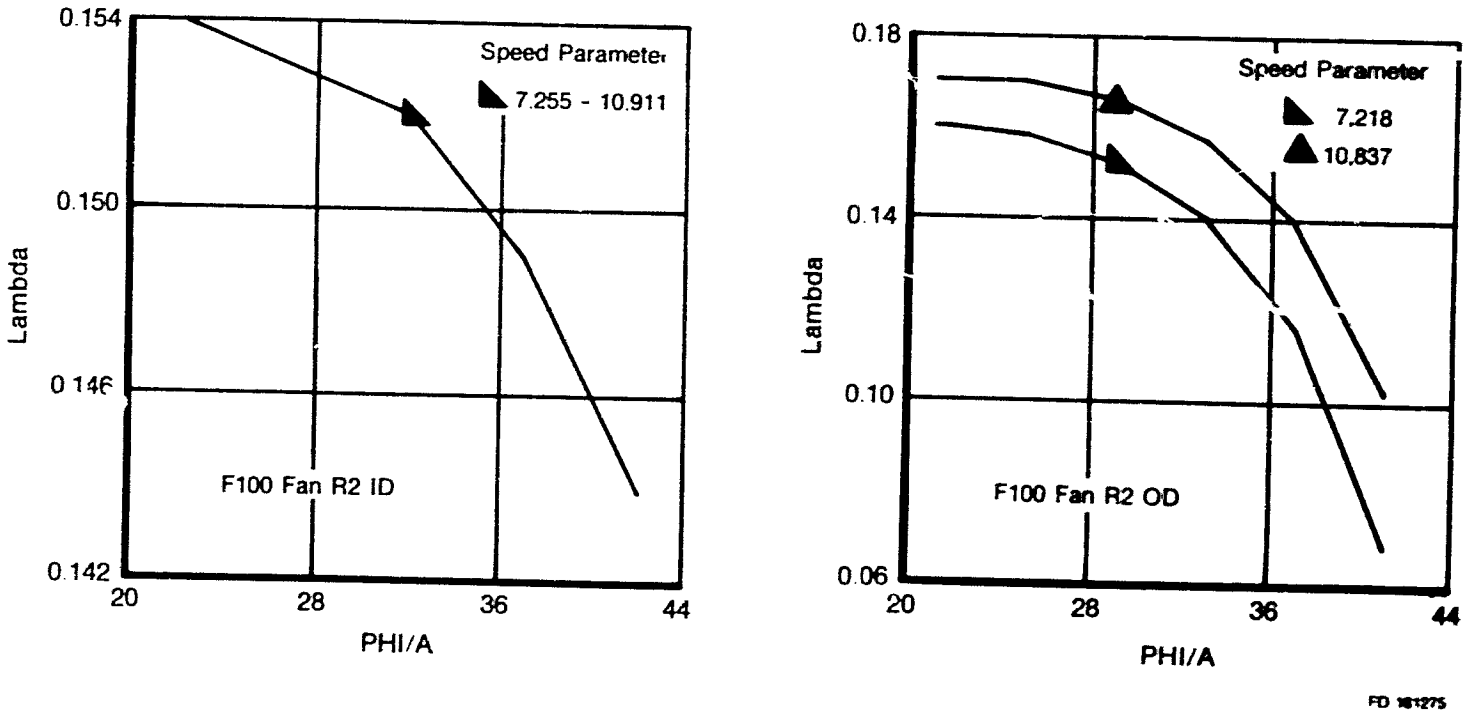

Figure 64. F100 Fan Rotor 2 Temperature Rise Characteristics

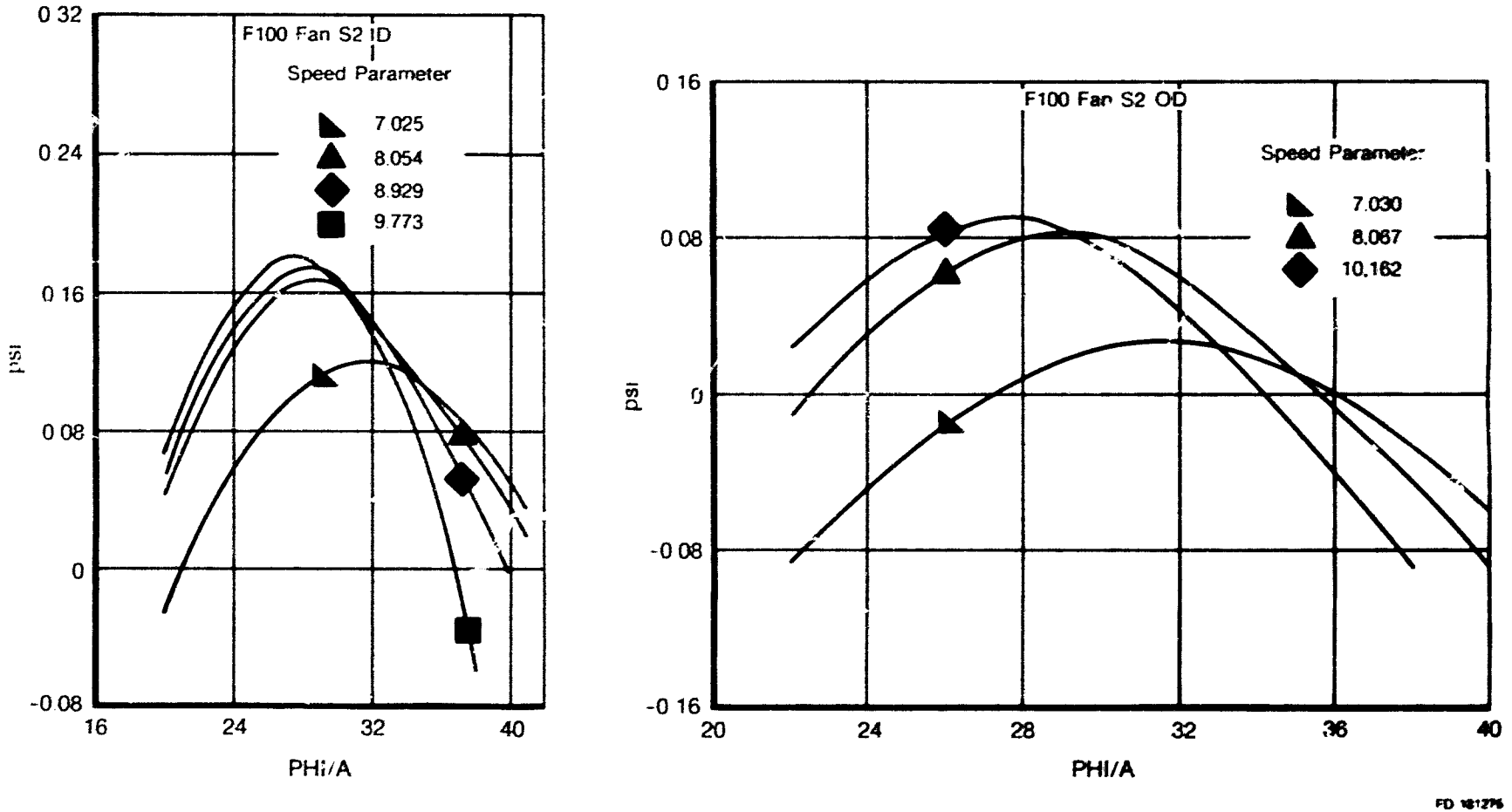

Figure 65. F100 Fan Stator 2 Pressure Rise Characteristics

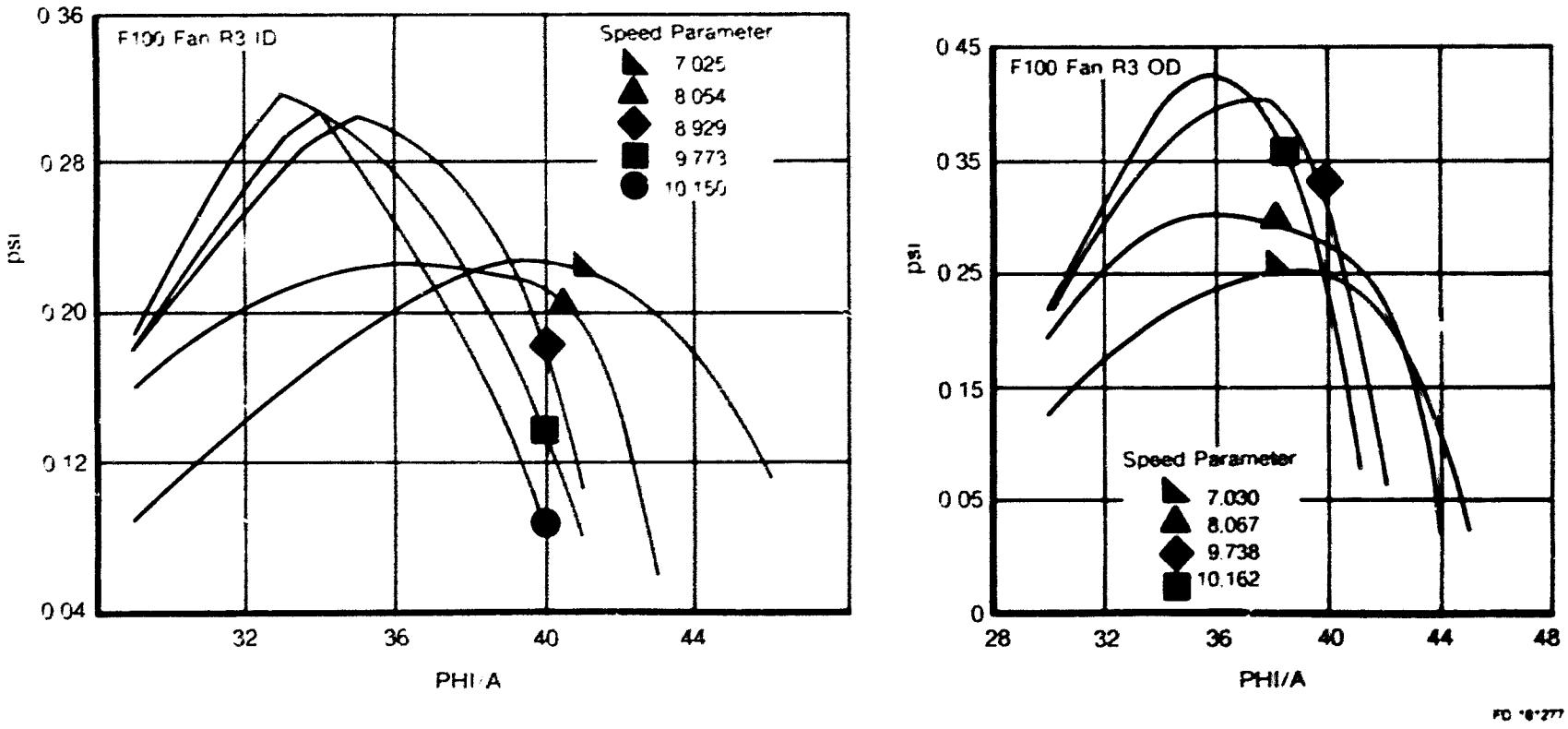

Figure 66. F100 Fan Rotor 3 Pressure Rise Characteristics

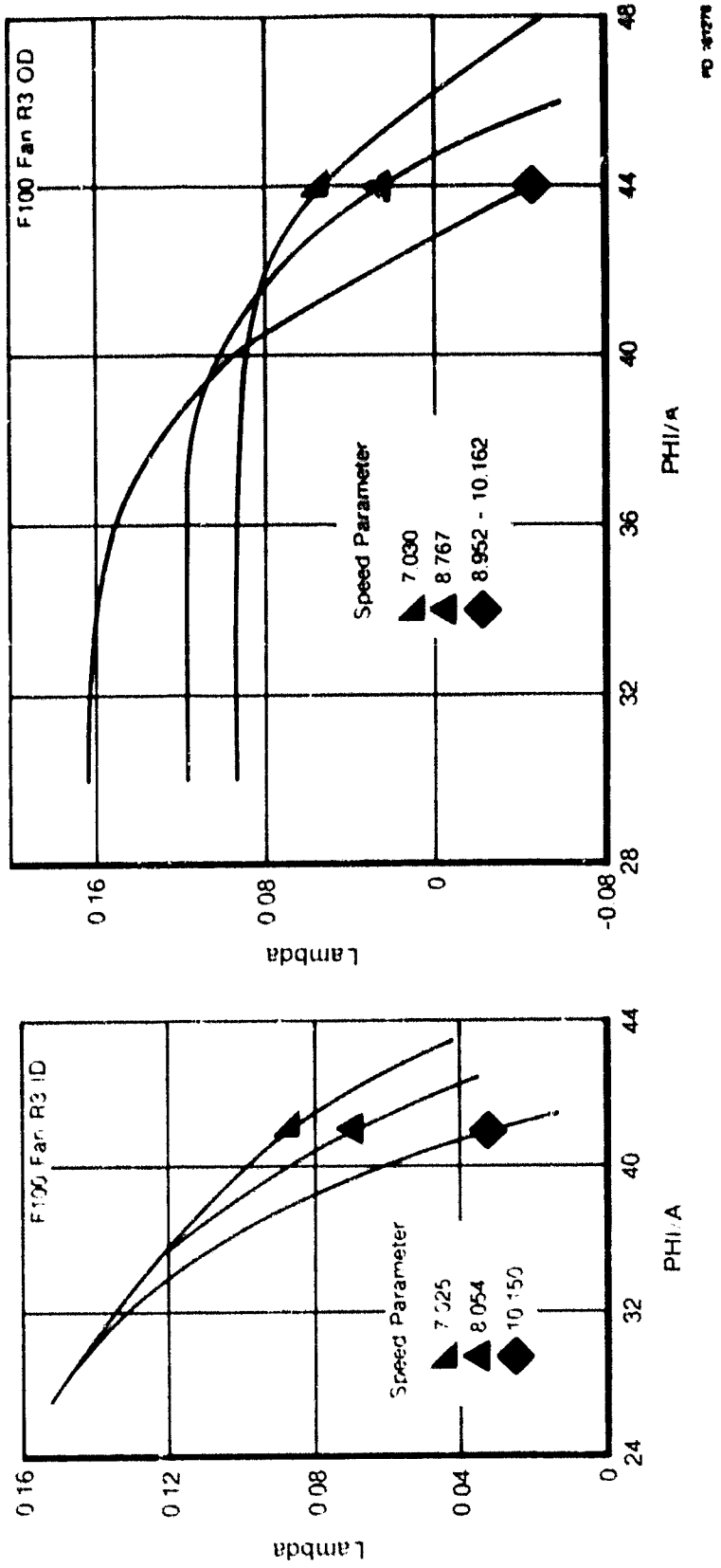

Figure 67. F100 Fan Rotor 3 Temperature Rise Characteristics

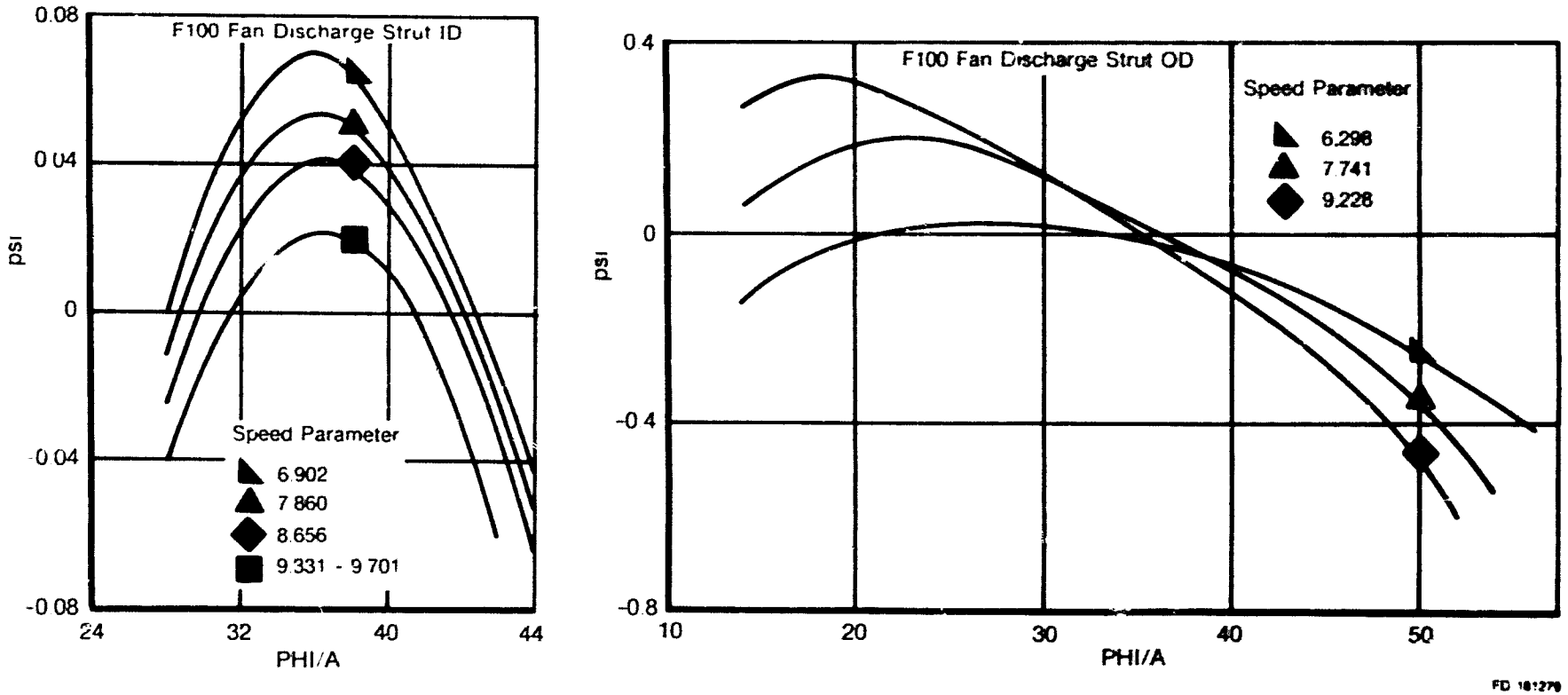

Figure 68. F100 Fan Discharge Strut Pressure Rise Characteristics

REFERENCES

1. Schuerman, J. A., K. E. Fisher, and P. W. McLaughlin, "High Frequency Dynamic Engine Simulation," NASA CR-135313, December 1977.

2. McAvlay, J. R., "Effect of Dynamic Variations in Engine-Inlet Pressure on the Compressor System of a Twin-Spool Turbofan Engine," NASA TM-X-2081, September 1970.

3. Seidel, Robert C., "Computer Programs for Calculation of Matrix Stability and Frequency Response from a State-Space System Description," NASA TM X-71581, July 1974.

4. Shultz, Donald G. and James L. Melsa, State Functions and Linear Control Systems, McGraw Hill, 1967.

5. Mazzawy, R. S., D. E. Haddad, and D. A. Fulkerson, "F100(3) Parallel Compressor Computer Code and User's Manual," PWA 5549-7, NAS3-20610, March 1978.